EXPERIMENTAL INVESTIGATION OF NANOPARTICLE ENHANCED OIL RECOVERY TECHNIQUES USING MICROMODELS

By

© Ayub Khezrnejad

A Thesis submitted to the

School of Graduate Studies

In partial fulfillment of the requirements for the degree of

Master of Engineerng

Faculty of Engineering and Applied Science

Memorial University of Newfoundland

October 2015

St. John's Newfoundland and Labrador

ABSTRACT

Nanotechnology has found widespread application in a diverse range of industries. Researchers are now investigating whether nanotechnology can be applied to enhance oil recovery. The goal of enhanced oil recovery is to manipulate the fluid-fluid properties (interfacial tension, viscosity), and fluid-rock properties (contact angle, relative permeability) to improve pore scale recovery efficiency.

In this study, nanofluids were prepared and injected into micromodels to study their effectiveness on oil recovery. Silicon oxide and aluminum oxide nanoparticles were used. Nanofluid viscosity and interfacial tension between nanofluid and oil was measured and modeled. Response Surface Methodology (RSM) was used to investigate the effect of the factors and their interactions. Fluid characterization data shows that nanoparticles are effective in both interfacial tension reduction and viscosity enhancement. The results from the micromodel studies indicate that adding a small amount of nanoparticles to the brine can enhance oil recovery by approximately 10 % - 20 %.

DEDICATION

All that I am or ever hope to be, I owe to my parents.

To the soul of my mother who encouraged me to be the best I can be. I feel she is always with me supporting and guiding.

To my beloved father for his love, support and encouragement

Thank You for Everything!

ACKNOWLEDGEMENTS

I would like to express the deepest appreciation to my dearest supervisors Dr. Lesley James and Dr. Thormod Johansen, who provided me guidance and support throughout this study: they continually and convincingly conveyed a spirit of adventure in regard to my research, and an excitement in regard to teaching. Without their guidance and persistent help this thesis would not have been possible. Furthermore, I would like to thank the staff of the Hibernia Enhanced Oil Recovery Research Group, Ms. Norah Hyndman, Mr. Edison Sripal, Ms. Kimberly Power, Mr. Shervin Ayazi, Mr. Mohammadreza Kowsari, Mr. Hossein Khorshidian, Ms. Mahsa Moayedi, and Mr. Maziyar Mahmoodi who provided help and constructive feedback.

I gratefully acknowledge the support of the Hibernia Management and Development Company Ltd. (HMDC), Chevron Canada, the Research and Development Corporation (RDC), the Natural Sciences and Engineering Research Council of Canada (NSERC), and the Canadian Foundation for Innovation for funding my research.

I would not have completed this road if not for my parents, Ali and Zohreh. I would like to thank you for your love and support throughout my life. My siblings and friends have also been the best of support along this journey, and encouraged me to move forward. Thank you all for your understanding and encouragement in my many moments of crisis.

Ayub Khezrnejad
Memorial University
September 2015

Table of Contents

ABSTRACT ii

DEDICATION iii

ACKNOWLEDGEMENTS iv

Table of Contents v

List of Tables xi

List of Figures xiv

List of Symbols, Nomenclature or Abbreviations xxii

1. Introduction 1

1.1 Enhanced Oil Recovery (EOR) 1

1.1.1 Primary Recovery 2

1.1.2 Secondary Recovery 3

1.1.3 Tertiary Recovery 3

1.2 Water Alternating Gas (WAG) 3

1.3 Main Recovery Mechanisms 4

1.4 Nanotechnology 5

1.5 Research Objectives 6

2. Literature Review 9

2.1 Introduction 9

2.1.1 Nanotechnology in Oil and Gas Applications 9

2.1.2 Nanotechnology in Enhanced Oil Recovery Research 10

2.2 Properties of Nanoparticles 13

2.2.1 General Definition 13

2.2.2 Nanoparticles Classification 14

2.2.2.1 Dimensionality 14

2.2.2.2 Morphology 15

2.2.2.3 Composition 15

2.2.2.4 Uniformity and Agglomeration State 16

2.2.3 Bulk to Nano Transition 16

2.2.4 Forces Governing Nanometer Scale Properties 17

2.3 Oil Recovery Fundamentals 19

2.3.1 Flow in Porous Media 19

2.3.2 Porosity and Pore Size Distribution 24

2.3.3 Permeability and Relative Permeability 25

2.3.4 Viscosity and Mobility Ratio 26

2.3.5 Interfacial Tension (IFT) 30

2.3.6 Contact Angle and Wettability....33
2.4 Nanotechnology Enhanced Oil Recovery Research....36
2.4.1 Core Flooding Studies....36
2.4.2 Micromodel Studies....46
2.4.3 Simulation and Mathematical Modeling Studies....53
3. Materials and Methods....58
3.1 Research Objectives....58
3.2 Design of Experiments....60
3.2.1 Response Surface Methodology (RSM)....60
3.2.2 Analysis of Variance (ANOVA)....61
3.2.3 Optimal Design of WAG Injection....62
3.2.4 Design of Waterflooding Experiments....63
3.2.5 Optimal Design of IFT Measurements....64
3.2.6 Optimal Design of Viscosity Measurements....66
3.3 Experimental Investigations....68
3.3.1 Fluids Preparation....69
3.3.2 Interfacial Tension Measurements....71
3.3.3 Viscosity Measurements....75

3.3.4 Micromodel Experiments 76

3.3.4.1 Micromodel Characterization 76

3.3.4.2 Experimental Setup 80

3.3.4.3 Experimental Procedure 81

3.3.4.4 Image Analysis 84

3.3.5 Error Analysis 85

4. Results and Discussion 87

4.1 WAG Experiments 87

4.2 IFT measurements 90

4.3 Modeling of the WAG Experiments 94

4.3.1 Effect of Type and Concentration of Nanoparticles 98

4.4 Modeling (IFT Experiments) 103

4.4.1 Silica Nanoparticles (SiO_2) – Low Pressure (20 psia) 106

4.4.2 Silica Nanoparticles (SiO_2) – High Pressure (8000 psia) 107

4.4.3 Alumina Nanoparticles (Al_2O_3) – Low Pressure (20 psia) 109

4.4.4 Alumina Nanoparticles (Al_2O_3) – High Pressure (8000 psia) 110

4.4.5 Interaction Effect 111

4.5 Waterflooding Experiments 116

4.5.1 Viscosity Measurements 121

4.5.2 Interfacial Tension Measurements 130

4.5.3 Capillary Number Analysis 131

5. Safety and Environmental Prospects 133

5.1 Potential Hazards 133

5.2 Precautions 134

5.3 Training 135

5.4 Personal Protective Equipment 135

6. Conclusions and Recommendations 136

6.1 Recommendations for Future Work 141

Appendix 143

A. Image Analysis 143

A.1 Micromodel Experiments 143

B. Error Analysis 150

B.1 Viscosity Measurements 150

B.1.1 Viscosity Calibration Experiment 153

B.2 Interfacial Tension Measurements 154

B.2.1 IFT Measurements Calibration 158

B.3 Waterflooding Micromodel 161

C. Raw Data 163

C.1 Micromodel Experiments 163

C.2 Interfacial Tension Measurements 172

C. 3 Viscosity Measurements 178

Bibliography 181

List of Tables

Table 1: Research summary of Nano-EOR techniques in core flooding experiments 38

Table 2: Research summary of Nano-EOR techniques using micromodels.....47

Table 3: Experimental research summary.....59

Table 4: Factors and levels of experimental design.....62

Table 5: Optimal design of WAG micromodel experiments.....63

Table 6: Design of waterflooding micromodel experiments 64

Table 7: Variables in the IFT experiments and their corresponding levels 65

Table 8: Optimal design of IFT measurements.....66

Table 9: Optimal design of viscosity measurements 67

Table 10: Salt concentrations used in the synthetic brine.....69

Table 11: Properties of nanoparticles.....70

Table 12: Properties nanoparticles dispersed in water.....71

Table 13: Technical features of the IFT meter.....73

Table 14: Pore dimensions (James 2009) 77

Table 15: Micromodel dimensions and characteristics (James 2009) 78

Table 16: PMMA micromodel characterization 79

Table 17: WAG experiments characterization 83

Table 18: The results of WAG micromodel experiments 88

Table 19: Analysis of variance for micromodel experiments 88

Table 20: IFT measurement results 91

Table 21: Analysis of variance results for the interfacial tension measurements 93

Table 22: Variables and their corresponding units 105

Table 23: Actual and coded values of variables 115

Table 24: Viscosity measurements 122

Table 25: Analysis of variance for viscosity measurements 124

Table 26: Interfacial measurements 131

Table 27: Capillary number for different scenarios of injection 132

Table 28: Oil recovery measurements by image analysis 150

Table 29: Silica nanofluid viscosity measurements (2.5 wt%, T=50°C, P=4010 psi) 152

Table 30: Standard deviation of viscosity measurements based on replicate runs 153

Table 31: Viscosity calibration results.....154

Table 32: IFT measurements for crude oil and alumina nanofluid (standard deviation).155

Table 33: Standard deviation of IFT measurements based on replicate runs 158

Table 34: Standard deviation for IFT of air/DI water system.....159

Table 35: Standard deviation for IFT of air/toluene system 160

Table 36: Standard deviation calculation for oil recovery of micromodel flooding.....162

List of Figures

Figure 1: Oil production classification (Burnett and Dann 1981) 2

Figure 2: Comparison of the sizes in nanoscale (Panneerselvam and Choi 2014) 6

Figure 3: Nanoparticles classification (Buzea et al. 2007) 14

Figure 4: Melting temperature of gold nanoparticles vs. particle diameter (Borel 1981) .17

Figure 5: A photo of water alternating gas flooding using a glass micromodel (Khezrnejad et al. 2014) 21

Figure 6: Micromodel waterflooding showing viscous fingering.....23

Figure 7: Micromodel polymer flooding showing a more stable flood front 23

Figure 8: Capillary desaturation curve (Lake 1989) 30

Figure 9: Oil-water interfacial tension before and after applying nanofluid (Roustaei et al. 2012) 32

Figure 10: The contact angle of a liquid with a surface in presence of air 33

Figure 11: Waterflooding micromodel (Maghzi et al. 2012).....36

Figure 12: FESEM image from limestone grain after flooding with TiO_2 nanofluid (Esfandyari Bayat et al. 2014).....43

Figure 13: FESEM image from limestone grain after flooding with SiO_2 nanofluid (Esfandyari Bayat et al. 2014).....43

Figure 14: Glass micromodel saturated with oil.....48

Figure 15: Emulsion generation using nanoparticles in the micromodel experiments (Li et al. 2013).....49

Figure 16: Using nanoparticles-stabilized foam for enhancing oil recovery of waterflooding in micromodel injection experiments (Nguyen et al. 2014).....51

Figure 17: The relation between oil recovery and injection volume of nanoparticles (Ju and Fan 2009).....55

Figure 18: Interfacial tension meter.....72

Figure 19: IFT meter software interface.....74

Figure 20: Rising drop method for IFT measurements.....74

Figure 21: Viscosity measurement setup.....75

Figure 22: Schematic diagram of viscosity measurement device.....76

Figure 23: Micromodel geometry (James 2009).....77

Figure 24: Photo captured during WAG injection.....78

Figure 25: PMMA micromodel 79

Figure 26: Schematic diagram of micromodel injection setup 81

Figure 27: Histogram graph of number of pixels vs. coded color before flooding [run #4] 84

Figure 28: Histogram graph of number of pixels vs. coded color after flooding [run #4] 85

Figure 29: Significant effects on the interfacial tension 94

Figure 30: Oil recovery vs. concentration for a 1:1 WAG ratio 96

Figure 31: Oil recovery vs. concentration for a 1:2 WAG ratio 96

Figure 32: Predicted oil recovery vs. actual experimental data 97

Figure 33: Interaction between nanoparticle type and WAG ratio (experimental results) 99

Figure 34: Oil in water emulsion observed during waterflooding with brine enriched with 0.08 g/ml SiO_2 nanoparticles [run #12].....100

Figure 35: No emulsion was observed during waterflooding with brine enriched with 0.08 g/ml Al_2O_3 nanoparticles [run #2].....100

Figure 36: Distribution of oil, brine with 0.08 g/ml Al_2O_3 nanoparticles, and air in the micromodel [run #2] 102

Figure 37: Distribution of oil and brine during waterflooding [run #7] 102

Figure 38: IFT vs. concentration in different states of pressure and temperature 104

Figure 39: Predicted IFT vs. actual experimental data 106

Figure 40: IFT vs. SiO_2 concentration for low pressure system (20 psia).....107

Figure 41: IFT vs. SiO_2 concentration for high pressure system (8000 psia).....108

Figure 42: IFT vs. Al_2O_3 concentration for low pressure system (20 psia).....109

Figure 43: IFT vs. Al_2O_3 concentration for high pressure system (8000 psia).....110

Figure 44: Interaction between concentration and temperature (4010 psia).....111

Figure 45: Interaction between pressure and temperature with no nanoparticles.....113

Figure 46: Interaction between pressure and temperature at high concentration of nanoparticles 114

Figure 47: Nonlinear behavior of interfacial tension.....116

Figure 48: Oil recovery vs. injected pore volume.....119

Figure 49: Ultimate recovery, recovery at breakthrough, and breakthrough time for the experiments.....120

Figure 50: Predicted viscosity vs. experimental viscosity measurements 125

Figure 51: Effect of nanoparticles concentration on alumina (Al_2O_3) nanofluid viscosity 126

Figure 52: Effect of nanoparticles concentration on silica (SiO_2) nanofluid viscosity....126

Figure 53: 3D map of viscosity vs. pressure and temperature (Al_2O_3, 1 wt%) 128

Figure 54: 3D map of viscosity vs. pressure and temperature (Al_2O_3, 5 wt%) 128

Figure 55: 3D map of viscosity vs. pressure and temperature (SiO_2, 1 wt%) 129

Figure 56: 3D map of viscosity vs. pressure and temperature (SiO_2, 5 wt%) 129

Figure 57: Silica nanofluid micromodel injection at t = 0 (min) 144

Figure 58: Silica nanofluid micromodel injection at t = 10 (min) 144

Figure 59: Silica nanofluid micromodel injection at t = 20 (min) 144

Figure 60: Silica nanofluid micromodel injection at t = 30 (min) 145

Figure 61: Silica nanofluid micromodel injection at t = 40 (min) 145

Figure 62: Silica nanofluid micromodel injection at t = 50 (min) 145

Figure 63: Silica nanofluid micromodel injection at t = 60 (min) 146

Figure 64: Silica nanofluid micromodel injection at t = 70 (min) 146

Figure 65: Silica nanofluid micromodel injection at t = 80 (min) 146

Figure 66: Silica nanofluid micromodel injection at t = 90 (min) 147

Figure 67: Silica nanofluid micromodel injection at t = 100 (min) 147

Figure 68: Silica nanofluid micromodel injection at t = 110 (min) 147

Figure 69: Silica nanofluid micromodel injection at t = 120 (min) 148

Figure 70: Silica nanofluid micromodel injection at t = 130 (min) 148

Figure 71: Silica nanofluid micromodel injection at t = 140 (min) 148

Figure 72: Silica nanofluid micromodel injection at t = 150 (min) 149

Figure 73: Silica nanofluid micromodel injection at t = 160 (min) 149

Figure 74: Silica nanofluid micromodel injection at t = 170 (min) 149

Figure 75: Silica nanofluid viscosity measurements (2.5 wt%, T=50°C, P=4010 psi) ...151

Figure 76: Silica nanofluid micromodel injection, t=0 min.....163

Figure 77: Silica nanofluid micromodel injection, t=10 min.....164

Figure 78: Silica nanofluid micromodel injection, t=20 min.....164

Figure 79: Silica nanofluid micromodel injection, t=30 min.....165

Figure 80: Silica nanofluid micromodel injection, t=40 min.....165

Figure 81: Silica nanofluid micromodel injection, t=50 min.....166

Figure 82: Silica nanofluid micromodel injection, t=60 min.....166

Figure 83: Silica nanofluid micromodel injection, t=70 min.....167

Figure 84: Silica nanofluid micromodel injection, t=80 min.....167

Figure 85: Silica nanofluid micromodel injection, t=90 min.....168

Figure 86: Silica nanofluid micromodel injection, t=100 min.....168

Figure 87: Silica nanofluid micromodel injection, t=110 min.....169

Figure 88: Silica nanofluid micromodel injection, t=120 min.....169

Figure 89: Silica nanofluid micromodel injection, t=130 min.....170

Figure 90: Silica nanofluid micromodel injection, t=140 min.....170

Figure 91: Silica nanofluid micromodel injection, t=150 min.....171

Figure 92: Silica nanofluid micromodel injection, t=160 min.....171

Figure 93: Silica nanofluid micromodel injection, t=170 min.....172

Figure 94: Interfacial tension between oil and alumina nanofluid (example #1) 173

Figure 95: Interfacial tension between oil and alumina nanofluid (example #2) 173

Figure 96: Interfacial tension between oil and alumina nanofluid (example #3) 174

Figure 97: Interfacial tension between oil and alumina nanofluid (example #4) 174

Figure 98: Interfacial tension between oil and alumina nanofluid (example #5) 175

Figure 99: Interfacial tension between oil and alumina nanofluid (example #6) 175

Figure 100: Interfacial tension between oil and alumina nanofluid (example #7) 176

Figure 101: Interfacial tension between oil and alumina nanofluid (example #8) 176

Figure 102: Interfacial tension between oil and alumina nanofluid (example #9) 177

Figure 103: Interfacial tension between oil and alumina nanofluid (example #10) 177

Figure 104: Viscosity measurements for DI water 178

Figure 105: Viscosity measurements for alumina nanofluid 179

Figure 106: Viscosity measurements for silica nanofluid.....179

Figure 107: Viscosity measurements for polymer solution 180

List of Symbols, Nomenclature or Abbreviations

All symbols, nomenclature and abbreviations are listed below alphabetically:

Al_2O_3: Aluminum oxide

ANOVA: Analysis of variance

C: Concentration (ppm or mg/L)

CDC: Capillary desaturation curve

Cor total: Corrected Total Sum of Squares

EOR: Enhanced Oil Recovery

Ø: Volume fraction of the solid sphere in the suspension

F value: Variance of the group means over mean of the within group variances

IFT: Interfacial tension (mN/m)

K: Permeability (mD)

Lack of fit: To determine an objective way of deciding when too much of the error in our prediction is due to lack of model fit

μ: Viscosity (cp)

μ_0: Viscosity of dispersion medium (cp)

Mean Square: An estimate of the population variance based on the variability among a given set of measures

N: Nanoparticle type

N_{vc}: Capillary number

P: Pressure (psi)

P&ID: Piping and instrumentation diagram

ppm: Part per million

Pure error: Error that occurs due to natural variation in the process

p-value: Tests the null hypothesis and the significance of the regression model

Residuals: The error variance for at least some of the treatment effects

RSM: Response surface methodology

σ: Interfacial tension (mN/m)

SiO_2: Silicon oxide

Sum of squares: The sum, over all observations, of the squared differences of each observation from the overall mean

T: Temperature (°C)

θ: Contact angle

v: Rate of displaced fluid

WAG: Water Alternating Gas

1. Introduction

1.1 Enhanced Oil Recovery (EOR)

Global demand for oil is expected to continue to increase for the foreseeable future prompting more exploration, the production of unconventional oil and gas, and the implementation of enhanced and improved oil recovery techniques to meet supply. Many novel enhanced oil recovery (EOR) methods have been proposed and applied to satisfy this demand. The major challenge is to increase recovery simultaneously at all scales; increase microscopic pore scale recovery and macroscopic field scale sweep and vertical efficiencies. **Figure 1** shows the common classification of oil recovery. Improved oil recovery (IOR) is commonly used in oil and gas industry to describe any process or processes used to economically increase the amount of oil production, which includes any physical, chemical, mechanical, and procedural techniques. Enhanced oil recovery is defined as the methods used to recover more oil than would be possible by employing only primary production or waterflooding. These recovery techniques are not recent inventions, and research on EOR began in the 1950's and has continued more or less uninterrupted to the present. Methods such as chemical injection, gas injection, or thermal techniques are commonly used to change the rock and fluid properties to economically improve the recovery factor.

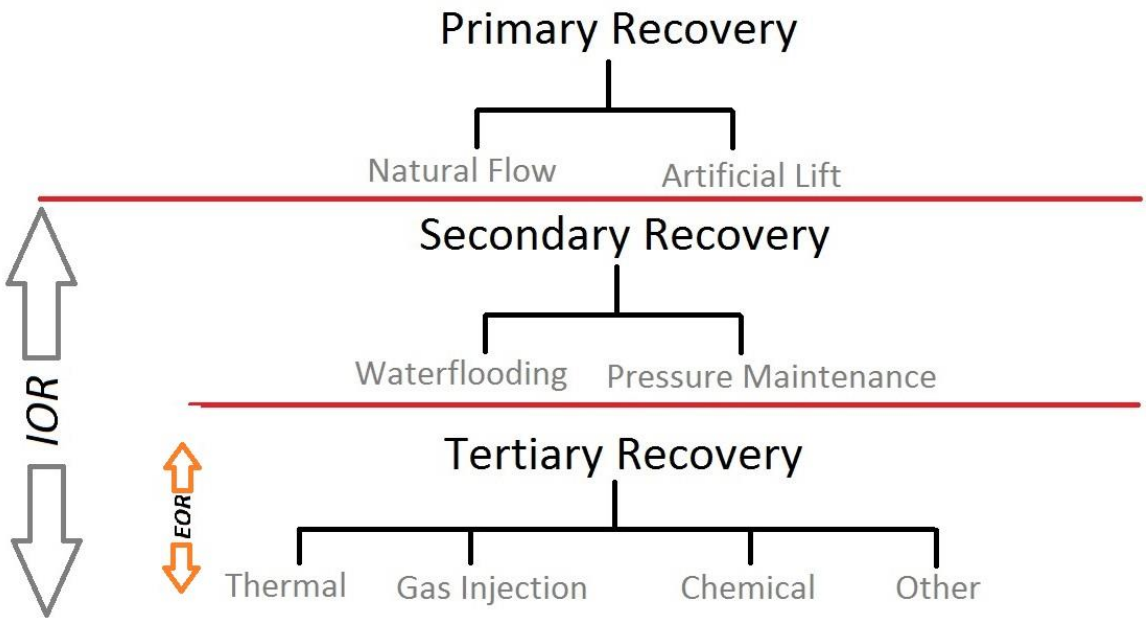

Figure 1: Oil production classification (Burnett and Dann 1981)

1.1.1 Primary Recovery

The natural pressure of the reservoir causes the oil to flow from the reservoir to the well that operates at a pressure less than reservoir pressure. By producing more oil from the reservoir, the reservoir pressure will decrease over the production lifetime. The possible drive mechanisms involved in primary recovery are:

- Oil/Gas expansion drive
- Water drive (influx)
- Compaction drive

1.1.2 Secondary Recovery

Secondary oil recovery methods are applied when the natural reservoir drive is no longer profitable. Secondary recovery depends on delivering an external energy into the reservoir by injecting fluids to increase reservoir pressure. Water or gas injection, for the purpose of pressure maintenance, is generally considered as secondary recovery.

1.1.3 Tertiary Recovery

Tertiary recovery or enhanced oil recovery (EOR) is used for the purpose of recovering post waterflood or gasflood residual oil from the reservoir by changing the physical and chemical properties of the rock and/or the fluid. Enhanced oil recovery methods are generally divided into four main groups:

- Thermal (steam/hot water injection, combustion, and etc.)
- Miscible/Immiscible gas injection (CO_2, hydrocarbon gas, nitrogen, air, and etc.)
- Chemical (alkali, surfactant, polymer, nanoparticles, and etc.)
- Other (microbial, electrical, leaching and etc.)

1.2 Water Alternating Gas (WAG)

Alternating water and gas injection (WAG) popularly known as “Water Alternating Gas Flooding” is applied to try and recover more residual oil at the microscopic and sweep efficiency recovery scale. The goal of WAG is to achieve high microscopic/pore scale

efficiency by injecting a gas phase then injecting water to improve vertical and overall sweep efficiency by minimizing fingering. The philosophy behind the WAG process is that by alternately flooding the reservoir with water and gas, gas can occupy portions of the pore space that is otherwise occupied by residual oil, while water when injected subsequently, will displace some of the remaining oil and injected gas, further reducing the residual oil saturation.

1.3 Main Recovery Mechanisms

The amount of the oil recovery in a reservoir is mainly affected by the volume of the oil contacted by the injected fluid or fluids. Pore scale mobilization or displacement of the oil is considered as the microscopic sweep efficiency. Microscopic efficiency depends on the factors such as interfacial tension between the reservoir and injected fluid/fluids, wettability of the reservoir rock, capillary pressure, and relative permeability. Macroscopic sweep efficiency controls the effectiveness of the displacing fluids to recover the reservoir oil in volumetric scale. Heterogeneities and anisotropy of the reservoir, mobility ratio (the mobility of the displacing fluid compared with the mobility of the displaced fluids), injection and production well locations, and the type of the rock reservoir are the factors that limit the macroscopic sweep efficiency.

1.4 Nanotechnology

Most researchers define nanotechnology as the study and control of phenomena and materials at length scales below 100 nm. **Figure 2** shows a comparison of the sizes of nanomaterials with those of other common materials. An unconstrained and practical definition for nanotechnology is given by Bawa et al. (2005) as:

> "The design, characterization, production, and application of structures, devices, and systems by controlled manipulation of size and shape at the nanometer scale (atomic, molecular, and macromolecular scale) that produces structures, devices, and systems with at least one novel/superior characteristic or property."

Nanotechnology has shown a great potential to initiate positive changes in several areas of the oil and gas industry, such as exploration, drilling, production, enhanced oil recovery, refining and distribution. The idea of using nanoparticles in EOR methods has been recently raised by researchers observing features such as emulsion generation without surfactant to help control mobility, interfacial tension reduction, wettability alteration, and long-distance oil transportation in the reservoir with nanoparticle stabilized emulsions. These fluid characteristics are factors in enhancing oil recovery. The use and effectiveness of nanoparticles in achieving favorable oil recovery is the topic of research that will be discussed and investigated in this thesis.

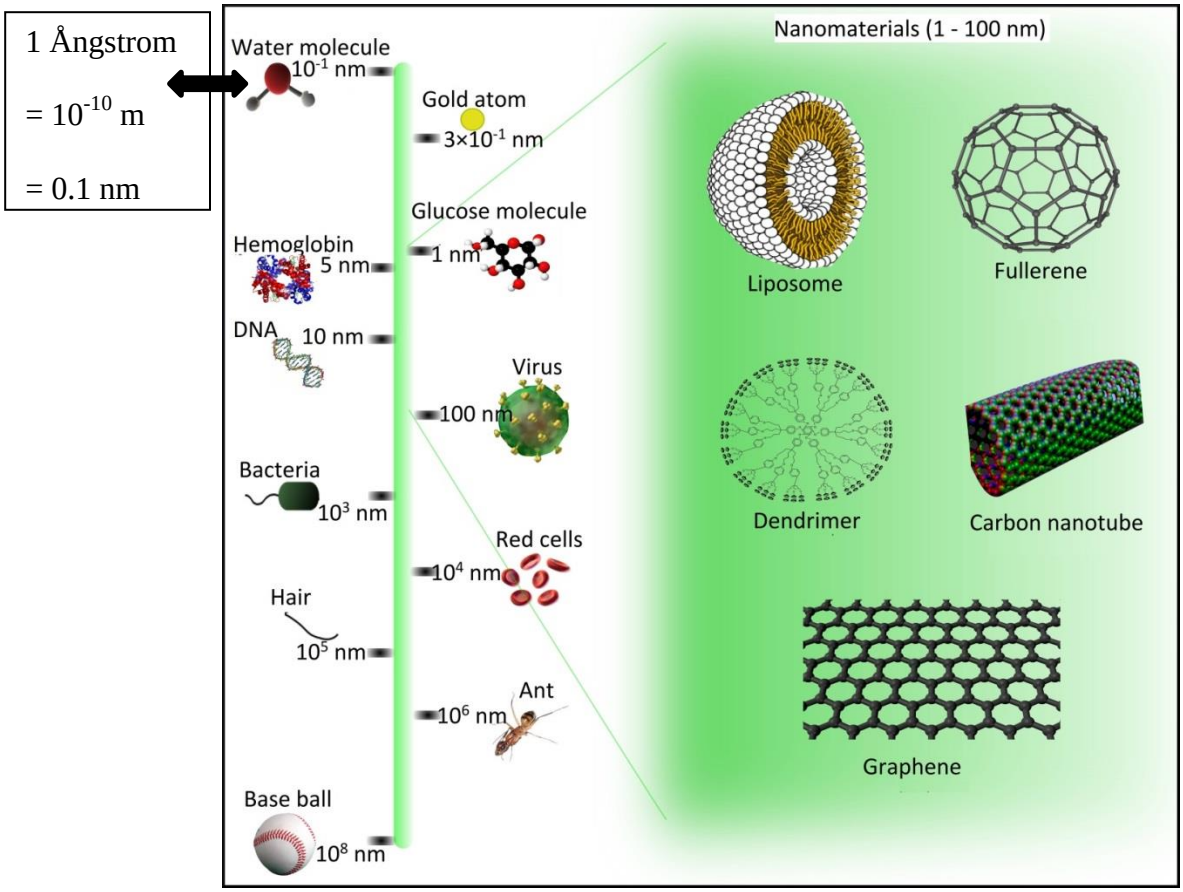

Figure 2: Comparison of the sizes in nanoscale (Panneerselvam and Choi 2014)

1.5 Research Objectives

Nanoparticles have shown a promising potential for enhancing the oil recovery due to their unique physical and chemical properties. The goal of this work is to better understand the oil recovery enhancement mechanism by nanoparticles. In this experimental work, this potential was studied to investigate how nanotechnology can help to improve the microscopic and/or macroscopic sweep efficiency. A series of water

alternating gas micromodel injection was performed to investigate the effect of adding nanoparticles to the water phase on oil recovery. Moreover, nanoparticle enhanced waterflooding was compared to polymer flooding to better understand the mechanisms of oil recovery improvement using nanoparticles. The results of polymer injection (with same viscosity of the nanofluid) were compared to the results of nanofluid injection to determine the role of nanoparticles in enhancing oil recovery. Is it the mobility ratio (viscosity effect) or interfacial tension reduction? The effect of nanoparticles on IFT reduction and viscosity enhancement was also studied in different ranges of pressure and temperature. It has been shown in the literature that nanoparticles are capable of reducing interfacial tension, and increasing the viscosity of water. However, most researchers measured the IFT and viscosity in a fixed condition (pressure and temperature). In order to understand the behavior of IFT and viscosity with respect to different factors and their interactions, we will change all the factors at the same time instead of changing one factor at a time, which only gives us an estimate of IFT and viscosity in a certain condition.

Important factors such as nanoparticle type, nanoparticle concentration, WAG ratio, pressure, and temperature were studied in this experimental work. A statistical method, Response Surface Methodology (RSM), was employed to study the effect of individual factors and their interactions on the response, and to fit the best possible model. By using RSM, the response can be correlated according to the corresponding factors. Additionally, the effect of the interactions between the factors on the response (oil

recovery/IFT/viscosity), and the nonlinearity of the model was also studied which has not been studied in the literature.

The possible mechanism for the oil recovery improvement using nanoparticles may be IFT reduction and viscosity enhancement. Adding nanoparticles to water phase is shown to be very effective in terms of enhancing oil recovery, and reducing the interfacial tension. The IFT/viscosity results were used to plan for micromodel EOR studies examining the effect of nanoparticles on recovery efficiency for which we illustrate the results.

2. Literature Review

2.1 Introduction

2.1.1 Nanotechnology in Oil and Gas Applications

Nanotechnology is influencing almost every industry, from consumer electronics to healthcare to telecommunications. This potential has not been yet completely studied in oil and gas exploration and production. However, nanotechnology applications in the oil industry are not completely new and nanoparticles have been successfully used in drilling muds for the past 50 years (Matteo et al. 2012).

Research by universities and institutes into the applications of nanotechnology in subsurface oil reservoirs is widely growing, and shown to be a potentially profitable area of investment. However, more effort is needed to apply nanotechnology to oil fields successfully (Friedheim et al. 2012). Future subsurface applications in developing novel injectant fluids for enhanced oil recovery make nanotechnology very promising area of research within the oil and gas industry (Kapusta et al. 2011).

Unique physical and chemical properties of nanoparticles such as corrosion resistance and mechanical strength make them a promising area of research specifically in EOR applications. Moreover, nanoparticles can be used as extremely sensitive downhole sensors for temperature, pressure and stress due to their optical, magnetic, and electrical

properties (Krishnamoorti 2006). Other emerging applications of nanotechnology are represented by the development of new types of smart fluids for improved/enhanced oil recovery (Matteo et al. 2012). Such a fluid can reduce the interfacial tension between the oil and the injected fluid, and increase the viscosity of the injected fluid at the same time, thus improving the microscopic and macroscopic sweep efficiency.

Chemical EOR processes such as polymer flooding, surfactant flooding, and alkaline injection are limited by high costs, potential corrosion of the formation and fluid loss during the flow through the reservoir (Kong and Ohadi 2010). Special characteristics of nanoparticles, especially their unique surface chemistry, may help to overcome these challenges. However, multidisciplinary research between chemists, physicists, and chemical and petroleum engineers is needed to apply nanotechnology successfully in oilfields. Also, theoretical investigations and simulation studies are required prior to any nano-technique to be used in the field to reduce the risk, and to select the best method (Ayatollahi and Zerafat 2012).

2.1.2 Nanotechnology in Enhanced Oil Recovery Research

The question is whether or not nanotechnology can play a role in helping to enhance oil recovery, and if so, how? The idea of using nanoparticles to enhance oil recovery has been recently raised by researchers observing features such as wettability alteration, interfacial tension (IFT) reduction, viscosity reduction, thermal conductivity enhancement

and long distance oil transportation in the reservoir with nanoparticle stabilized emulsions (Chol 1995; Maghzi et al. 2011; Ayatollahi and Zerafat 2012; Hendraningrat and Torsæter 2014; Li and Torsæter 2014; Jafari et al. 2015). However, the function of nanotechnology in the oilfield is still a subject of discussion and debate.

Use of EOR methods involves enormous risks in terms of technical feasibility, reserves recovery, and resources commitment. Low primary recovery is attributed to oil gravity, viscosity, and the drive mechanism (Choudhary et al. 2012). The main challenges of EOR such as low sweep efficiency, costly EOR agents and processing/storage facilities, possible formation damage, difficulty in transportation of EOR agents (especially for offshore fields), scaling results from laboratory pore/core scale to field scale predictions and, the lack of analytical tools, all hinder the wider use of EOR processes.

An important benefit of using nanoparticles is that they are much smaller than the size of the pores and throats in the porous medium, which decrease the possibility of pore/throat plugging. Higher thermal conductivity of nanoparticles make them very promising in future applications for heavy oil/bitumen recovery. Literature suggests that nanoparticles can be effective in terms of IFT reduction which improves the microscopic efficiency. Moreover, specific types of nanoparticles can increase the viscosity of the injected fluid significantly, which improves the mobility ratio and macroscopic sweep efficiency. Overall, the experimental results suggest that nanoparticle enhanced water injection is a

promising as an EOR process (Qiu 2010; Agenet et al. 2012; Ayatollahi and Zerafat 2012; Friedheim et al. 2012; Maghzi et al. 2012).

According to current research and technical literature, the new generation of nano-agents should: i) affect the properties of the injected fluid, in terms of viscosity, density, thermal conductivity and specific heat; and ii) modify the fluid-rock interaction properties, for example in terms of wettability. As the particles size decreases to the nano scale, the nanofluid properties/behavior tends to be governed by molecule forces instead of bulk material properties (Bensaba 2013).

Potential nanoparticles to be used for in EOR include oxides of aluminum, zinc, magnesium, iron, zirconium, nickel, tin and silicon (Ogolo et al. 2012). Single-walled-carbon-nano-tube and silica nanohybrids are very promising materials: if delivered at the oil-water interface, they may react with and modify the oil properties to increase oil mobilization (Matteo et al. 2012).

Silica nanoparticles have been widely studied for EOR purposes (Maghzi et al. 2011; Maghzi et al. 2012; Ogolo et al. 2012; Khezrnejad et al. 2014; Jafari et al. 2015). Special surface characteristics of this type of nanoparticles make them effective agents for enhancing water-flooding oil recovery. It is suggested that silica nanoparticle concentration of 0.02 to 0.03 (wt %) is desirable to enhance oil recovery (Ju et al. 2006). According to the wettability of the surface of these nanoparticles, they can be classified

into two types: lipophobic and hydrophilic polysilicon nanoparticle and hydrophobic lipophilic polysilicon nanoparticle (Ju and Fan 2009).

2.2 Properties of Nanoparticles

2.2.1 General Definition

Most researchers define nanotechnology as the study and control of phenomena and materials at length scales below 100 nm. An unconstrained and practical definition for nanotechnology is given by Bawa et al. (2005) as:

"The design, characterization, production, and application of structures, devices, and systems by controlled manipulation of size and shape at the nanometer scale (atomic, molecular, and macromolecular scale) that produces structures, devices, and systems with at least one novel/superior characteristic or property."

Typically, any particle smaller than 100 nm and larger than 1 nm is considered a nanoparticle. The importance of nanoparticles is in their specific physical and chemical properties which might be different from the properties of the bulk material (Pal et al. 2011). There are different methods of classifying nanoparticles. For example, nanoparticles can be classified based on their dimensionality, morphology, composition, uniformity, and/or agglomeration.

2.2.2 Nanoparticles Classification

Engineered nanoparticles such as metal nanoparticles or nanotubes can be manufactured for a specific purpose. Moreover, nanoparticles can form naturally or by accident. Nanoparticles can be classified based on their dimensionality, morphology, composition, and uniformity and agglomeration (Buzea et al. 2007). **Figure 3** shows general classification of nanoparticles.

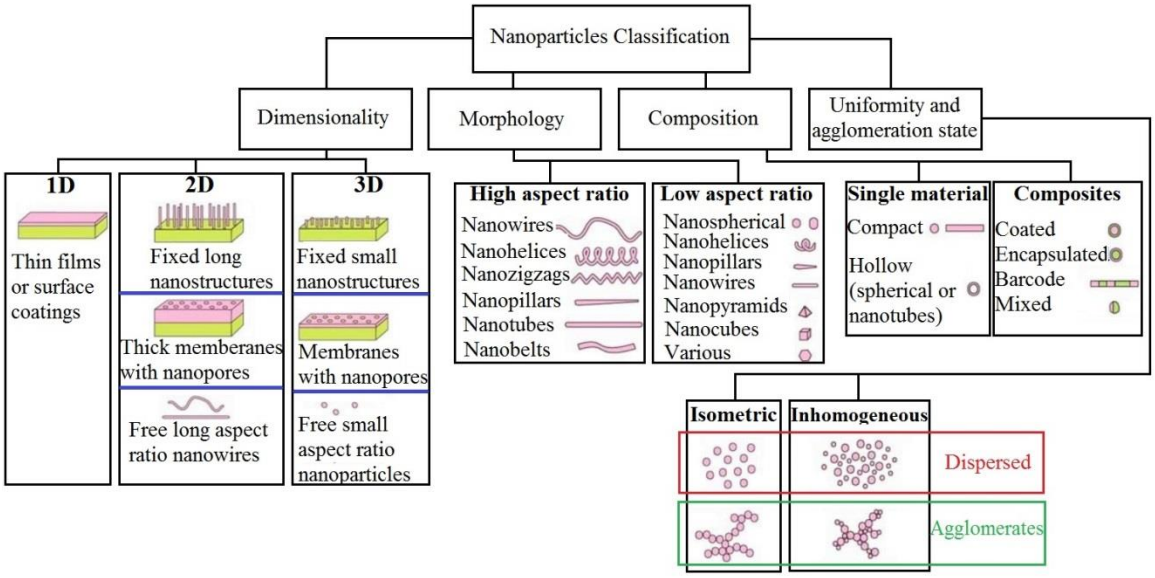

Figure 3: Nanoparticles classification (Buzea et al. 2007)

2.2.2.1 Dimensionality

As shown in **Figure 3**, nanoparticles can be classified based on their dimension. Nanoparticles with nanoscale in only one dimension fall into 1D group. This type of nanoparticles are generally used as thin films for surface coating or in fabricating

electronic, optoelectronic, electrochemical, electromechanical devices (Buzea et al. 2007; Xia et al. 2003). Nanoparticles having nanometer scale size in two dimensions are in the category of 2D nanoparticles. They are typically used for small particle separation and filtration (Buzea et al. 2007). Materials having nanometer scale in all three dimensions are called 3D nanoparticles. Free nanoparticles with various morphologies, vastly used in variety of industries, are considered as 3D nanoparticles.

2.2.2.2 Morphology

Generally, the aspect ratio in nanotechnology is defined as the ratio of the longest measure of an object size along a specified direction to the shortest perpendicular one, or simply length to diameter of an object (Buzea et al. 2007; Chen et al. 2008). According to this definition, nanoparticles morphology can be divided into two main categories of high and low aspect ratio. Based on the application, nanoparticles exist as powder, suspension, or colloids. When deciding to choose a specific nanoparticle for a particular application, shape, flatness, and aspect ratio are very important parameters to consider.

2.2.2.3 Composition

Nanoparticles can also be classified based on their composition. Nanoparticles can be synthesized from one single material or a mixture of several materials (Buzea et al. 2007). One interesting application of composite nanoparticles in EOR is that by surface modifying a nanoparticle, the wettability state of the particle can be changed to the

desired wettability state. For example, it is possible to change the wettability of a reservoir rock by using engineered surface modified nanoparticles.

2.2.2.4 Uniformity and Agglomeration State

As shown in **Figure 3**, nanomaterials can be isometric or irregular in terms of shape. Surface chemistry and physical/chemical properties of nanoparticles dictate if a specific nanoparticle can be dispersed in a specific medium (Buzea et al. 2007; Bensaba 2013). Brine is normally used in waterflooding. It is a challenge to uniformly disperse nanoparticles in brine. For example, silica nanoparticles tend to agglomerate in brine which is undesirable due to the potential core blockage. By silica nanoparticles surface modifying, we can overcome this problem, and uniformly disperse them in brine (wettability alteration of nanoparticles).

2.2.3 Bulk to Nano Transition

Nanoparticles behave differently, and have different properties than their bulk. Therefore, they are considered as a different state of matter, and we can say that nanotechnology is a bridge between bulk material and atomic or molecular structures. As the number of atoms in a particle fall below 100 atoms (approximately 100 nm), the physical and chemical properties of the particle might become different than the bulk properties (Owens and Poole Jr. 2008). For example, **Figure 4** shows how the melting point of a gold particle decreases significantly as its number of atoms fall below 100 atoms (Borel 1981). Silica

nanoparticles are widely used for EOR research due to their unique properties (Maghzi et al. 2011; Maghzi et al. 2012; Ogolo et al. 2012; Khezrnejad et al. 2014; Jafari et al. 2015). Literature suggests that silica nanoparticles have the ability to reduce interfacial tension, and alter wettability alteration. These functions are achievable only at the nanometer scale due to unique physicochemical properties of nanoparticles.

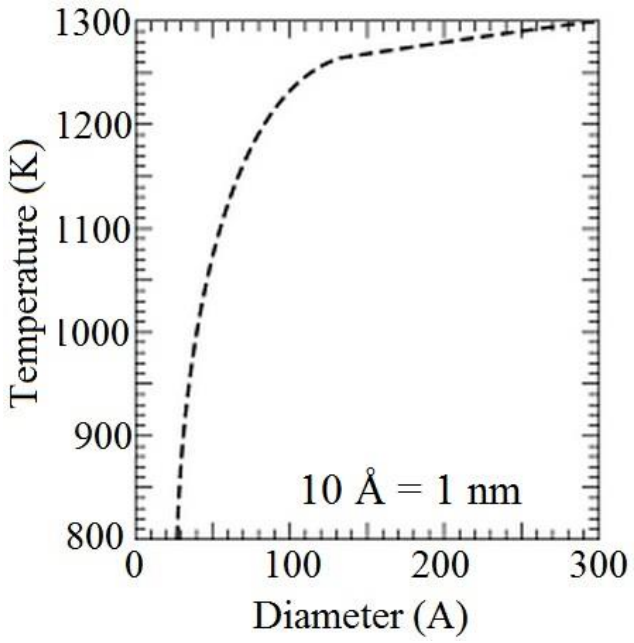

Figure 4: Melting temperature of gold nanoparticles vs. particle diameter (Borel 1981)

2.2.4 Forces Governing Nanometer Scale Properties

When a nanoparticle is injected into a porous medium, four phenomena may occur: adsorption, desorption, blocking, and transport (Ju et al. 2006). Both attractive and repulsive forces are important while studying the transport of nanoparticles. For example,

considering a suspension of nanoparticles in water as the injected fluid to the porous media, when the total energy of this system is negative, the attractive force is larger than repulsion between particles and porous walls, leading to further adsorption. Otherwise, desorption of nanoparticles from the porous walls will occur. Dynamic equilibrium between adsorption and desorption is controlled by the total energy between particles and porous walls. Clearly, blocking will take place if the diameter of particles is larger than the size of the pore throat, or when several particles smaller than the pore size gather together to block the pore throat. Transport of nanoparticles in porous media is governed by diffusion and convection. Diffusion at the molecular level occurs due to the kinetic energy of the random motion of the molecules (Ju, et al. 2006; Ju and Fan 2009).

There are three important effects due to nanoparticles transport in porous media: i) wettability alteration, ii) change in oil displacement mechanism and the effective pore diameter due to wettability alteration, and iii) pore blockage. Nanoparticles can achieve a certain state of wettability by surface modifying process (Mohajeri et al. 2015). The pore walls wettability may be changed due to nanoparticle adsorption and consequently, the relative permeability of the oil and water phases will be changed. The mechanism of oil displacement in the small pores and the effective pore diameters for oil flow in the porous medium will be changed due to wettability alteration. Finally, the adsorption of particles on the porous surface and blocking of the small pore throats may lead to a reduction in porosity and absolute permeability (K) of the porous media (Ju et al. 2006). Overall, by

designing a nanoparticle with specific physicochemical properties, we can achieve some desirable EOR conditions such as wettability alteration, IFT reduction, and viscosity enhancement. However, it should be noted that there are some undesirable phenomena that could happen due to nanoparticles transport in porous media like pore blockage.

2.3 Oil Recovery Fundamentals

2.3.1 Flow in Porous Media

Darcy's law is the most common flow equation used to describe the fluid flow inside porous media. **Eq. 1** describes the general form of Darcy's law used for single flow in porous media:

$$Q = \frac{KA}{\mu L}\Delta P, \text{ ----- } \textbf{Eq. 1}$$

where, Q (m^3/s) is the total flux, K (m^2) is the absolute permeability of the porous media, A (m^2) is the cross sectional area of the flow, μ (Pa.s) is the viscosity of the injected fluid, L (m) is the total length of the porous media, and ΔP (Pa) is the pressure difference between the inlet and the outlet of the porous media.

When we have multiphase flow inside porous media, relative permeability comes into the flow equation to differentiate between immiscible phases. Relative permeability (k_r) of a

phase is the dimensionless measure of effective permeability of that phase. Darcy's law for multiphase flow in porous media is described in the **Eq. 3**:

$$k_{ri} = \frac{k_i}{K}, \text{ ----- } \mathbf{Eq.\ 2}$$

$$Q = \frac{k_i A}{\mu_i L} \Delta P = \frac{K k_{ri} A}{\mu_i L} \Delta P, \text{ ----- } \mathbf{Eq.\ 3}$$

where, k_{ri} is the relative permeability of phase (i), k_i is the effective permeability of phase (i), and μ_i is the viscosity of phase (i).

The existence of two or more immiscible fluids in a porous rock depends on capillary pressure. The curvature on the interface of two immiscible fluids causes pressure difference (capillary pressure) on the interface. Macroscopic capillary pressure for a specific reservoir rock is a unique function of the fluid phase saturation, the wettability of the rock (denoted by the contact angle θ), and the interfacial tension between the fluids (σ) (Brown 1951). **Figure 5** shows how capillary pressure causes curvature on the interface of immiscible fluids. This photo was taken from water alternating gas (WAG) experiment on a glass micromodel.

$$p_c = p_{non-wetting\ phase} - p_{wetting\ phase} = \frac{2\gamma cos\theta}{r}, \text{ ----- } \mathbf{Eq.\ 4}$$

where, γ is the interfacial tension between two fluids, θ is the contact angle, and r is the effective radius.

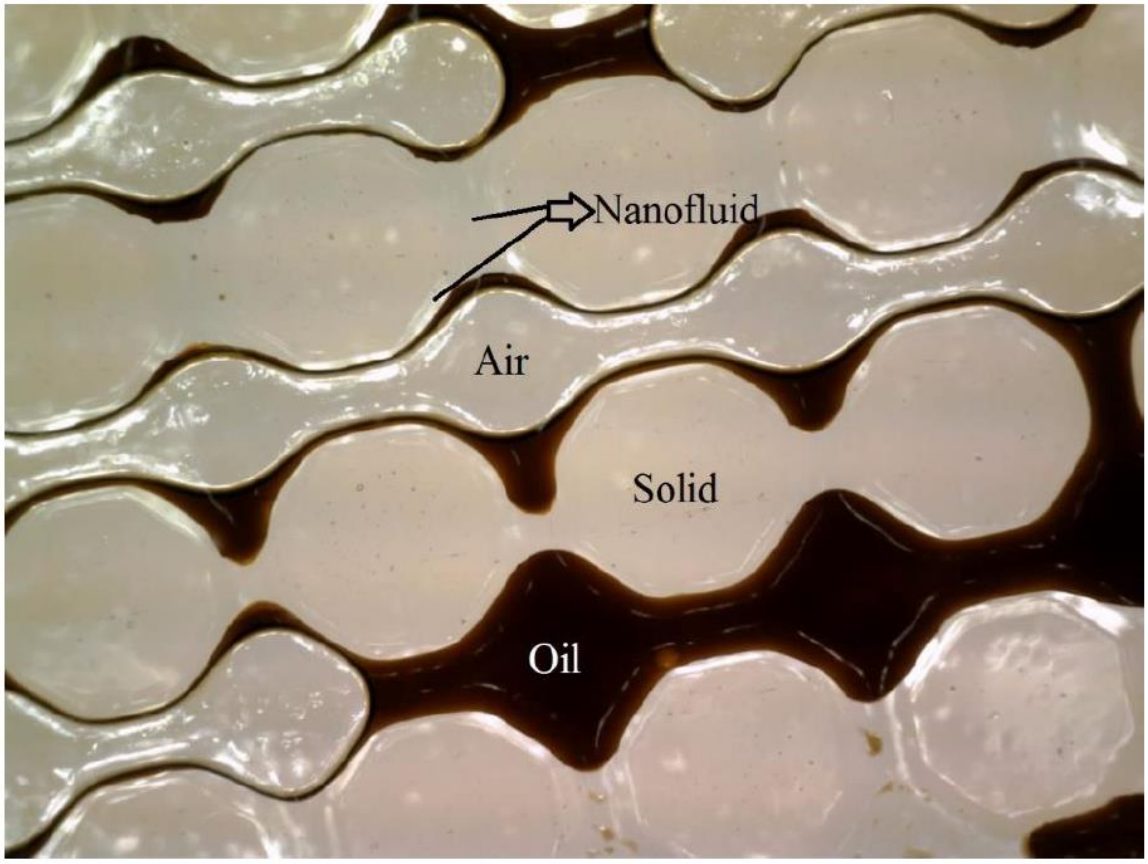

Figure 5: A photo of water alternating gas flooding using a glass micromodel (Khezrnejad et al. 2014)

Mobility ratio is another important factor in fluid flow, which is defined as the mobility of an injectant fluid (in waterflooding case, water) by the mobility of the displaced fluid (in waterflooding case, oil). It is the mobility ratio that controls the macroscopic displacing sweep efficiency of a certain flooding. The equation below depicts the general description of mobility ratio.

$$M = \frac{\frac{k_r}{\mu}(displacing\ fluid)}{\frac{k_r}{\mu}(displaced\ fluid)}, \text{ ----- } \mathbf{Eq.\ 5}$$

where, M is the mobility ratio, k_r is relative permeability, and μ is the viscosity of the fluid. When the injected fluid is miscible with the displaced fluid, the permeabilities are equal, and mobility ratio becomes the ratio of viscosities (Cheek and Menzie 1955).

Viscous fingering and gravity override are two undesirable phenomena that affect the oil recovery negatively. When the viscosity of the injected fluid is lower than the viscosity of the displaced fluid, the less viscous fluid tends to move faster. In this case, the displacing fluid front is not flat. This unstable front causes lower areal sweep efficiency. **Figure 6** and **7** show the comparison between waterflooding ($\mu_{\text{injected fluid}}$ = 1 cP) and polymer flooding ($\mu_{\text{injected fluid}}$ ~ 2.3 cP) during micromodel injection. These two photos were taken at the same time of injection. As shown in the figures, the front movement is more stable and piston like in polymer flooding.

The difference in the densities of the fluids inside the reservoir causes gravity override. For example, in case of immiscible gas injection the difference in densities of the injected fluid and displaced fluid (oil) is significant, which causes the gas to move up in the reservoir. Gravity override causes unstable movement of the front, thus lowering the areal sweep efficiency.

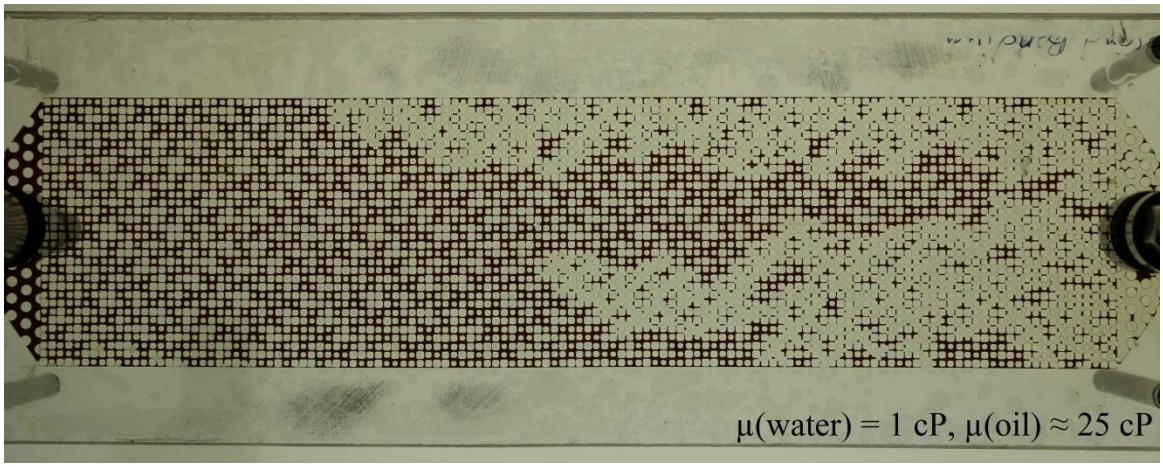

Figure 6: Micromodel waterflooding showing viscous fingering

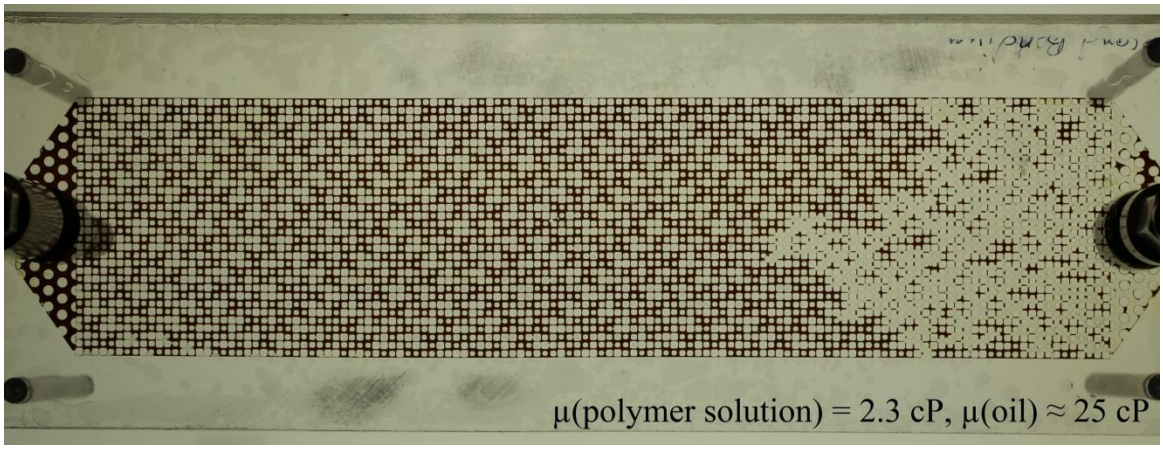

Figure 7: Micromodel polymer flooding showing a more stable flood front

The overall efficiency of any enhanced oil recovery process depends on both macroscopic and microscopic sweep efficiencies. In order to achieve optimum macroscopic sweep efficiency, viscous fingering and gravity override should be minimized. Maximum macroscopic sweep efficiency is achievable by having a stable and piston like front movement. The viscosities and densities of the fluids and the reservoir rock

heterogeneities highly affect the macroscopic sweep efficiency. On the other hand, microscopic sweep efficiency strongly depends on interfacial tension and the wettability state of the rock. For example, polymers are usually used to increase the viscosity of the injected fluid; hence, improving the mobility ratio and macroscopic sweep efficiency. On the other hand, surfactants are usually added to the injected fluid to reduce the interfacial tension, which is improving the microscopic sweep efficiency (Bagrezaie and Pourafshary 2014). Nanotechnology is a very promising area of research for EOR purposes due to the ability of nanoparticles to reduce the interfacial tension and to alter the wettability of the reservoir rock (Ayatollahi and Zerafat 2012; Maghzi et al. 2012; Khezrnejad et al. 2014; Jafari et al. 2015).

2.3.2 Porosity and Pore Size Distribution

Porosity is defined as the volume of pore space divided by the total volume of the rock. Porosity is the parameter that depicts the ability of a rock to hold a fluid. Usually, two different types of porosity are assigned to a certain reservoir rock: total porosity and effective porosity. Total porosity is the ratio of total pore space volume over the total volume of the rock. However, effective porosity is the ratio of interconnected pore volume over the total volume of the rock (Hook 2003).

Pore geometry within the reservoir rock is a key factor in fluid flow inside porous media. Pore size distribution of a rock is typically measured by microscope on a thin section of

rock, or by injecting mercury under pressure. The process for indirect measurement of pore size distribution is converting capillary pressure into pore size. For a clean sandstone rock, pore size distribution is usually bell-shaped (Netto 1993).

2.3.3 Permeability and Relative Permeability

Permeability is the capacity and ability of a porous media (reservoir rock) to transmit a fluid. According to Darcy's law, the flow rate going through a porous media strongly depends on the permeability of the porous media, viscosity of the fluid and the pressure drop. Dimensional analysis on Darcy's law shows that the unit of permeability is $[L]^2$. In oil and gas industry, the unit of permeability is called Darcy. However, millidarcy (mD) is the unit used in the field scale.

$$[K] = \frac{[\frac{L^3}{T}][\frac{M}{LT}][L]}{[L^2][\frac{M}{LT^2}]} = [L^2], \text{ ----- } \mathbf{Eq.\ 6}$$

Absolute permeability is defined as the ability of rock to transmit a certain fluid when the rock is fully saturated with this particular fluid (single phase flow). In presence of multi fluids inside porous media, the capacity and ability of the rock to transmit a particular fluid is called effective permeability of that fluid. Relative permeability of a particular fluid is the ratio of effective permeability over absolute permeability.

2.3.4 Viscosity and Mobility Ratio

Understanding of reservoir fluid properties such as viscosity, interfacial tension, and thermal conductivity is crucial in EOR processes. By manipulating the fluid properties such as viscosity, we can enhance oil recovery significantly. For example, interfacial tension reduction is a target of most of chemical flooding to increase the amount of residual oil recovery, and improve microscopic sweep efficiency. Viscosity enhancement is usually performed to improve the mobility ratio and macroscopic sweep efficiency.

Viscosity is the measure of intrinsic fluid flow resistance. Viscosity plays an important role in the fluid flow inside porous media. The two main forces controlling fluid flow in porous media are: the viscous and capillary forces. Capillary number was proposed to depict the relationship between these two forces (Chatzis and Morrow 1984; Lake 1989).

$$N_C = \frac{Viscous\ forces}{Capillary\ forces} = \frac{\nu\mu}{\gamma}, \text{ ----- } \mathbf{Eq.\ 7}$$

where μ and ν are the dynamic viscosity and characteristic velocity of the displaced fluid, and γ is the interfacial tension between the two fluids. To improve the efficiency of common waterflooding ($N_C \approx 10^{-7}$), the capillary number should increase by the means of viscosity enhancement, wettability alteration, or interfacial tension reduction (Lake 1989; Nguyen et al. 2012). The desirable capillary number for enhanced oil recovery has to be in the range 10^{-4} to 10^{-3} (Taber et al. 1997).

Polymers are commonly used for viscosity enhancement (Novy and Sloat 1975; Wang et al. 2006; Wang et al. 2010; Morelato et al. 2011; Fletcher et al. 2013). However, challenges like stability of polymers under harsh downhole reservoir conditions, cost, and required facilities hinder enhanced oil recovery by the means of polymer flooding (Ayatollahi and Zerafat 2012; Kurenkov et al. 2002). Adding nanoparticles to water increases the viscosity; hence, improves the mobility ratio (Fei et al. 2011; Zhi-Yong et al. 2013). Nanofluids are shown to be very effective in terms of wettability alteration and interfacial tension reduction (Khezrnejad et al. 2014; Maghzi et al. 2011; Roustaei et al. 2012). Moreover, Zhang et al. (2011) along with other researchers demonstrated that specially designed nanoparticles are significantly more stable than polymers and surfactants in harsh reservoir condition (Jafari et al. 2015; Yu et al. 2014). All these features make nanofluids very promising EOR technique for improving both microscopic and macroscopic sweep efficiency.

Nowadays, medium, heavy and extra heavy oil reservoirs are more crucial due to light crude production peaking and increasing global demand for oil. The high viscosity of heavy oil reserves make them technically and economically challenging to produce. Steam is the most commonly used heat carrier for thermal methods. Steam-oil reaction can be enhanced by the addition of metal nanoparticles that reduces viscosity of heavy oil (Greff and Babadagli 2011).

Iron, nickel, copper and their oxides nanoparticles have a great potential to significantly reduce the viscosity of heavy oil. Heat transfer improvement can be considered as another important feature of the metal particles which can cause a faster recovery of heavy oil/bitumen. This is not yet well understood and the effect of metal nanoparticles on heat transfer through heavy-oil and its possible impacts on viscosity reduction remain a topic of debate in literature.

Einstein's equation (Einstein 1905) relates viscosity of a dilute liquid suspension of non-interacting uniform solid (μ) and the viscosity of the dispersion medium (μ_0):

$$\mu = \mu_0(1 + 2.5\emptyset) \text{ ----- } \mathbf{Eq.\ 8}$$

where ∅ is the volume fraction of the solid sphere in the suspension. According to this equation, addition of nanoparticles will increase the viscosity of the oil. This contradiction may arise if we do not consider any interaction between the particles and the oil, which is one of the assumptions of the equation. The type and concentration of metal particles should be optimized in such a way that the effect of the reactions overcomes the increase in the viscosity due to the physical effects as given by the above equation.

Low thermal conductivity of heavy oil is an important limitation for energy efficient thermal recovery techniques (Shokrlu and Babadagli 2010). It is well known that metal nanoparticles have a high thermal conductivity, and they can be used to enhance the

thermal conductivity of fluids. There is a controversy in the literature about the use of nanoparticles as thermal enhancement agents (Zhang et al. 2007; Shokrlu and Babadagli 2010) and further research is needed to clarify this controversy.

Shah (2009) investigated the possibility of improving gas injection for heavy oil recovery by using metal nanoparticles. The research was focused on the following points: reducing the viscosity of the heavy oil using super critical CO_2 and Viscosity Reducing Injectant (VRI) saturated by nanoparticles; exploiting the thermal properties of nanoparticles for enhanced heat transfer to heavy oil; exploring the effects of poly di methyl siloxane and metal nanoparticles on density and viscosity for reducing mobility and viscous fingering phenomena; and studying EOR processes on Berea sandstone cores, saturated with Alaska North Slope heavy oil, using CO_2 and CO_2 nanofluid gas core flood experiment (Shah 2009).

Greff and Babadagli (2011) showed that nano-nickel catalysts increase the efficiency of heavy oil production by means of viscosity reduction and heat transfer enhancement. Metal nanoparticles can catalyze the breaking of carbon-sulfur bonds within asphaltenic components, and consequently lower the viscosity dramatically. Li et al. (2007) reported significant viscosity reduction by the use of nickel nanoparticles in heavy oil production process. The type and concentration of the particles are reported to be important factors affecting the degree of viscosity reduction (Shokrlu and Babadagli 2010).

2.3.5 Interfacial Tension (IFT)

Interfacial Tension (IFT) is the energy difference (between two fluids) at the molecular level in the vicinity of two immiscible fluids. IFT plays a significant role in fluid distribution and movement in the rock, wettability of the solid surface and most significantly on the oil recovery efficiency from the reservoir. IFT affects the capillary forces compared to viscous forces in oil reservoirs, if is the most important parameter affecting residual saturation of the phases during imbibition and drainage processes in porous media.

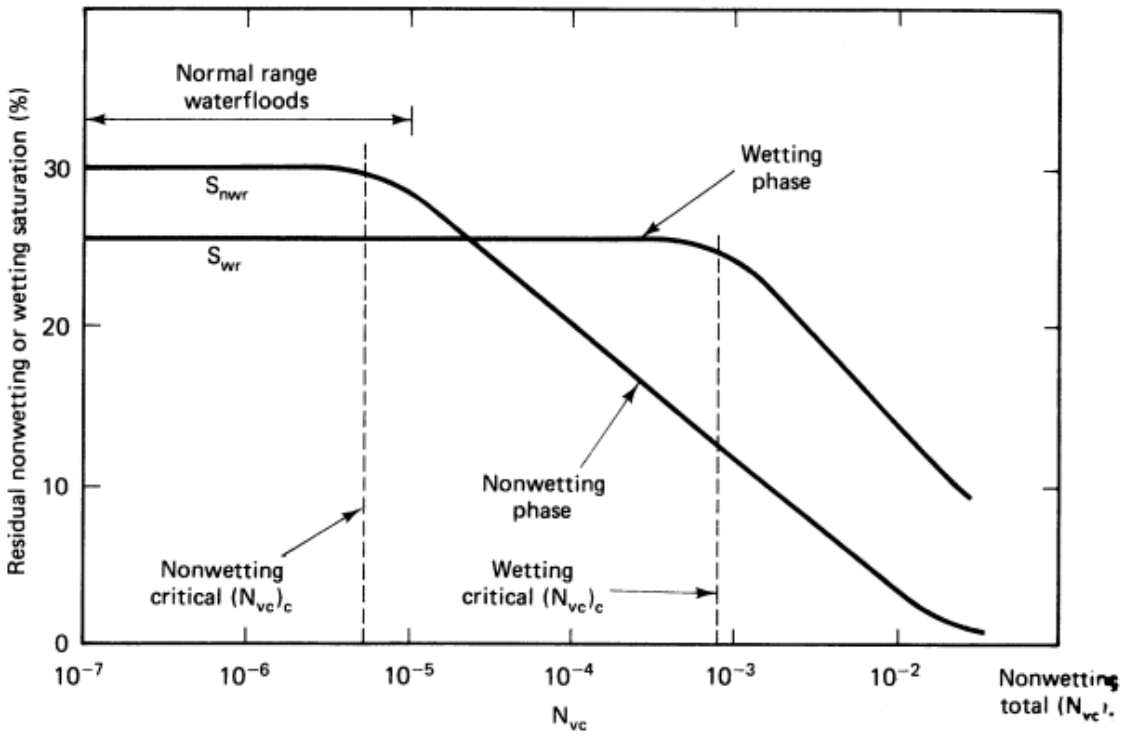

Figure 8: Capillary desaturation curve (Lake 1989)

The capillary desaturation curve, as shown in **Figure 8**, is a conventional technique used in the oil industry to relate residual saturation to capillary number.

Capillary number (N_C) is an empirical number that is used to express the relationship between the two main forces (viscous and capillary) that controls the oil displacement process. In order to increase the oil recovery, the required Nc has to be in the range of 10^{-4} to 10^{-3} (Taber et al. 1997). Injection of polymer can increase the mobility ratio and consequently increase the capillary number. Polymer injection is highly effective but expensive. Another way to increase the capillary number is by reducing the IFT or changing the wettability of the rock to a more water-wet condition. Surfactants can reduce the IFT to ultra-low value (Mohanty 2004). But surfactants may not be proper agents for harsh reservoir conditions, and the loss rate of surfactant during waterflooding is high. Also, the transportation of surfactant and polymer to the oil fields is expensive. Nanoparticles similarly achieve this task and they can be very effective agents under harsh down-hole reservoir conditions (Chakraborty et al. 2012). Nguyen et al. (2012) showed the potential of using silica nanoparticles as an EOR agent for high pressure and high temperature offshore reservoirs.

Roustaei et al. (2012) reported significant reduction in IFT by using nanofluid. As shown in **Figure 9**, interfacial tension between oil and water has a value of 26.3 (mN/m) before applying of nanofluids. However, in the presence of nanofluids, it reduces to 2.55

(mN/m) and 1.75 (mN/m). The figure shows the IFT reduction by using two different types of nanoparticles: hydrophobic and lipophilic polysilicon (HLP) and naturally wet polysilicon (NWP).

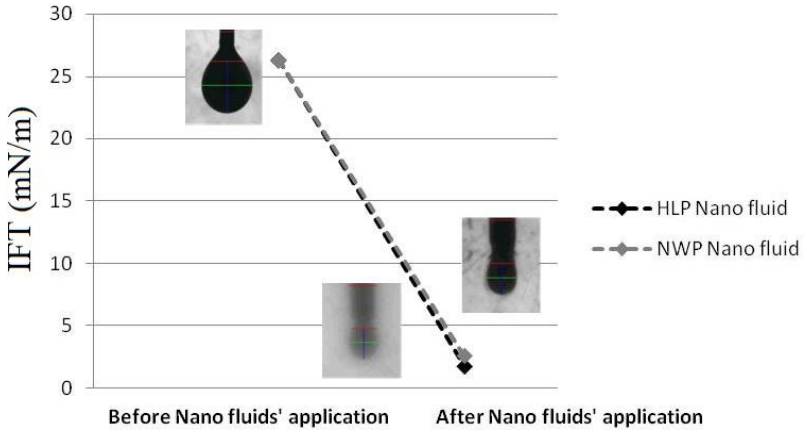

Figure 9: Oil-water interfacial tension before and after applying nanofluid (Roustaei et al. 2012)

Capillary pressure acts as a barrier for displacement of oil in the porous media in the waterflooding process. However, its negative effect can be decreased by the impact of nanoparticles on oil-water interfacial tension and rock wettability. The reduction of interfacial tension decreases the work of deformation needed for oil droplets to move through pore throat (Sharma et al. 1985; Kumar et al. 1989).

Nanoparticles, especially silica nanoparticles, have great potential to reduce the capillary pressure, which can be attributed to the specific attraction of nanoparticles to absorb onto the interface of water-oil-rock phases and alter the wettability and reduce IFT. Besides

that, in the medium of surfactants, nanoparticles can be additionally absorbed by the surfactant, and increase the efficiency of surfactant injection (Hunter et al. 2008).

2.3.6 Contact Angle and Wettability

The interaction between reservoir rock and fluid/fluid inside the reservoir is a very important factor affecting the fluid flow in porous media. Wettability is one of these factors that affect both relative permeability and capillary pressure, and consequently the oil recovery coefficient. As mentioned before, nanoparticles can be used for altering the wettability of reservoir rock. In the following section, the mechanism of wettability alteration will be explained.

Wettability is the tendency of the reservoir rock surface to preferentially contact a particular fluid in a multiphase or fluid system. Surface wettability is determined by measuring the contact angle of a liquid drop on a particular surface. When the contact angle is greater than 90°, the liquid does not wet the surface and when the contact angle is less than 90°, the liquid wets the surface (**Figure 10**).

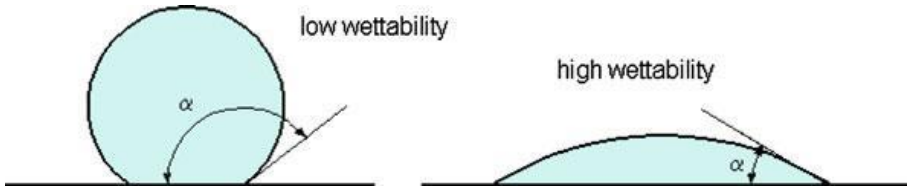

Figure 10: The contact angle of a liquid with a surface in presence of air

It is well established that the waterflood sweep efficiency in a slightly water-wet reservoir is lower than that in a strongly water-wet reservoir (Ju and Fan 2009). Also, early waterflooding experimental works show oil recovery increasing with increasing water-wetness. Conversely, there are also many examples of enhanced waterflood recovery with change from water-wet conditions to weakly water-wet and oil-wet conditions in the literature (Agbalaka et al. 2008). Therefore, the optimum wetting condition to reach maximum waterflood oil recovery remains a topic of debate. Also, lab research shows that changes in wetting states have resulted in improved gas-flood and WAG recoveries.

Rock wettability is strongly affected by:

1) The adsorption or desorption of constituents in the oil phase.
2) Reservoir rock mineralogy.
3) The film deposition and spreading ability of the oleic phase (Agbalaka et al. 2008).

The aim of injecting a nanofluid into the oil reservoir is to change the wettability of the rock from oil-wet to water-wet or the other way around. Therefore, the rock may be considered as having mixed wettability while injecting nanofluid into the reservoir (El-Amin et al. 2013). Many studies have been done investigating the effect of wettability on fluid flow in the porous media (Dixit et al. 2000; Van Dijke and Sorbie 2003; Dehghan et al. 2010; Yadali Jamaloei and Kharrat 2010; Zhao et al. 2010). However, there are only a few papers available in literature about the effect of nanoparticles on wettability alteration of a porous medium (Ju, et al. 2006; Ju and Fan 2009; Maghzi et al. 2011; Maghzi et al.

2012). Therefore, the role of nanoparticles on wettability alteration of medium surfaces has not been yet completely clarified.

Maghzi et al. (2011) revealed that silica nanoparticles increased the oil recovery during polymer flooding by 10%. Also, the results of this work showed that aging with dispersed silica nanoparticles in water, could make a strongly water-wet surface. The change of wettability of a surface by nanoparticles is possibly due to nanoparticle adsorption onto the surface. Polymer flooding EOR method can be modified by the addition of silica nanoparticles. This increases the sweep efficiency by means of the polymer. Additionally, the presence of the nanoparticles in the polymer solution can alter the surface wettability. Some researchers at the University of Kansas attempted to create a new class of polymer-type nanoparticles that can be incorporated with EOR injection fluids. With their ultra-small size and very high surface area/volume ratios, nano-polymers can penetrate into small pore throats without being trapped and the amount of expensive injection can be decreased (Matteo et al. 2012).

Figure 11 shows that the waterflooding microscopic efficiency can be improved by the use of silica nanoparticles. The results of Maghzi et al.'s work (2012) revealed that nanoparticles can alter wettability of the surface to more water-wet condition which leads to oil recovery enhancement.

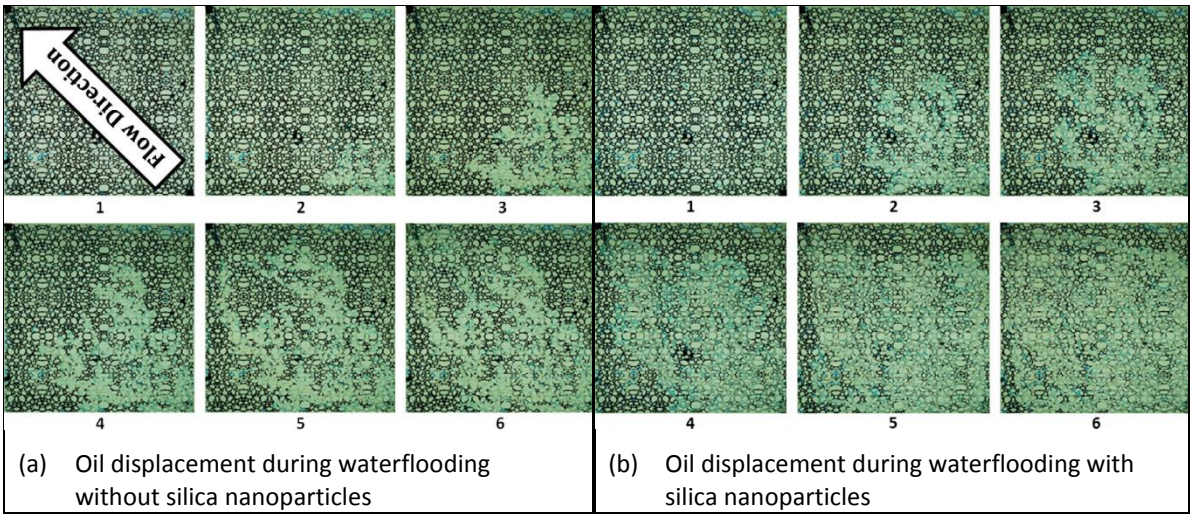

(a) Oil displacement during waterflooding without silica nanoparticles

(b) Oil displacement during waterflooding with silica nanoparticles

Figure 11: Waterflooding micromodel (Maghzi et al. 2012)

2.4 Nanotechnology Enhanced Oil Recovery Research

The desire is to inject a fluid (s) that will exploit/alter the governing parameters, previously discussed, to enhance the oil recovery. In the following sections, we will review what research has been done to understand how nanotechnology alters these main rock (porosity and permeability), fluid (density, viscosity and interfacial tension), and fluid-rock (contact angle) properties.

2.4.1 Core Flooding Studies

Core flooding is a common experiment in oil and gas research. Core flooding is approximate 1D flooding of real reservoir rock (6 – 18" long slice of a composite core) at reservoir conditions. There are many experimental investigations in literature studying the effect of nanoparticles on oil recovery using a core flooding process. Researchers in

universities and institutions allocated a lot of effort and time in the last decade to investigate the effect of using nanoparticles for enhanced oil recovery purposes, especially using core flooding experiments. **Table 1** summarizes the research that has been done to investigate the effect of Nano-EOR techniques on core flooding experiments.

Rodriguez et al. (2009) performed series of core flooding experiments to investigate the transport mechanism of nanoparticles in porous media. This experimental work indicates that transport of nanoparticles in porous media is significantly less challenging (even in low permeable areas) in comparison with other types of colloidal dispersions. Surface modified silica nanoparticles were used in the core flooding experiments to measure the nanoparticles retention in core plugs. This study shows that nanoparticle retention is not significant, which can be attributed to i) small size of nanoparticles in comparison with pore size, and ii) surface modification of nanoparticles, causing the nanoparticles to stay uniformly dispersed during core flooding. Factors such as flow rate, salinity, pH value of the injected fluid, etc. can affect the homogeneity and agglomeration state of nanoparticles in the injected fluid. Overall, in these specific set of experiments the retention of nanoparticles was found to be insignificant. However, more extensive studies are needed to make this general judgment. The authors did not consider the charge of the nanoparticles nor the interaction with salt or mineral ions.

Onyekonwu and Ogolo (2010) investigated the effect using polysilicon nanoparticles on oil recovery in core flooding experiments. Oil recovery efficiency was reported to be in the range of 50 to 80 percent while using nanoparticles. Wettability alteration and interfacial tension reduction were suggested as the two main mechanisms of improving oil recovery. Moreover, concentrations of lower than 3 grams of nanoparticles per liter of injected fluid were recommended for core flooding experiments.

Table 1: Research summary of Nano-EOR techniques in core flooding experiments

Author (year)	Nanoparticle type	Flooding type	Nanoparticle concentration	Nanoparticle size	Base fluid	Core sample	Oil properties
Rodriguez et al. (2009)	Surface treated SiO_2	Waterflooding	Up to 20 wt%	5 or 20 nm	NaCl brine	Limestone, Berea and Boise sandstone	–
Onyekonwu and Ogolo (2010)	Polysilicon nanoparticles	Waterflooding	2 – 3 g/L	10 – 60 nm	Brine 30000 ppm	Sandstone	28 °API 41 cP
Espinosa et al. (2010)	Surface treated silica	CO_2 foam flooding	0.05 – 0.50 g/L	5 nm	DI water and 4% NaCl brine	–	–
Aminzadeh et al. (2012)	Surface treated silica	Stabilized CO2 in water foam flooding	5 wt%	5 nm	2 wt% NaBr brine	Boise sandstone	–
Metin et al. (2012)	SiO_2	Waterflooding	1 – 35 wt%	5 – 25 nm	0.05 NaCl brine	Berea sandstone, Limestone	–
Hendraningrat et al. (2013)	Hydrophilic SiO_2	Waterflooding	0.05 wt%	7 – 40 nm	3 wt% NaCl brine	Berea sandstone	0.826 g/cm^3 – 5.1 cP
Li et al. (2013)	Hydrophilic SiO_2	Waterflooding	0.01, 0.05, and 0.10 wt%	7 nm	3 wt% NaCl brine	Berea sandstone	0.826 g/cm^3 – 5.1 cP
Sharma et al. (2014)	Hydrophilic SiO_2	Waterflooding	1 wt%	15	10.3 g/L brine	Berea sandstone	33.03 °API
Esfandyari Bayat et al. (2014)	Al_2O_3 – TiO_2 – SiO_2	Waterflooding	0.005 wt%	40 nm 10 – 30 nm 20 nm	DI water	Limestone	0.863 g/cm^3 – 21.7 cP

Sun et al. (2014)	Partially hydrophobic modified SiO_2	Nanoparticle stabilized foam flooding	0.5 wt%	14 nm	0.5 wt% NaCl brine	Sand pack	0.9139 g/cm^3 – 413 mPa.s
Nguyen et al. (2014)	Coated silica	Nanoparticle stabilized foam flooding	1 % (w/v)	12 nm	Ethanol – DI water	Berea sandstone	14, 24, and 37 °API
Ehtesabi et al. (2014)	TiO_2	Waterflooding	0.01 and 0.05	–	5000 ppm brine	–	0.92 g/cm^3 – 41.21 cP
Mo et al. (2014)	SiO_2	Nanoparticle stabilized CO_2 foam injection	–	17 – 20 nm	2% NaCl	Dolomite, Berea, Limestone	
Singh and Mohanty (2014)	Alumina coated silica nanoparticles	Foam injection	1 wt%	20	Ultra-pure water	Berea sandstone	30 cP
Joonaki et al. (2014)	Al_2O_3, Fe_2O_3, and SiO_2	Waterflooding	0 – 4 g/L	40, 20 – 35, 10 – 30 nm	25000 ppm Brine	Sandstone	29.56 °API – 40.38 cP
Roustaei et al. (2015)	SiO_2	Waterflooding	1 – 6 g/L	20-70	5 wt% NaCl	Carbonate rock	33 °API – 11.014 cP
Jafari et al. (2015)	SiO_2	WAG injection	700 ppm	14 nm	5000 ppm NaCl brine	Berea sandstone	0.8845 gr/cm^3 – 10.07 cP

Espinosa et al. (2010) and Aminzadeh et al. (2012) used silica nanoparticles to produce stabilized CO_2 in water foam. The results of core flooding experiments indicated that using nanoparticles stabilized CO_2 in water foam is a promising mobility control method while using CO_2 as the injected gas. Moreover, gravity override can be avoided using nanoparticles in the CO_2 injection process (Aminzadeh et al. 2012). Jafari et al. (2015) used silica nanoparticles in CO_2 to investigate the effect of nanoparticles on heavy oil recovery during water alternating CO_2 core flooding experiments. The results of this work demonstrate that the oil recovery efficiency was improved by approximately 5 percent by using silica nanoparticles.

Metin et al. (2012) studied the dynamic viscosity of nanofluids during core flooding experiments. Silica nanoparticles were used for this experimental work. The results show Newtonian behavior of nanofluids during flooding. The viscosity of the nanofluid was found to be strongly dependent on the concentration of the nanoparticles. For most cases nanoparticle retention inside the core sample was found to be insignificant. However, in sandstone core plug cases, significant amount of nanoparticle retention was observed due to clay swelling. Silica nanoparticles have been widely used as EOR agents in laboratory scale due to their unique physical and chemical properties that can deliver favorable EOR mechanisms such as IFT reduction and wettability alteration. Moreover, using silica nanoparticles is more cost effective comparing to other types of nanoparticles. In this study, the effect of interaction between factors on viscosity has been overlooked.

Hendraningrat et al. (2013) found an approximately 5 to 10 % improvement in oil recovery by waterflooding enriched with hydrophilic silica nanoparticles in core flooding experiments. This experimental work studied the effect of important factors such as particle size, rock permeability, wettability, injection flow rate, and temperature. The experimental results indicate that the highest recovery was obtained from cores with initial wettability of intermediate/oil wet after flooding with nanofluid. This can be attributed to the ability of hydrophilic silica nanoparticles in changing the wettability state of the rock from intermediate/oil wet to water wet. However, the interaction effects have not been clarified in this work. Li et al. (2013) also used hydrophilic silica nanoparticles

(7 nm) in core flooding experiments. The core sample was Berea sandstone in this experimental investigation. The results of core flooding experiments show 4 – 5 % improvement in oil recovery using silica nanoparticles in brine compared to waterflooding.

Zaid et al. (2014) investigated the effect of using aluminum oxide (Al_2O_3) and zinc oxide (ZnO) nanoparticles on oil recovery. The results of this work demonstrate that nanoparticles have the ability to create stable emulsions. Emulsions generation might be beneficial in terms of oil recovery; however, the process of separating oil from the emulsion can be challenging. The emulsions created between oil and water interface have significantly higher viscosity, providing more force to push residual oil to the outlet. Interfacial tension between oil and nanofluid was also studied in this experimental work. The results indicate significant IFT reduction using nanoparticles. Oil recovery of core flooding experiments was compared for two cases of nanofluid and surfactant flooding. They observed 117 % increase in the oil recovery of residual oil in place using nanoparticles compared to surfactant. Moreover, aluminum nanoparticles were found to be more efficient compared to zinc oxide in terms of oil recovery improvement. They suggest that this oil recovery improvement using nanoparticles might be due to emulsion generation. The emulsion that is created between the two interfaces has a higher viscosity than its original components, providing more force to push the trapped oil.

Sharma et al. (2014) also studied the effect of using nanoparticles on emulsion generation at high pressure (13.6 MPa) and four temperatures (313, 333, 353, and 363 K). This experimental work suggests that stabilized emulsion created by nanoparticles can improve the oil recovery by two mechanisms of thermal stability and stabilized flow behavior. They observed a 23 % increase in oil recovery using nanoparticles compared to waterflooding (core flooding experiments). Replicate experiments are needed to measure the experimental error and get confidence in data. Replicate core flooding experiments would add more value to this work.

The results of Esfandyari Bayat et al. (2014)'s work indicate 5 to 10 % increase in oil recovery using nanoparticles in core flooding experiments. Three different types of nanoparticles were used in this work: aluminum oxide (Al_2O_3), titanium dioxide (TiO_2), and silicon oxide (SiO_2). The core sample was intermediate wet limestone rock. Core flooding experiments were performed in different temperatures. This experimental work indicates wettability alteration of core sample to water wet condition (contact angle measurements). The limestone thin sections with initial wettability state of oil wet (θ = 90°) were aged in nanofluids for 48 hours. Then the wettability of the limestone slices were measure by analyzing the picture of the oil drop on the rock surface in the presence of nanofluid (at 26 °C). The contact angle measured for Al_2O_3, TiO_2, and SiO_2 cases were 71°, 57°, and 26° respectively. **Figure 12** and **13** shows that nanoparticles can stick to the surface of the rock and change the wettability. Moreover, considerable oil viscosity

reduction was observed after flooding with nanofluid (due to thermal conductivity enhancement of the injected fluid).

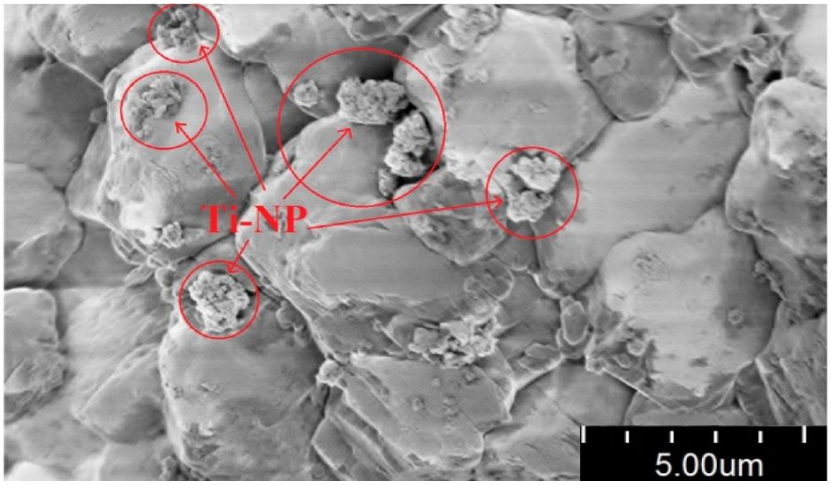

Figure 12: FESEM image from limestone grain after flooding with TiO_2 nanofluid (Esfandyari Bayat et al. 2014)

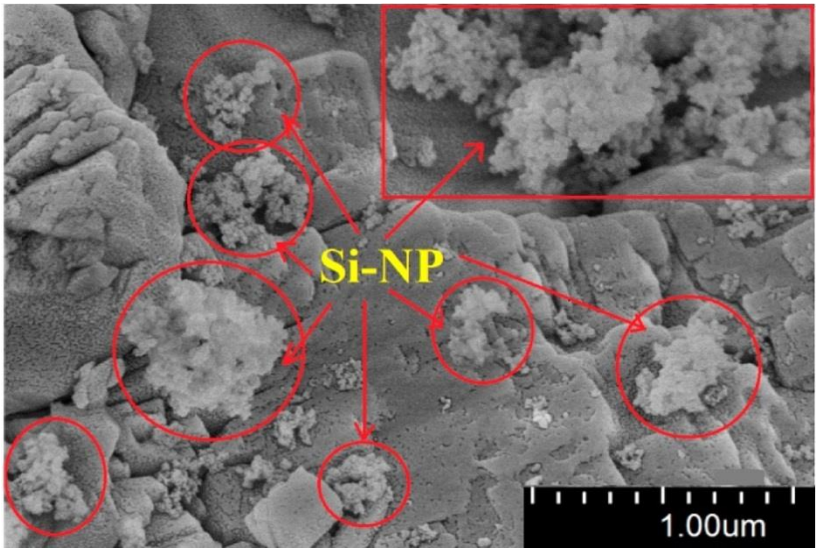

Figure 13: FESEM image from limestone grain after flooding with SiO_2 nanofluid (Esfandyari Bayat et al. 2014)

Sun et al. (2014) studied the effect of using modified hydrophobic silica nanoparticles on oil recovery and nitrogen foam stability. The results of this work indicated that nitrogen foam stabilized by silica nanoparticles has a high temperature tolerance compared to foam stabilized by surfactant. The optimum concentration of nanoparticles was found to be 1.5 wt% in brine for core flooding. The foam stability shake tests were performed in an oven to control the temperature. Nguyen et al. (2014) studied the effect of nanoparticles on CO_2 foam stability. The foam stabilized by nanoparticles was found to be stable after 10 days. Surfactant based foam was found to stay stable only for 1 day. Moreover, 15 % oil recovery improvement was observed using nanoparticle stabilized foam.

Roustaei and Bagherzadeh (2015) performed series of core flooding experiments using silica nanoparticles. The results indicate approximately 10 to 20 % increase in oil recovery using silica nanoparticles. Oil wet carbonate rock was used as the porous media in this work. The results demonstrated wettability alteration of the rock from oil wet to strongly water wet after flooding with the nanofluid. This study suggested 4 grams/liter as the optimum concentration of nanoparticles in brine for core flooding. The authors did not perform replicate experiments nor examine the role of IFT reduction using nanoparticles.

Most experimental work suggests wettability alteration from oil wet to water wet as a recovery improvement method. Other possible mechanisms of oil recovery improvement by nanoparticles are: IFT reduction and viscosity improvement. Extensive work should

investigate and quantify the role of different factors contributing to oil recovery using nanoparticles.

Many more researchers reported the oil recovery improvement using nanoparticles in core flooding experiments. Ehtesabi et al. (2014) reported 14 % oil recovery improvement by using TiO_2 nanoparticles. Mo et al. (2014) investigated the effect of using nanosilica stabilized foam on oil recovery of core flooding experiments. The results indicated that oil recovery increased approximately 30 % by using nanofluids compared to waterflooding (pressure from 1200 psi to 2600 psi, and temperature from 20 °C to 60 °C). Singh and Mohanty (2014) reported 20 percent oil recovery improvement by using hydrophilic nanoparticles stabilized foam in core flooding experiments. Joonaki and Ghanaatian (2014) also reported approximately 20 % increase oil recovery. They used SiO_2 and Al_2O_3 as nanoparticles EOR agents. Moreover, IFT reduction (from ~6 to ~2 dyne/cm) and wettability alteration (from ~130° to ~90°, examined using contact angle measurements analyzing oil droplet in the presence of nanofluid) was observed in this experimental work. Nazari Moghadam et al. (2015) studied a wide range of nanoparticles for enhanced oil recovery (ZrO_2, $CaCO_3$, TiO_2, SiO_2, MgO, Al_2O_3, CeO_2, and carbon nanotube). They reported approximately 9 percent oil recovery improvement by using nanoparticles in core flooding experiments.

2.4.2 Micromodel Studies

Physical pore network micromodels are used for the visualization of mechanisms of multiphase fluid flow in porous media. Modern image processing tools allow for easy phase saturation mapping in the transparent micromodels (Emami Meybodi et al. 2011). The experimental data from physical micromodels can be used for validation of numerical simulations (Øren and Pinczewski 1995; Laroche et al. 1999). In EOR studies, an appropriate micromodel represents a reservoir rock with specific characteristics such as the scale of the homogeneity and state of wettability. To understand multiphase flow in porous media, a large number of studies on physical micromodels have been carried out (Maghzi et al. 2012; Dong et al. 1995; Bahralolom and Orr 1988; Sayegh and Fisher 2008). Micromodels, in general, have been used to understand multiphase flow in porous media starting from Chatzis and Morrow (1981), Morrow et al. (1986), up to James et al. (2008). Further, micromodels have been used specifically for studying the effects of nanoparticles in multiphase flow (Maghzi et al. 2012; Li and Torsæter 2014; Hendraningrat and Shidong 2012), and in water alternating gas injection (Sohrabi et al. 2000, 2004; Van Dijke et al. 2003).

Figure 14 shows a glass micromodel saturated with oil. **Table 2** shows the summary of research done on the application of nanotechnology in EOR using pore network micromodels.

Table 2: Research summary of Nano-EOR techniques using micromodels

Author (year)	Nanoparticle type	Flooding type	Nanoparticle concentration	Nanoparticle size	Base Fluid	Micromodel type	Oil Properties
Maghzi et al. (2011)	SiO_2	Polymer flooding	1000 ppm	14 nm	DI water	Glass	1400 (kg/m^3), 85 cP
Maghzi et al. (2012)	Hydrophilic SiO_2	Water flooding	0.1 to 5 wt%	14 nm	200000 ppm brine	Glass	19 °API 870 mPas
Hendraningrat and Shidong (2012)	Hydrophilic SiO_2	Water flooding	0.1 to 1.0 wt%	15 to 50 nm	3 wt% NaCl brine	Glass	0.806 (gr/cm^3), 2 cP
Maghzi et al. (2013)	SiO_2	Polymer flooding	1000 ppm	14 nm	DI water	Glass	840 (kg/m^3), 85 cP
Li et al. (2013)	Hydrophilic SiO_2	Water flooding	0.01, 0.05, and 0.10 wt%	7 nm	3 wt% NaCl brine	Glass micromodel	0.826 (gr/cm^3), 5.1 cP
Maghzi et al. (2014)	Hydrophilic SiO_2	Polymer flooding	0.1 to 5 wt%	14 nm	1400 to 84000 ppm brine	Glass (laser etching)	25 °API, 1000 cP
Sun et al. (2014)	Partially hydrophobic SiO_2	Foam Flooding	0.0 to 2.0 wt%	14 nm	0.5 wt% NaCl brine	Glass etched micromodel	0.913 (gr/cm_3), 413 mPas
Nguyen et al. (2014)	Silica coated nanoparticles	Nano stabilized CO_2 foam flooding	1% (w/v)	7 nm	DI water	Glass	Light (37 °API), Medium (24 °API), and Heavy (14 °API)
Khezrnejad et al. (2014)	SiO_2 and Al_2O_3	Water alternating gas injection	0 to 1000 ppm	5 to 100 nm	36000 ppm brine	Glass	~0.85 (gr/cm_3), ~25 cP
Hamedi-Shokrlu and Babadagli (2014)	Nickel nanoparticles	Water flooding	0.05 wt%	20 – 100 nm	DI water	Glass	Kerosene
Gharibshahi et al. (2015)	SiO_2	Water flooding	4 wt%	14 nm	Water	Glass	933 (kg/m_3), 870 mPas
Mohebbifar et al. (2015)	SiO_2 and TiO_2	Water flooding	0 to 3000 ppm	7 and 21±5 nm	Synthetic brine	Glass	21 °API, 200 cP
Mohajeri et al. (2015)	ZrO_2 nanoparticles	Water flooding	100 ppm	14 nm	–	Glass	21.2 °API, 130.4 cP

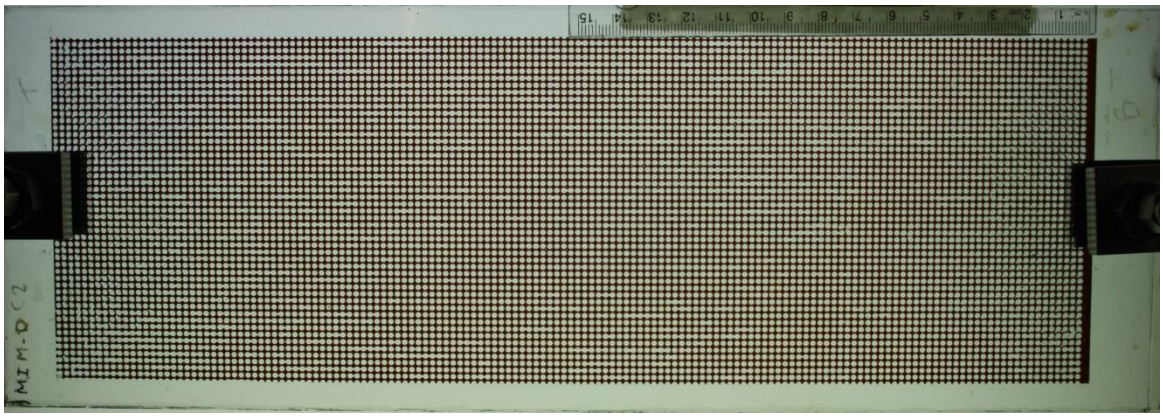

Figure 14: Glass micromodel saturated with oil

Maghzi et al. (2011, 2013, and 2014) used silica nanoparticle in a polymer solution, and studied the effect of nanoparticles on oil recovery in micromodel injection. The results of this work demonstrated that nanoparticles have the ability of changing the wettability of micromodel to strong water wet condition. Oil recovery was improved by 10 % using silica nanoparticles. Maghzi et al. (2012)'s work revealed that oil recovery increases by increasing the nanoparticle concentration in deionized (DI) water during micromodel flooding. For concentrations of 0.1 and 3.0 wt%, 8.7 and 26 % oil recovery improvement was reported. Moreover, the concentration of 3 wt% was reported as the optimum concentration of nanoparticles in DI water. After flooding with nanofluid, strong water-wetness was observed in the micromodel. It should be noted that glass is generally water wet. However, in this work the glass micromodel was saturated with heavy oil, which can change the wettability of the micromodel. The possible interaction between polymer and nanoparticles could add more value to this study.

Hendraningrat and Shidong (2012) used hydrophilic nanoparticles in brine during micromodel injection to study IFT reduction, nanoparticles retention in the porous media and permeability impairment. Permeability reduction was reported due to pore blockage by nanoparticles. This pore blockage is due to nanoparticles agglomeration in the injected fluid, which can be avoided by uniformly dispersing nanoparticles.

Li et al. (2013) used hydrophilic silica nanoparticles (7 nm) for improving brine flooding during water-wet glass micromodel injection. Interfacial tension and contact angle were monitored at different concentrations of nanoparticles. The results of this work revealed stable emulsion generation using nanoparticles. **Figure 15** shows a photo taken form the glass micromodel during the flooding, showing the stable oil in water emulsion. Studying the effect of concentration on emulsion generation could be very beneficial to this experimental work.

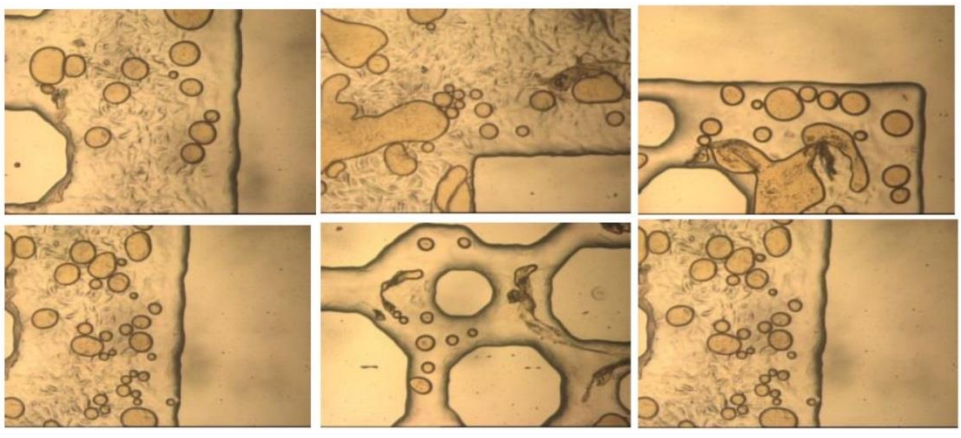

Figure 15: Emulsion generation using nanoparticles in the micromodel experiments (Li et al. 2013)

Sun et al. (2014) studied the effect of using partially hydrophilic modified SiO_2 nanoparticles on nitrogen foam micromodel injection. Nguyen et al. (2014) reported 15 percent oil recovery improvement by using nanoparticle-stabilized CO_2 foam during micromodel injection experiments. By using nanoparticle in the foam, the size of oil in water emulsion was decreased significantly. **Figure 16** shows a qualitative and quantitative description of how nanoparticle-stabilized foam injection increases both microscopic and macroscopic sweep efficiencies. As shown in the figure, for all three cases of light, medium and heavy oil, the area which the foam is in contact with the oil is larger compare to waterflood. Also, it can be clearly seen that the effect of viscous fingering is dampened by using nanoparticle stabilized foam (mobility control).

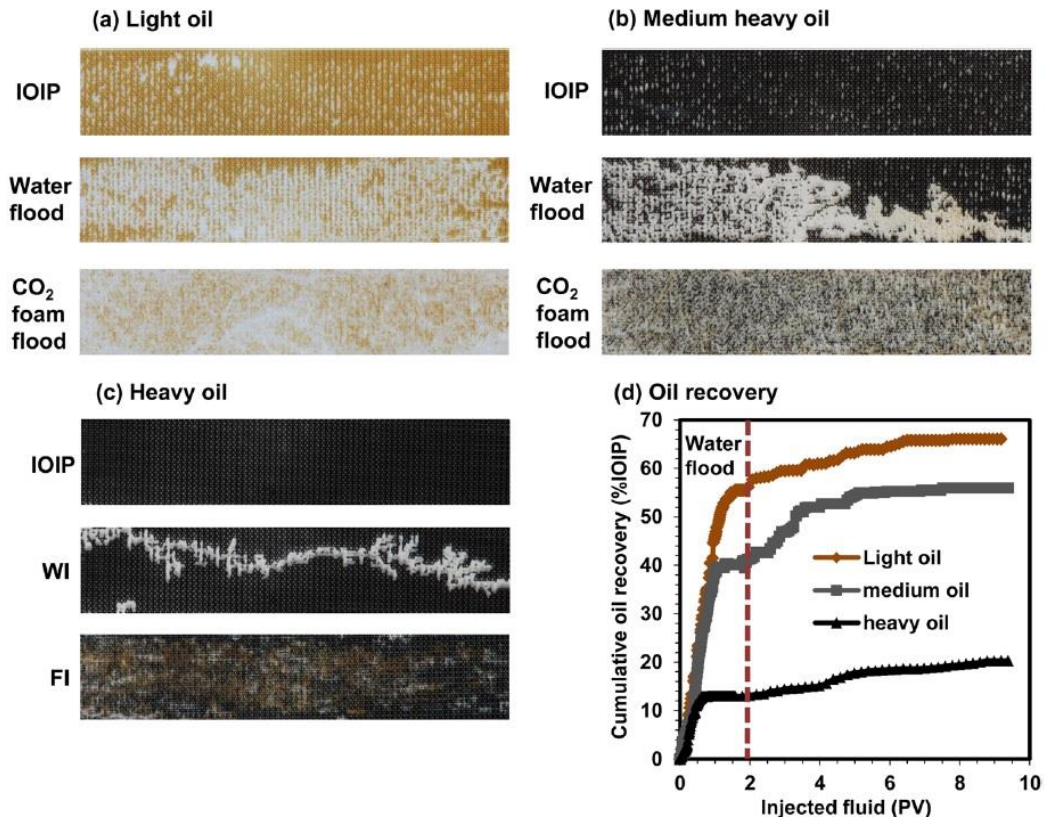

Figure 16: Using nanoparticles-stabilized foam for enhancing oil recovery of waterflooding in micromodel injection experiments (Nguyen et al. 2014)

Khezrnejad et al. (2014) used two different types of nanoparticles (SiO_2 and Al_2O_3) to study the effect of nanoparticles on oil recovery efficiency in glass micromodel injection. Significant IFT reduction was reported using nanoparticles in brine. In this work, the effect of different factors such as WAG ratio and nanoparticle concentration on oil recovery was studied. The results of this experimental study revealed that oil recovery can be improved by 15 to 20 percent using nanoparticles. Higher oil recovery was obtained using silica nanoparticles over alumina. Silica nanoparticles shown to be more efficient in terms of oil recovery compared to alumina nanoparticles. This might be explained by the

higher IFT reduction using SiO_2. Moreover emulsion generation was observed when SiO_2 nanoparticles were used.

Hamedi-Shokrlu and Babadagli (2014) studied the stabilization and transportation of nanonickel particles in micromodel injection process. Nickel nanoparticles were used due to their high thermal conductivity, which make them perfect to be used as catalyst. Gharibshahi et al. (2015) compared the results of experimental micromodel injection with CFD simulation. Silica nanofluid was used as injected fluid. The effect of pore heterogeneity and connectivity, tortuosity, and pore shape on EOR, breakthrough time and fluid trapping was studied. The results of this work indicate that nanoparticles can be highly efficient in terms of viscous fingering reduction.

Mohebbifar et al. (2015) reported 78 % recovery by using nanoparticles in micromodel flooding experiments. Wettability alteration (from oil wet to water wet), thinning oil film, IFT reduction, and emulsion generation were reported in this experimental work. The results demonstrated that nanoparticle can be highly efficient for improving the microscopic sweep efficiency. Wettability alteration from oil wet to water wet is not necessarily a recovery improvement mechanism. The reason for oil recovery improvement could be wettability alteration along with other factors. Therefore, it is needed to study the effect of each factor individually and along with other factors. Mohajeri et al. (2015) used ZrO_2 nanoparticles to improve the efficiency of surfactant

flooding process during micromodel experiments. The results show approximately 40 percent oil recovery improvement by using nanofluid over water.

2.4.3 Simulation and Mathematical Modeling Studies

There are only few studies dealing with mathematical modeling of nanoparticle transport in porous media (Ju et al. 2006; Ju and Fan 2009; El-amin et al. 2013). Ju et al. (2006), and Ju and Fan (2009) developed a mathematical model of nanoparticle transport in porous media. A simulator was developed to study the effect of migration and adsorption of nanoparticles to the pore walls and wettability alteration in a one-dimensional two-phase mathematical model.

Distribution of particle concentration, the reduction in porosity and absolute permeability, nanoparticles volume retention on the pore walls and in pore throats along a dimensionless distance, and oil production performance was also studied. The main assumptions of this mathematical model are:

1. One-dimensional flow
2. Isothermal condition
3. Incompressible rock and fluids
4. Homogeneous nanofluid
5. Darcy flow (gravity is neglected)
6. Constant viscosity and density of the fluids

7. Newtonian fluids
8. No chemical reaction

Then, continuity equations were solved to describe the flow of nanofluid inside a porous medium. Brownian diffusion effect was considered since nanoparticles were only existed in water phase (nano scale).

The results of their work revealed:

- Water phase permeability of specific type of sandstone increased from 1.6 to 2.1 times of its original value.
- There was a decrease in absolute permeability because of nanoparticle adsorption on the pore surfaces and nanoparticle capture at the pore throats.
- 1.5-2.0 PV of injection with total concentration 5 vol. % silica nanoparticles was recommended to enhance water injection capability for the low permeability oil fields.
- Since nanoparticles have the ability to increase the tendency of strong water-wettness by adsorption on porous surfaces, it can be used to improve oil recovery in the oil fields flooded by water. As mentioned before the wettability state that leads to higher oil recovery is a subject of debate in literature. **Figure 17** shows how oil recovery has been improved from 52.2% to 69.8% after injection of 2.0 PV nanofluids. The recovery improved by 17.6%.

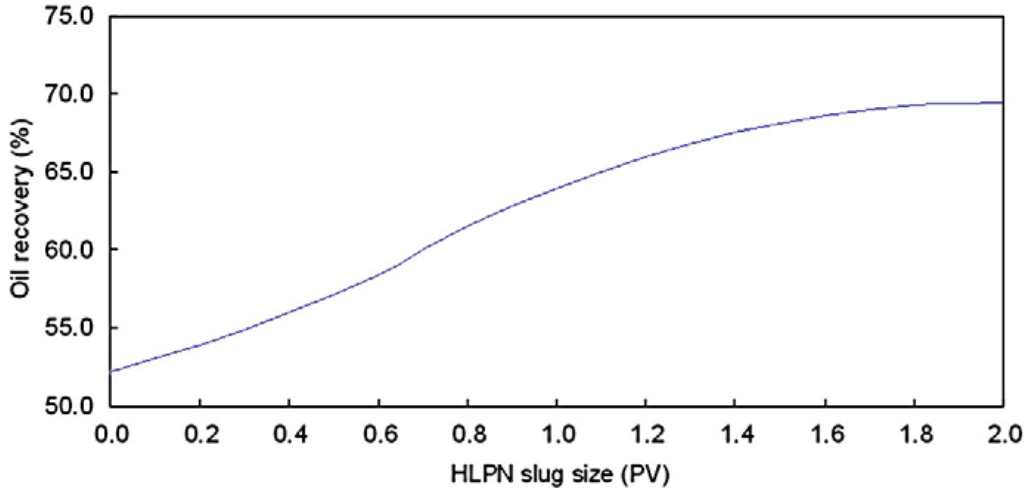

Figure 17: The relation between oil recovery and injection volume of nanoparticles (Ju and Fan 2009)

Liu and Civan (1993) developed a mathematical model for fine migration in porous media. In their work, the releases of in-situ fines, retention of external particles and in-situ fines, and inter phase transfer of particles are represented by empirical rate expressions. Pore plugging and porosity variation cause a reduction in permeability. Therefore, the effects of relative permeabilities, capillary pressure and wettability of fine particles and pore surfaces on two-phase flow are considered in this model. The results of this work can be useful for predicting formation damage during fines migration and, more importantly, for developing mathematical models of nanoparticle transport in porous media. Simulation studies carried out by the model indicate that formation damage due to particle invasion is strongly influenced by the particle wettability (Liu and Civan 1993).

El-Amin et al. (2013) mathematically modeled and numerically simulated imbibition of nanoparticles-water suspension into a water-oil system in porous media. Negative

capillary pressure and various types of correlations were considered in this model. Buoyancy and capillary forces, and Brownian diffusion were considered in solving mass conservation and constitutive equations. The results of this work indicate considerable changes in the rock and fluid properties such as: absolute and relative permeability, porosity, capillary pressure and surface wettability.

In order to improve the CO_2 sequestration process, nanoparticles can be added to the CO_2 phase to increase the density contrast between the CO_2 rich brine and the underlying resident brine and, consequently, decrease onset time of instability and increase convective mixing. El-Amin et al. (2013) developed mathematical models to describe nanoparticles transport carried by injected CO_2 in porous media. Buoyancy and capillary forces as well as Brownian diffusion were considered in this model and numerical simulators were used to simulate the nanoparticle transport in CO_2 storage.

Gharibshahi et al. (2015) used computational fluid dynamics (CFD) to study the effects of pore morphology and pore size distribution in a 2D micromodel on oil recovery factor. To this end, the momentum and mass transfer equation were solved using Fluent software. Parameters such as heterogeneity of pores, connectivity of pore with and without throat lines, tortuosity, and pore shape were studied. Also the simulation results were compared to the experimental results to confirm that the model is suitable for a real case of flooding. Gambit (Fluent Inc.) software was used to create micromodel patterns. Moreover,

MATLAB and C++ programming was performed to generate the random distribution of model. The results of heterogeneous pore network modeling show that oil recovery obtained from the model has a good agreement with the experimental results. Moreover, models with random distribution of pores are shown to have a good agreement with the experimental results. The least relative error of approximately 5 percent was captured between the model and the experimental results.

3. Materials and Methods

In this experimental study, statistical design of experiments was combined with experimental methods to optimize the factors involved in EOR process. Both statistical and experimental methods used in this study will be discussed in this chapter. Moreover, the materials used for the experiments will be specified.

3.1 Research Objectives

Nanotechnology has shown a great potential in EOR processes. However, there are some uncertainties regarding the application of nanotechnology in EOR. In this experimental study, we tried to optimize the factors involving in nanotechnology EOR techniques. Factors like type of nanoparticle, concentration of nanoparticles in the injected fluid, WAG ratio, interfacial tension, viscosity, pressure, and temperature were studied. Micromodel studies were conducted under waterflooding and water alternating gas injection schemes. Detailed measurements of viscosity and interfacial tension were conducted to understand the role of interfacial tension reduction versus mobility ratio in improving oil recovery using nanoparticle enhanced water. **Table 3** shows the research summary of this study.

In the water alternating gas micromodel experiments, the effect of WAG ratio, different types of nanoparticles, and concentration of nanoparticles on oil recovery were studied.

Air was used as the gas phase in the experiments. Nanoparticles were added to brine to enhance the oil recovery through two possible mechanisms: mobility control (viscosity enhancement of water), and interfacial tension reduction (microscopic efficiency improvement).

Table 3: Experimental research summary

Type of micromodel flooding	Type of nanoparticle	Base Fluid	Fluid characterization experiments	Type of Micromodel	Studied Factors
Water alternating gas injection (12 runs)	SiO_2 (powder) and Al_2O_3 (powder)	36000 ppm brine	IFT (24 runs)	Glass	Nano type, concentration, and WAG ratio (WAG experiments) – Pressure, temperature, concentration, and nanotype (IFT)
Waterflooding (8 runs)	SiO_2 (dispersed in water) and Al_2O_3 (dispersed in water)	DI water	IFT (4 runs) and viscosity (24 runs)	PMMA	Nanotype, viscosity, and IFT (waterflooding experiments) – Pressure, temperature, concentration, and nanotype (viscosity)

In order to better understand the mechanism of oil recovery improvement by using nanoparticles, viscosity and interfacial tension measurements were performed. The effect

of pressure, temperature, two different types of nanoparticles, and nanoparticles concentration was investigated.

The research question is whether oil recovery using nanoparticle enhanced water is due to a more favorable mobility ratio (increased water phase viscosity) or is it due to the effect of the enhanced surface chemistry? In this study, we examine the role of increased viscosity of the water phase on oil recovery using nanoparticle enhanced water and polymer enhanced water with similar viscosity. First, the nanoparticle enhanced water is characterized. A statistical design of experiments technique, Response Surface Methodology, is used to investigate the effect of the type of nanoparticles (silicon oxide and aluminum oxide nanoparticles), concentration of the nanoparticles, pressure, and temperature on viscosity. The effect of interactions between the factors on viscosity is also studied. Second, the viscosity measurement results are used to plan micromodel and coreflooding laboratory scale enhanced oil recovery experiments at low pressure and temperature conditions. The results can be used to help elucidate the role of increasing viscosity versus surface chemistry on oil recovery.

3.2 Design of Experiments

3.2.1 Response Surface Methodology (RSM)

Response surface methodology (RSM) is a mathematical and statistical tool employed to investigate a functional relationship between a response of interest and a set of related

variables. Response surface methodology gives us a strong tool to fit the best model including significant factors and their interactions (Anderson and Whitcomb 2005). Instead of changing one factor at a time, which is the common design used by most experimental researchers, RSM can be employed to see the effect of interactions as well as the effect of individual factors. Further, any nonlinearity can be detected and applied to the model. Response surface methodology is a statistical method for designing an experiment. Therefore, the user should be aware that even the best statistical model is an approximation to reality.

3.2.2 Analysis of Variance (ANOVA)

The term "analysis of variance (ANOVA)" was first coined in 1918 by Sir R.A. Fisher. Generally speaking, ANOVA is a particular form of statistical hypothesis testing which is often used in the analysis of experimental data. A statistical hypothesis test is a method of making decisions using data. Variance analysis (ANOVA) is a statistical tool capable of modeling the relationship between the variables and the response. Furthermore, the interactions between the factors and nonlinearity can also be analyzed. ANOVA is a technique that is used to measure the effect of each factor and their interaction on the response by computing the variance (by dividing the sum of squared error over degrees of freedom). ANOVA provides a method to accurately investigate the regression model by analyzing the null hypothesis.

Variance analysis is the statistical technique used in RSM to model the response according to individual factors and interactions. ANOVA is a technique that is used to measure the effect of each factor and their interaction on the response by computing the variance by dividing the sum of squared error over degrees of freedom. Because of this feature and other characteristics, ANOVA provides a method to accurately investigate the regression model.

3.2.3 Optimal Design of WAG Injection

Instead of changing one factor at a time, Response Surface Methodology (RSM) was employed to investigate the individual effect of each factor: concentration, nanoparticle type, WAG ratio, and their interactions on oil recovery (response). Response surface methodology is a tool to assist in modeling a response based on significant factors and interactions. In this study, Design Expert Software® was used for the design of experiments. **Table 4** shows the dependent variables.

Table 4: Factors and levels of experimental design

Factor	Low level	High Level
C: Concentration	0 (wt%)	0.1(wt%)
N: Nanoparticle Type	SiO_2	Al_2O_3
W: WAG ratio	1:1	1:2

Statistical design of experiments (optimal design) was used to design the number of experiments required using specific values when investigating three factors: nanoparticle concentration, type of nanoparticles used, and WAG ratio on the oil recovery. Optimal

design allows us to best possible model for the response corresponding to available variables with the minimum number of runs.

Table 5: Optimal design of WAG micromodel experiments

Run	Type	WAG Ratio	Nanoparticle Concentration (wt%)
1	SiO_2	1:2	0.02
2	Al_2O_3	1:2	0.08
3	Al_2O_3	1:1	0.02
4	Al_2O_3	1:1	0.10
5	SiO_2	1:2	0.02
6	SiO_2	1:2	0.10
7	Brine	1:1	0.00
8	Al_2O_3	1:2	0.08
9	Brine	1:2	0.00
10	SiO_2	1:1	0.04
11	Al_2O_3	1:1	0.06
12	SiO_2	1:1	0.08

Table 5 shows the design of the number of micromodel experiments based on optimal design. The micromodel experiments were carried out by run # to avoid bias. Concentration is a quantitative factor, and both the type of nanoparticles and WAG ratio are qualitative factors. The optimal design suggests different values for concentration to postulate the best model.

3.2.4 Design of Waterflooding Experiments

In this set of experiments, the efficiency of EOR using two different types of nanoparticles (alumina and silica) was compared to DI water/polymer flooding. Nanoparticles can improve both macroscopic (viscosity enhancement) and microscopic

(interfacial tension reduction) sweep efficiencies. By comparing nanofluid injection with polymer injection (viscosity enhancement), we might be able to see how nanoparticles can enhance oil recovery (viscosity, surface chemistry, or both?). Different scenarios of injection for waterflooding micromodel experiments are defined in **Table 6**. Moreover, the effect of injection flow rate was also studied. The * sign indicates the replicate runs.

Table 6: Design of waterflooding micromodel experiments

Run #	Injected Fluid	Viscosity (cP)	Injection flow rate (ml/min)
1	DI water	1.00	0.010
*2	Polymer (10 ppm)	1.75	0.010
3	Polymer (10 ppm)	1.75	0.005
*4	Polymer (10 ppm)	1.75	0.010
5	Polymer (20 ppm)	2.30	0.010
6	Polymer (20 ppm)	2.30	0.005
7	SiO_2 nanofluid (5 wt%)	1.06	0.010
8	Al_2O_3 nanofluid (5 wt%)	1.75	0.010

3.2.5 Optimal Design of IFT Measurements

It has been shown in the literature that nanoparticles are capable of reducing interfacial tension between the oil and water. However, most researchers have measured the IFT in a fixed condition (pressure and temperature). In order to understand the behavior of IFT with respect to different factors and their interaction, we need to change all the factors at the same time instead of changing one factor at a time, which only gives us an estimate of IFT in a certain condition. In this study, response surface methodology was employed to investigate the individual effect of each factor: concentration of nanoparticles in the brine

phase (C), pressure (P), temperature (T), nanoparticle type (N), and their interactions on the response (IFT).

In this study, Design Expert Software® was used for the design of experiments. **Table 7** shows the dependent variables.

Table 7: Variables in the IFT experiments and their corresponding levels

Factor	Units	Low level	High Level
C: Concentration	ppm	0	1000
P: Pressure	psi	20	8000
T: Temperature	°C	20	80
N: Nanoparticle Type		SiO_2 (-1)	Al_2O_3 (+1)

As it was done with the micromodel experiments, optimal design was used. Optimal design allows us to fit the best possible model for the response corresponding to available variables with minimum number of runs. **Table 8** shows the design of 24 IFT experiments based on optimal design. Concentration, pressure, and temperature are quantitative factors, and type of nanoparticles is qualitative factor. The optimal design suggests a different value for the quantitative factors to postulate the best model. The * sign in the table indicates the replicate runs.

Table 8: Optimal design of IFT measurements

Run	Type	Concentration (ppm)	Pressure (psia)	Temperature (°C)
1	SiO_2	735	6244	51.2
2	Al_2O_3	580	20	30.5
3	Al_2O_3	1000	20	80.0
*4	SiO_2	412	8000	80.0
5	Al_2O_3	1000	3092	20.0
6	Al_2O_3	0	20	20.0
7	SiO_2	0	20	80.0
*8	Al_2O_3	500	4010	50.0
9	Al_2O_3	635	8000	27.8
10	SiO_2	0	3850	20.0
*11	Al_2O_3	500	4010	50.0
12	Al_2O_3	0	4968	80.0
*13	Al_2O_3	500	4010	50.0
14	Al_2O_3	0	8000	20.0
15	SiO_2	1000	3901	80.0
16	SiO_2	0	3850	20.0
17	Al_2O_3	1000	8000	80.0
*18	SiO_2	412	8000	80.0
19	SiO_2	1000	8000	20.0
*20	SiO_2	0	8000	54.6
21	Al_2O_3	47	690	57.9
22	SiO_2	1000	20	20.0
23	SiO_2	625	20	59.9
*24	SiO_2	0	8000	54.6

3.2.6 Optimal Design of Viscosity Measurements

As discussed in the introduction, nanoparticles are capable of increasing the viscosity of water. However, most of these viscosity measurements were conducted under fixed pressure and temperature. In order to understand the behavior of viscosity with respect to different factors and their interactions, we need to change all the factors at the same time.

Response surface methodology (optimal design) was employed to investigate the effect of each factor: concentration of nanoparticles, pressure, temperature, nanoparticle type, and their interaction on the response (viscosity).

Table 9: Optimal design of viscosity measurements

Run	Nanoparticle type	Concentration (ppm)	Pressure (psia)	Temperature (°C)
*1	SiO_2	5000	8000	80.0
*2	Al_2O_3	5000	3012	80.0
*3	Al_2O_3	5000	8000	20.0
*4	Al_2O_3	0	8000	80.0
5	Al_2O_3	2500	4010	50.1
6	SiO_2	0	4110	80.0
*7	SiO_2	2900	4728	69.8
8	SiO_2	0	4110	80.0
9	SiO_2	650	8000	57.2
10	Al_2O_3	2500	4010	50.1
11	Al_2O_3	0	20	80.0
*12	SiO_2	0	20	20.0
13	Al_2O_3	150	778	42.5
14	SiO_2	5000	4110	20.0
15	SiO_2	0	8000	20.0
16	SiO_2	5000	4110	20.0
17	Al_2O_3	2500	4010	50.1
18	SiO_2	5000	20	54.5
*19	Al_2O_3	3125	8000	73.1
20	Al_2O_3	0	4848	20.0
21	Al_2O_3	5000	20	20.0
22	SiO_2	2875	20	80.0
23	SiO_2	5000	20	54.5
24	SiO_2	3115	20	24.4

In this study, Design Expert Software® was used for the design of experiments. **Table 9** shows the design of 24 viscosity measurements based on optimal design. Concentration,

pressure, and temperature are quantitative factors varying from 0 to 5000 ppm, 20 to 8000 psia, and 20 to 80 °C respectively. To avoid any bias, experiments were performed randomly.

The VISCOlab PVT viscometer (manufactured by Cambridge Viscosity) was used for measuring the viscosity. A billet for the range of 0.25 to 5 cP was used for the experiments. After loading the pump, the system was set to the desired temperature and pressure. Before measuring any data, the system was bled through the relief valves to rid the system of any air. Then, viscosity was measured under stable pressure and temperature conditions. After running each test, the system was flushed with an appropriate solvent to clean all the lines and fittings, and then vacuumed. Bias was avoided by performing the experiments in random order.

3.3 Experimental Investigations

Two different types of micromodel EOR study were performed. First, water alternating gas (WAG) micromodel experiments were conducted to investigate the effect of using nanoparticles on ultimate oil recovery. The effect of nanoparticle concentration and WAG ratio was also studied. Second, a series of waterflooding experiments were performed in a different micromodel to better understand the mechanism of enhancing oil recovery by using nanoparticles (viscosity, surface chemistry or both?). Along with the micromodel experiments, fluid properties (viscosity and IFT) were also characterized.

3.3.1 Fluids Preparation

In the WAG micromodel experiments, the synthetic brine used in the experiments was formulated with 36330 ppm total dissolved salts in distilled water. **Table 10** shows the brine composition based on individual salt concentrations. The brine composition was designed to mimic the sea water composition offshore Newfoundland.

Table 10: Salt concentrations used in the synthetic brine

Salt	Concentration (g/ml)	Concentration (ppm)
NaCl	0.02850	28532
CaCl	0.00190	1902
KI	0.00095	951
Na_2SO_4	0.00095	951
$NaHCO_3$	0.00019	190
$MgSO_4$	0.00380	3804
Total	0.03629	36330

It should be mentioned that DI water was used as the reference fluid in the waterflooding micromodel experiments.

In the WAG micromodel experiments, two different types of nanoparticles (powder) were used to enhance the physical chemical properties of the brine. The properties of dispersed nanoparticles (manufactured by Sky Spring Nanomaterials Inc.) are tabulated in **Table 11**.

Table 11: Properties of nanoparticles

Type	Description	Average Particle Size (nm)	Purity (%)	Specific Surface Area (m^2/g)
Al_2O_3	White nanopowder	5	99.9	300
SiO_2	White nanopowder	5-15	99.8	100-140

Triton X-100 surfactant was added to the synthetic brine during the preparation of the nanofluid aqueous phase to prevent the flocculation of nanoparticles after being dispersed. It was observed that in order to disperse 1000 ppm nanoparticles, 200 ppm of surfactant was required. Once combined, an ultrasonic probe was used to completely disperse the nanoparticles added to this solution at a frequency of 20 KHz for 30 minutes. To confirm the homogeneity and the stability of the prepared solution, the solution was placed for 48 hours in a closed transparent bottle away from destabilizing factors such as light and heat. Upon visual inspection, neither precipitation nor other visible alterations were detected.

In the waterflooding micromodel experiments, two different types of nanoparticles (dispersed in water) were used to enhance the physical and chemical properties of DI water (viscosity enhancement and interfacial tension reduction). The properties of the dispersed nanoparticles (manufactured by US Research Nanomaterials, Inc.) are tabulated in **Table 12**. It should be noted that the silica (SiO_2) nanoparticles used in the experiments were amorphous, and the alumina (Al_2O_3) nanoparticles were gamma type. In order to completely disperse the nanoparticles in the DI water, an ultrasonic device was used. The

sonication process was performed on the nanofluid for 30 minutes. To confirm the homogeneity and stability of the prepared solution, the solution was placed in a closed transparent bottle away from degrading factors such as light and heat for two weeks. Visual inspection showed neither precipitation nor other visible alterations indicating a stable nanoparticle suspension. The polymer used in these set of experiments was Flopaam 3430S (manufactured by SNF Floerger).

Table 12: Properties nanoparticles dispersed in water

Type	Description	Average Particle Size (nm)	Purity (%)	pH value
Al_2O_3	Gamma	10	99.9	2-5
SiO_2	Amorphous	5-35	99.9	8-11

The hydrocarbon fluid used in the experiments was stock tank crude oil from offshore Newfoundland with approximately 32-35 ºAPI. The injected gas used in the WAG experiments was air.

3.3.2 Interfacial Tension Measurements

The synthetic brine used in the experiments was formulated with 36330 ppm total dissolved salts in distilled water. **Table 10** shows the brine composition based on individual salt concentrations. The brine composition was selected to represent as closely as possible the sea water composition offshore Newfoundland. The hydrocarbon fluid used in the experiments was stock tank crude oil from offshore Newfoundland with approximately 32-35 ºAPI.

An Interfacial Tension Meter (IFT 700, manufactured by Vinci Technologies) was used to determine the IFT between the oil and the nanofluid (liquid-liquid interface) under reservoir conditions.

The experimental setup is shown in **Figure 18**. The setup consists of three main parts: computer system, cell, and the camera. The technical features of IFT 700 setup are tabulated in **Table 13**. As shown, this setup allows us to go up to 10000 psi and 180 ºC.

Figure 18: Interfacial tension meter

Table 13: Technical features of the IFT meter

Item	Type/model/specification
IFT standard measurements	0.1 to 100 (mN/m)
Cell Volume	20 (cc)
Operating pressure	700 (bar) or 10000 (psi)
Operating temperature	Ambient to 180 (°C)
Wetted parts	Stainless steel, PTFE, Viton
Pump	Two hand pumps of 20 (cc)
Connections	1/8" LP Autoclave or Butech type (15000 psi)

For the IFT measurements, silica and alumina nanoparticles were used as it is mentioned before in the micromodel experiments. The properties of SiO_2 and Al_2O_3 are shown in **Table 11**.

The pendant drop method was used for IFT measurements. An oil drop was created and put in contact with the nanofluid in a cell at reservoir condition. A camera connected to a computer records the shape of the oil droplet to derive the interfacial tension. The Drop Analysis System software allows fast calculation of surface and interfacial tension. Very good stability of the drop, a very important factor during IFT measurements, was observed during these experiments. The pendant drop method was used to measure the IFT between oil and nanofluid. Basically, a drop (oil) is generated from the end of a capillary needle in a bulk fluid (nanofluid) varying pressure and temperature, up to reservoir condition. With a calibrated and accurate video lens system, the complete shape of the drop is analyzed. The drop is analyzed based on the Laplace equation (nonlinear equation of differential equation) to get IFT. It should be mentioned that these numerical

calculations are done by the software, and the IFT will be given to the user directly. Since the density of the oil is lower than the density of nanofluid, rising drop method was used in the experiments. **Figure 19** shows the software interface. An example of the IFT measurement by using rising drop method is shown in **Figure 20**.

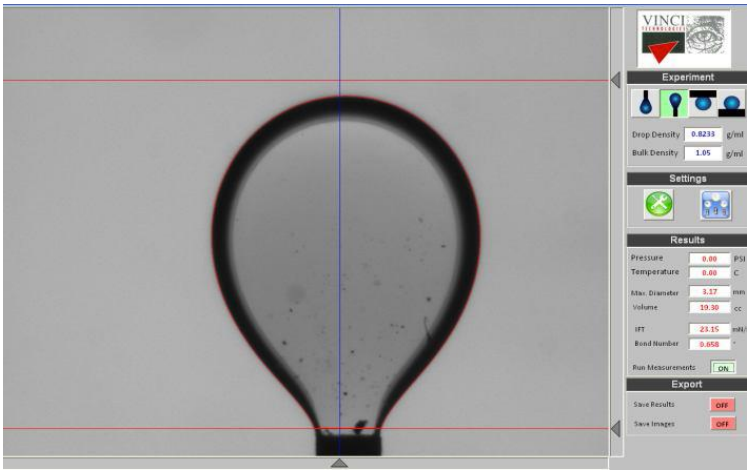

Figure 19: IFT meter software interface

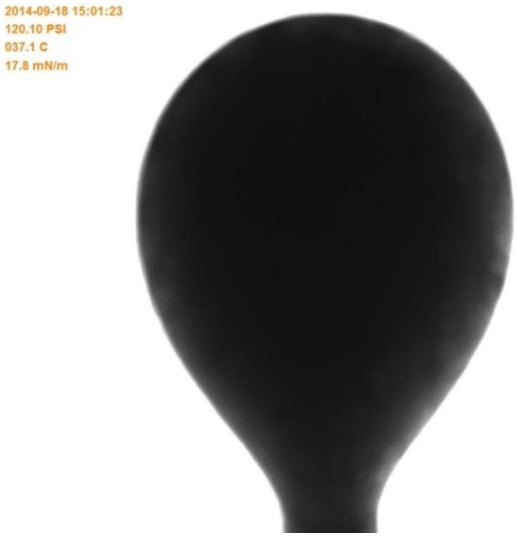

Figure 20: Rising drop method for IFT measurements

3.3.3 Viscosity Measurements

The VISCOlab PVT viscometer (manufactured by Cambridge Viscosity) was used for measuring the viscosity. A billet for the range of 0.25 to 5 cP was used for the experiments. After loading the pump, the system was set to the desired temperature and pressure. Before measuring any data, the system was bled through the relief valves to rid the system of any air. Then, viscosity was measured under stable pressure and temperature conditions. After running each test, the system was flushed with an appropriate solvent to clean all the lines and fittings, and then vacuumed. Bias was avoided by performing the experiments in random order. **Figure 21** shows the experimental setup for viscosity measurements. A schematic diagram of the viscosity measurements setup is shown in **Figure 22**.

Figure 21: Viscosity measurement setup

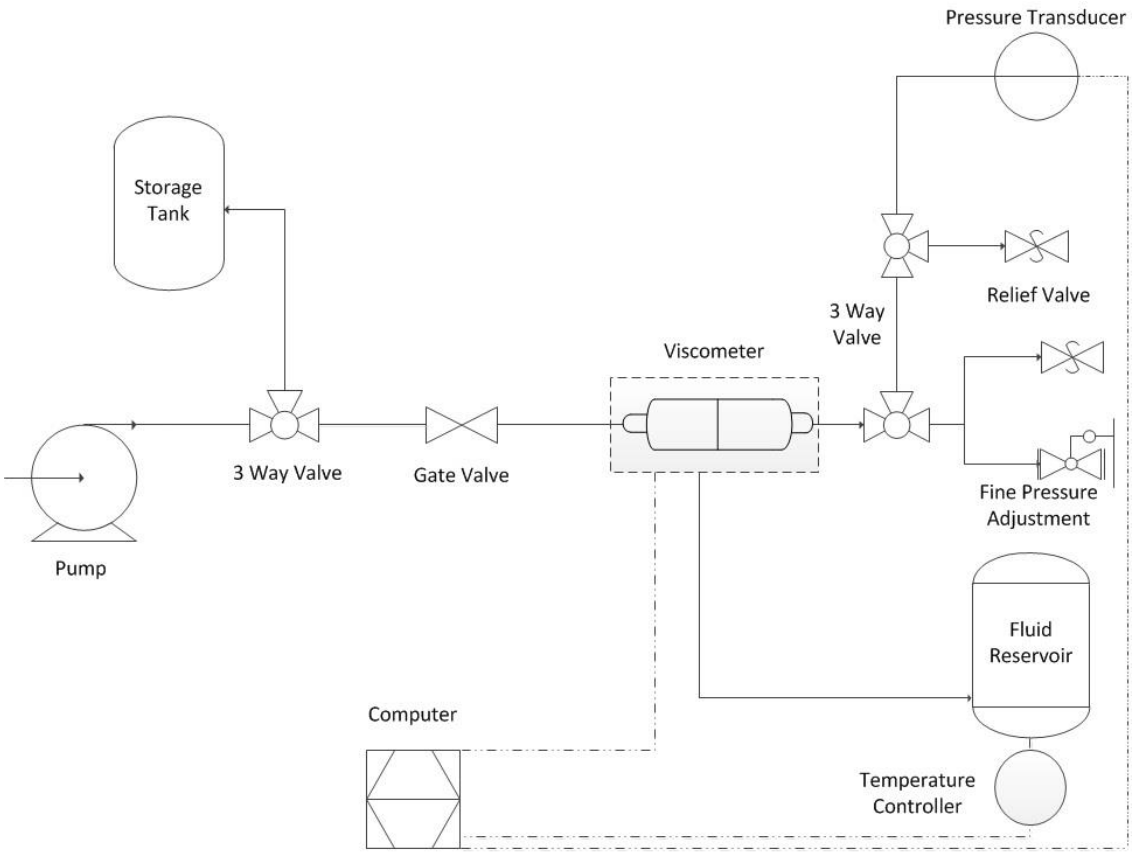

Figure 22: Schematic diagram of viscosity measurement device

3.3.4 Micromodel Experiments

3.3.4.1 Micromodel Characterization

A glass micromodel was used as the porous medium for WAG experiments. **Figure 23** shows the geometry of the micromodel. **Figure 24** shows a real photo taken during flooding, which demonstrates the strong water-wetness of the glass micromodel. The pore size dimensions are shown in **Table 14**. The important parameters are pore body and pore

throat width, which are 1.28 and 0.45 mm respectively. The micromodel dimensions and characteristics are tabulated in **Table 15**. The permeability value of 131 Darcy indicates a highly permeable porous medium. It should also be noted that the porosity of 0.42 is higher than real porosity values.

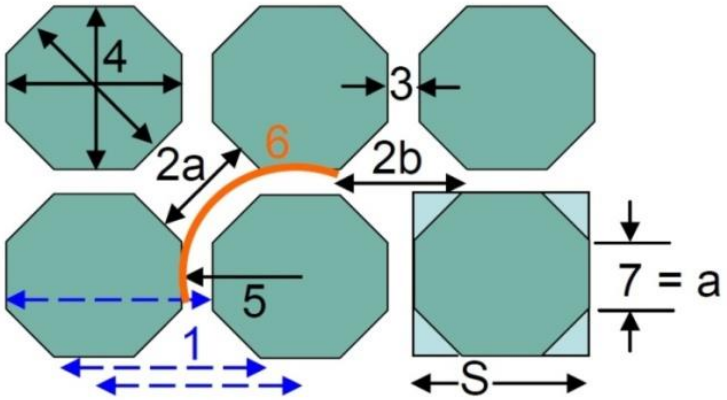

Figure 23: Micromodel geometry (James 2009)

Table 14: Pore dimensions (James 2009)

Tag #	Description	Dimension (mm)
1	Pore to Pore	2.04
2a	Pore Body	1.28
2b	Pore Body (1)-(7)	1.38
3	Pore Throat Width	0.45
4	Particle Size	1.59
5	Diffusion Distance	1.245
6	Flow Path	2.61
7	Pore Throat Length	0.66

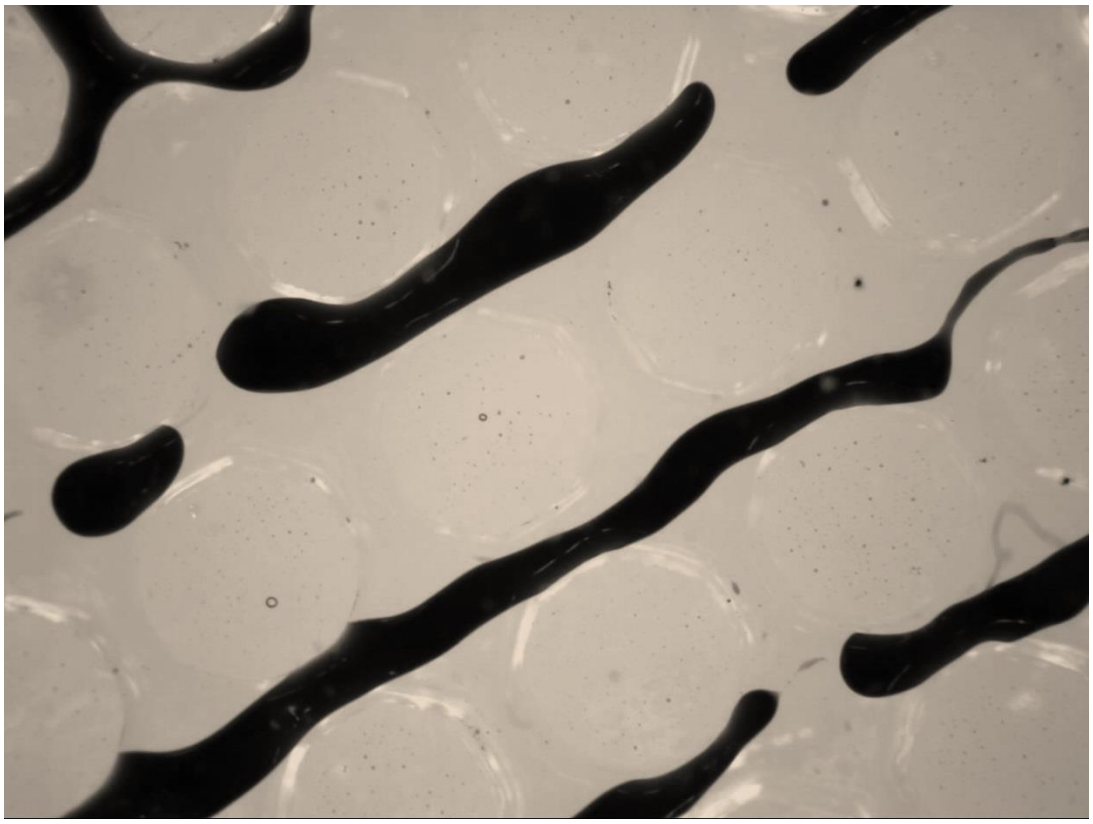

Figure 24: Photo captured during WAG injection

Table 15: Micromodel dimensions and characteristics (James 2009)

Description	Dimension
Length (cm)	30.4
Length (#pores)	149
Width (cm)	10.0
Width (#pores)	49
Pore Volume (cm^3)	1.6
Porosity	0.42
Permeability (Darcy)	131

A micromodel fabricated from polymethyl methacrylate (PMMA) was used as the porous medium in the waterflooding micromodel experiments. **Figure 25** shows a photo of the micromodel saturated with oil. **Table 16** shows the properties of the micromodel.

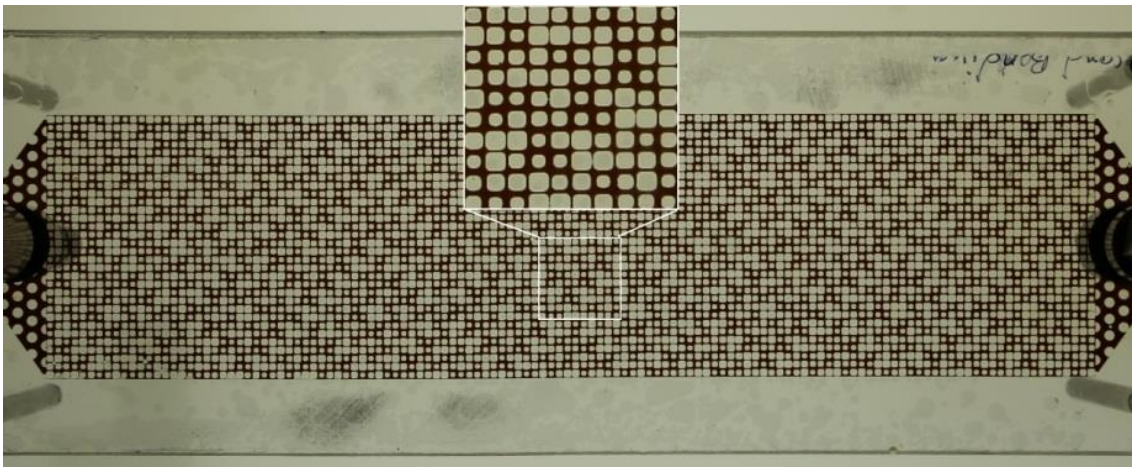

Figure 25: PMMA micromodel

Table 16: PMMA micromodel characterization

Description	Dimension
Length (cm)	25.6
Width (cm)	6.4
Average depth (μm)	160
Porosity	0.43
Pore Volume (cm^3)	1.15
Permeability (Darcy)	2.9

As shown in the table, the permeability of this micromodel is closer to real reservoir rock permeability (2.9 Darcy). However, the porosity of 0.43 is higher than the real case. Porosity of the micromodel was measured by image processing. Micromodel was vacuumed, and then fully saturated with oil. A picture was taken from the micromodel.

By dividing the number of black pixels to the total pixels (image processing), the porosity was measured. The pore volume of the micromodel was measure by injecting DI water with a constant flow rate into the micromodel. The interval between the time that water was introduced to the micromodel and the time that water front reached the outlet was monitored. Then, pore volume was measured. From the pore volume and porosity data, average depth of micromodel can be calculated. For measuring permeability, DI water was injected with constant flow rate. The inlet and outlet pressure was monitored. The known parameters are: viscosity of DI water, pressure drop, the length of the micromodel, injection flow rate, and cross sectional area. The absolute permeability can be calculated from Darcy's equation.

As it was discussed before, two sets of micromodel experiments were performed to study the effect of using nanoparticles in EOR. First, glass micromodel injection tests were performed to visualize the nanoparticle enhanced WAG process. Second, PMMA micromodel injection was performed to compare nanofluid injection with DI water/polymer injection.

3.3.4.2 Experimental Setup

A schematic diagram of micromodel injection setup is shown in **Figure 26**. A high accuracy pump (KDS Gemini 88 syringe pump) was used to inject the fluids in constant rate mode.

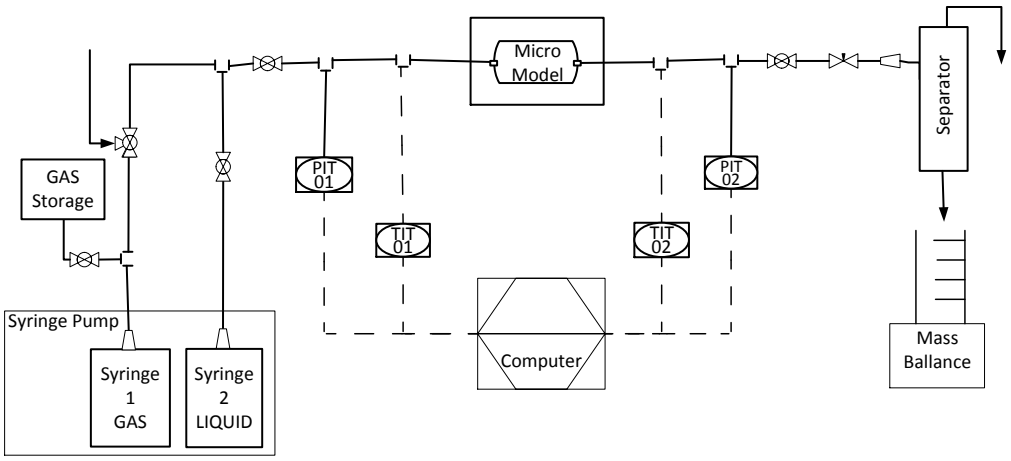

Figure 26: Schematic diagram of micromodel injection setup

3.3.4.3 Experimental Procedure

All connections must be attached properly by following the proper fittings procedures for tube fittings. Prior to running any experiments, a pressure test must be conducted to ensure that the system is safe to use for the desired experimental condition. In this case, a pressure test using water up to 40 psi was conducted before starting the experiments. If at any time during the pressure test a leak is discovered, the location of the leak should be noted, the pressure test should be stopped and the system should be depressurized, and the cause of the leak should be investigated and remedied.

The following procedure was used to conduct nanofluid/water-alternating-gas enhanced oil recovery experiments in a low pressure (ambient) micromodel system.

1. The glass micromodel was cleaned by flushing with toluene and acetone (2 pore volumes toluene and 2 pore volumes acetone).
2. The glass micromodel was completely dried in an oven.
3. After cleaning, the injection fluids (nanofluid and air) were loaded in the syringe pumps.
4. Brine was injected up to the inlet through the temporary line.
5. The micromodel inlet valve was closed.
6. The micromodel and downstream tubing was vacuumed to remove any air and reduce the probability of trapping air during the primary brine imbibition.
7. The outlet valve was closed.
8. By opening the inlet, system was drained by brine.
9. The outlet valve was opened.
10. Oil was loaded into a temporary line.
11. Oil was injected into the glass micromodel and to the outlet.
12. Slugs of nanofluid and air were injected to the glass micromodel consecutively.

Table 17 outlines the details of the experimental runs. For a WAG ratio of 1:1, 1 slug of water was followed by 1 slug of air. For a WAG ratio of 1:2, 1 slug of water was followed by 2 slugs of air.

Table 17: WAG experiments characterization

WAG ratio 1:1				WAG ratio 1:2			
Phase	Flow rate (ml/min)	Number of cycles	Duration (minutes)	Phase	Flow rate (ml/min)	Number of cycles	Duration (minutes)
Liquid	0.0193	6	30	Liquid	0.0193	6	30
Gas	0.0387	6	15	Gas	0.0387	6	30

The following procedure was used to conduct the nanofluid/polymer solution/DI waterflooding experiments at the low pressure (ambient conditions) micromodel system:

1. The PMMA micromodel was cleaned by flushing with hexane (2 pore volumes).
2. The micromodel was completely dried using compressed air.
3. The injection fluids were loaded in the syringe pumps.
4. DI water was injected up to the inlet through the temporary line.
5. The micromodel inlet valve was closed.
6. The micromodel and downstream tubing were vacuumed to remove any air and reduce the probability of trapping air during the primary imbibition.
7. The outlet valve was closed.
8. By opening the inlet, the system was drained by DI water.
9. The outlet valve was opened.
10. Oil was loaded into a temporary line.
11. Oil was injected into the glass micromodel and to the outlet.
12. Slugs of desired fluid injected to the glass micromodel.

3.3.4.4 Image Analysis

The oil saturation in the micromodel experiments can be measured at any time by image analysis. Standard image analysis using MATLAB® software was used to determine the oil recovery. The difference between the initial state of the black pixels and the final state was interpreted as oil recovery. **Figure 27** and **28** show the pixel histograms for run #4 (**Table 2**). A number was assigned to each color from 0 (black) to 250 (white). The range between 0 to 150 was considered as oil as per the software recommendations.

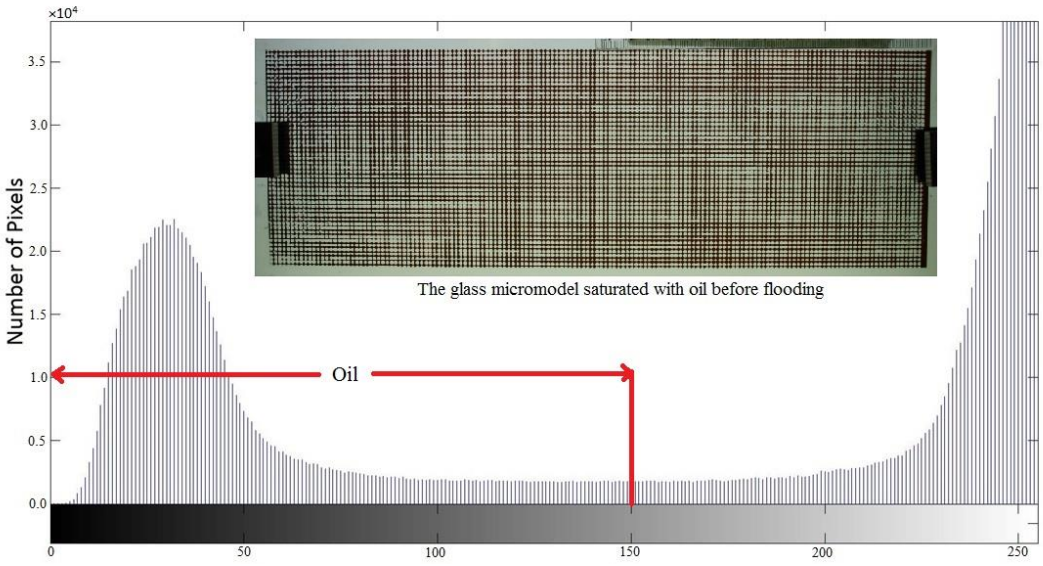

Figure 27: Histogram graph of number of pixels vs. coded color before flooding [run #4]

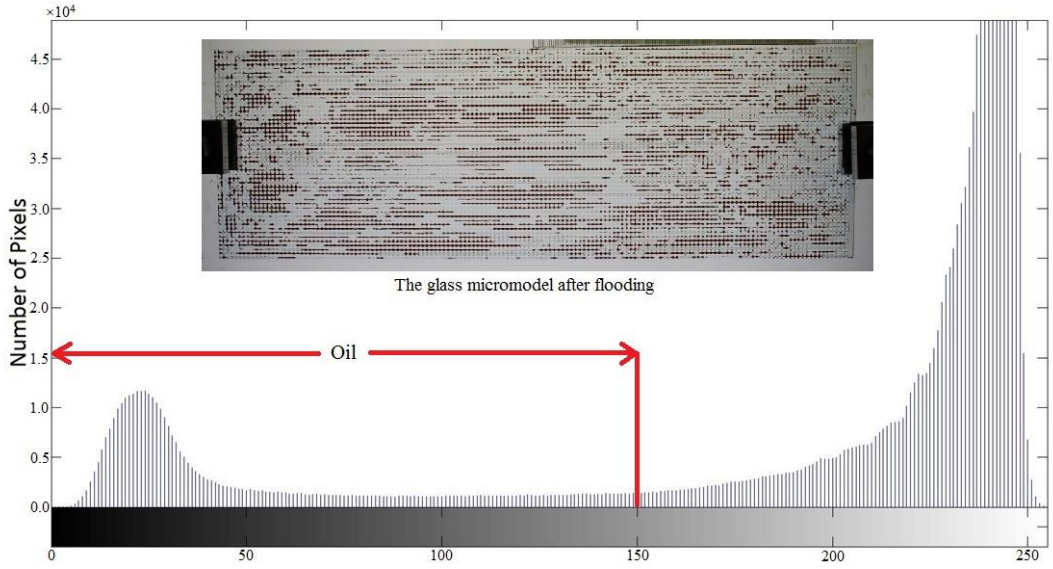

Figure 28: Histogram graph of number of pixels vs. coded color after flooding [run #4]

In **Figure 27** and **28**, the horizontal axis represents the color coded by numbers starting from zero. The vertical axis indicates the number of pixels. By summing up the number of pixels between 0 to 150, the oil saturation can be calculated. Oil recovery was defined as:

$$Oil\ recovery\ (\%) = \left[\frac{initial\ oil\ saturation - final\ oil\ saturation}{initial\ oil\ saturation}\right] 100\% \text{ ----- } \mathbf{Eq.\ 9}$$

3.3.5 Error Analysis

Experimental investigations usually have different sources of error that need to be taken into account when reporting the results. The degree of the closeness of a measurement to a reference value is defined by the accuracy the system (systematic error). Precision

(random error) of a measurement system dictate the reproducibility and repeatability of the measurements.

In this work, calibration test was performed before the experiments to make sure that the experimental results are accurate. The detailed results of calibration experiments will be discussed in **Appendix B**. Moreover, different numbers of replicate runs were performed to measure the precision of the system. The detailed results of random error measurements are also discussed in **Appendix B**.

4. Results and Discussion

4.1 WAG Experiments

Optimal design was used to perform the experiments. Optimal design is a statistical type of design of experiments. The number of experiments varies according to the number of quantitative and qualitative factors. The optimal design is a response surface methodology method that gives us the minimum number of runs to analyze the response according to available factors. Design Expert software® was used to generate the experimental runs.

Table 18 shows the results of the water alternating gas micromodel experiments. Ultimate oil recovery was measured by using image analysis. The procedure of measuring oil recovery by image analysis is discussed in **Appendix A**. The maximum oil recovery (63.1%) was obtained while using 0.1 weight percent of silica (SiO_2) nanoparticles and a WAG ratio of 1:2. The minimum oil recovery was 45.7% during brine injection with a WAG ratio of 1:1.

Table 18: The results of WAG micromodel experiments

Run	Type	WAG Ratio	Nanoparticle Concentration (wt%)	Oil Recovery (%)
1	SiO_2	1:2	0.02	60.1
2	Al_2O_3	1:2	0.08	61.1
3	Al_2O_3	1:1	0.02	56.4
4	Al_2O_3	1:1	0.10	58.8
5	SiO_2	1:2	0.02	61.7
6	SiO_2	1:2	0.10	63.1
7	Brine	1:1	0.00	45.7
8	Al_2O_3	1:2	0.08	60.3
9	Brine	1:2	0.00	46.7
10	SiO_2	1:1	0.04	62.6
11	Al_2O_3	1:1	0.06	59.8
12	SiO_2	1:1	0.08	65.1

Table 19: Analysis of variance for micromodel experiments

Source	Sum of Squares	Degree of Freedom	Mean Square	F value	p-value (Prob>F)
Model	669.59	4	167.40	163.72	< 0.0001
A: Sqrt(Concentration)	424.99	1	424.99	415.67	<0.0001
B: Nanoparticle Type	27.97	1	27.97	27.35	0.0005
AB	8.77	1	8.77	8.57	0.0168
A^2: Concentration	84.51	1	84.51	82.66	< 0.0001
Residuals	9.20	9	1.02		
Lack of Fit	8.61	7	1.23	4.15	0.2081
Pure Error	0.59	2	0.30		
Cor Total	678.79	13			

Table 19 shows the analysis of variance results for the WAG micromodel experiments. The prediction interval provides the upper and lower levels for the 95% confidence level. Therefore, if the p-value, which tests the null hypothesis and the significance of the regression model, is larger than 0.05, the probability tends to accept the hypothesis and it

does not perform the 95% confidence interval. In other words, when the p-value is smaller than 0.05 the source is considered as significant. The analysis of variance is model dependent so it is up to the user to suggest models that describe the data. We systematically tried and compared several different models (linear, quadratic, etc.) with the inclusion and elimination of higher order and interaction terms. The goal was to find the simplest model to best fit results found. The results of the ANOVA table demonstrate that WAG ratio does not have a significant effect on oil recovery. It should be mentioned that WAG ratio is an important parameter in enhanced oil recovery. However, in this particular set of experiments, WAG ratio is not playing an important role in the statistical model. Smaller p-value indicates the more significant of the source on the response. As shown in **Table 19**, square root of concentration and concentration shown to have the most effect on oil recovery.

The significant factors affecting oil recovery for these experiments are:

- Square root of concentration
- Nanoparticle type
- Interaction between square root of concentration and nanoparticle type
- Concentration of nanoparticles in the nanofluid

Square root of concentration was used as the main factor instead of concentration in order to fit the simplest and best possible model.

4.2 IFT measurements

The results of the IFT measurements are tabulated in **Table 20**. These 24 runs were designed to optimally model IFT with respect to four different factors. A calibration experiment was performed using air/DI water/toluene to ensure that the results are accurate. The details of calibration experiment are discussed in **Appendix B**. In the classic design of experiments, one factor will be changed at a time and other factors will be constant, however, interaction between the factors cannot be seen. In these experiments, all the factors are changing at the same time, and each run is different than other runs (except the replication for measuring pure error and lack of fit). The importance of this kind of design (response surface methodology) is that the effect of interaction and nonlinearity can be detected easily, and considered in the model. For example, it is important to know how IFT will change by changing pressure in a high temperature environment. In other words, what is the effect of the interaction between pressure and temperature on IFT?

The * sign in the table indicates the replicate runs. Based on the replicate runs, the standard deviation of ±0.35 mN/m was calculated for this particular set of experiments. Three particular experiments were repeated, and standard deviation was calculated for each one of them. Then, the combined (average) standard deviation was reported as the

total standard deviation. The detail of standard deviation calculation will be discussed more in **Appendix B**.

Table 20: IFT measurement results

Run	Type	Concentration (ppm)	Pressure (psia)	Temperature (°C)	IFT (mN/m)±0.35
1	SiO_2	735	6244	51.2	1.97
2	Al_2O_3	580	20	30.5	4.42
3	Al_2O_3	1000	20	80.0	2.28
4*	SiO_2	412	8000	80.0	2.26
5	Al_2O_3	1000	3092	20.0	3.09
6	Al_2O_3	0	20	20.0	26.90
7	SiO_2	0	20	80.0	17.78
8*	Al_2O_3	500	4010	50.0	4.48
9	Al_2O_3	635	8000	27.8	3.90
10	SiO_2	0	3850	20.0	26.01
11*	Al_2O_3	500	4010	50.0	3.95
12	Al_2O_3	0	4968	80.0	16.42
13*	Al_2O_3	500	4010	50.0	4.08
14	Al_2O_3	0	8000	20.0	26.73
15	SiO_2	1000	3901	80.0	1.19
16	SiO_2	0	3850	20.0	27.80
17	Al_2O_3	1000	8000	80.0	1.42
18*	SiO_2	412	8000	80.0	2.78
19	SiO_2	1000	8000	20.0	2.66
20*	SiO_2	0	8000	54.6	16.96
21	Al_2O_3	47	690	57.9	18.40
22	SiO_2	1000	20	20.0	2.84
23	SiO_2	625	20	59.9	3.54
24*	SiO_2	0	8000	54.6	18.68

Table 21 shows the interpretation of the interfacial tension measurements. In these experiments, we tried to model IFT according the important parameters affecting it. The first step was to include all the important factors that we could control. Therefore, it was decided to include four factors: concentration of nanoparticles, pressure, temperature, and

the type of nanoparticles. After finalizing the factors and their corresponding levels, optimal design was used to design the experiments. Finally, analysis of variance was performed on the results to determine which factors are significant. As was previously mentioned, the prediction interval provides the upper and lower levels for the 95% confidence interval. When a p-value is smaller than 0.05 the source is considered as significant. Therefore, if the p-value, which tests the null hypothesis and the significance of the regression model, is larger than 0.05, the probability tends to accept the hypothesis and it does not perform the 95% confidence interval. The analysis of variance is model dependent so it is up to the user to suggest models that describe the data. We systematically tried and compared several different models (linear, quadratic, etc.) with the inclusion and elimination of higher order and interaction terms for both the micromodel and IFT experiments. The goal was to find the simplest model to best fit the results. Modeling the IFT, the significant factors are listed below. These are illustrated in **Figure 29**.

- Concentration of nanoparticles in the nanofluid (C)
- Pressure (P)
- Temperature (T)
- Interaction between concentration and temperature (CT)
- Interaction between pressure and temperature (PT)
- $(\text{Concentration})^2$ (C^2)

Nanoparticle type (N) and the interaction between nanoparticle type and pressure (PN) were also included in the model to reduce the amount of error in the IFT correlation. The p-value for nanoparticle type and PN interaction are 0.0551 and 0.0627 respectively. Therefore, it was decided to include these two factors in the model to increase the accuracy of IFT prediction.

Table 21: Analysis of variance results for the interfacial tension measurements

Source	**Sum of squares**	**Degree of freedom**	**Mean square**	**F-value**	**p-value**
Model	51.970	8	6.500	780.48	< 0.0001
C (Concentration)	34.730	1	34.730	4172.17	< 0.0001
P (Pressure)	0.270	1	0.270	32.04	< 0.0001
T (Temperature)	2.360	1	2.360	284.05	< 0.0001
N (Nanoparticle Type)	0.036	1	0.036	4.32	0.0551
CT (Concentration × Temperature)	0.380	1	0.380	45.28	< 0.0001
PT (Pressure × Temperature)	0.098	1	0.098	11.74	0.0037
PN (Pressure × Nanoparticle Type)	0.034	1	0.034	4.04	0.0627
C^2 (Concentration^2)	4.470	1	4.470	536.72	< 0.0001
Residuals	0.120	15	$8.323*10^{-3}$		
Lack of fit	0.067	10	$6.672*10^{-3}$	0.57	0.7874
Pure error	0.058	5	0.012		
Cor total	52.090	23			

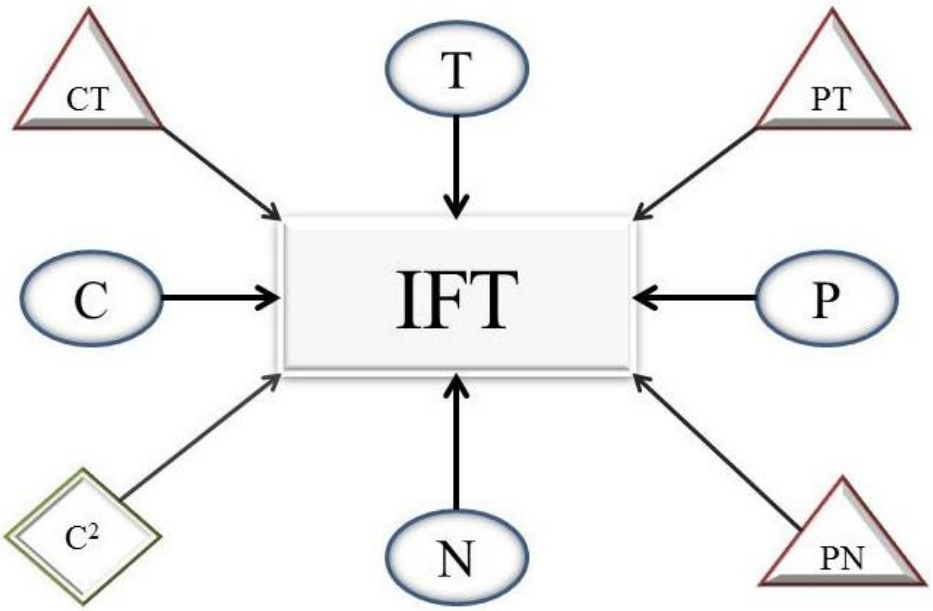

Figure 29: Significant effects on the interfacial tension

4.3 Modeling of the WAG Experiments

Experimentally, by looking at **Table 18**, we see oil recovery increasing with nanoparticle concentration in brine. However, after a critical concentration, the increase in oil recovery was statistically insignificant. **Figures 30** and **31** show the effect of concentration on oil recovery for a WAG ratio of 1:1 and 1:2, respectively. The dashed lines indicate the 95% confidence interval bands for the predictive model shown in correlations corresponding to the analysis of variance in **Table 19**, and the points are the experimental results. Both show recovery increasing with increasing concentration until recovery starts to plateau at approximately 0.04 g/ml nanoparticles, after which the change in oil recovery is insignificant. The possible mechanisms for the increased oil recovery in these

experimental tests are: interfacial tension reduction and emulsion generation, each of which will be discussed subsequently. As shown in **Figures 30** and **31**, both concentration and square root of concentration are shown on the x axis. As it was mentioned before, square root of concentration was used to better fit the statistical model to the experimental points.

The ANOVA table (**Table 19**) demonstrates that the regression model is significant, and the lack of fit is not significant. According to the p-value for "Lack of Fit", there is a 20.81% chance that a "Lack of Fit F-value" this large could occur due to noise. After trying several models with the interaction and higher terms included and excluded, the predicted model with the best fit was found to include the concentration (A^2) and the square root of concentration (A), type of nanoparticle (B), and the interaction between type of nanoparticles and concentration (AB) as significant factors. The model and experimental data suggest that silica nanofluid is slightly more efficient. The experimental results and predicted model both suggest a non-linear effect of nanoparticle concentration on oil recovery.

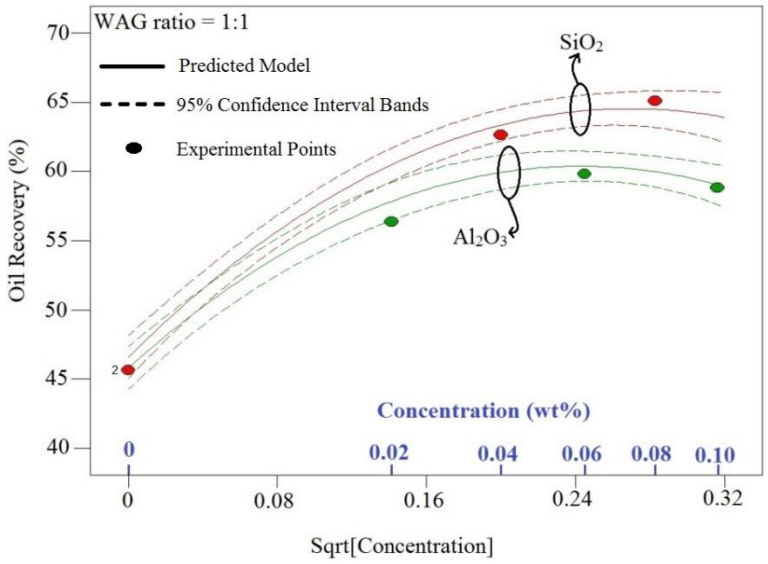

Figure 30: Oil recovery vs. concentration for a 1:1 WAG ratio

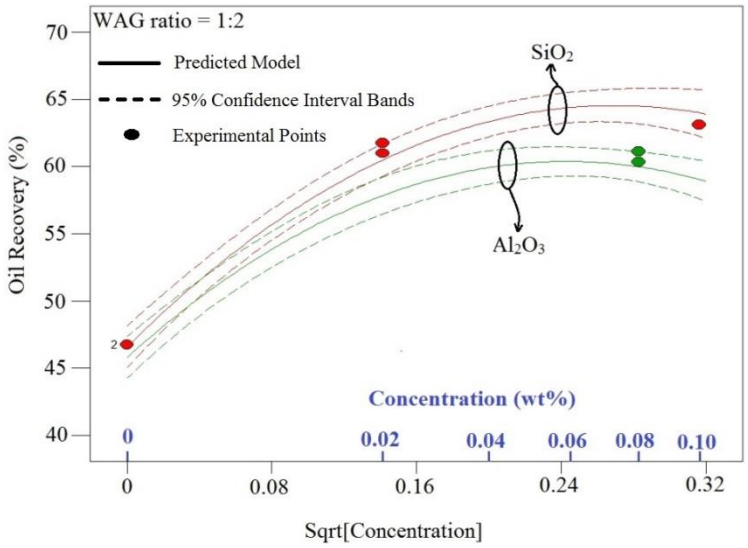

Figure 31: Oil recovery vs. concentration for a 1:2 WAG ratio

Oil recovery was correlated based on concentration. The model prediction based on variance analysis, suggests the following equations for oil recovery. The predicted model

for oil recovery (%) based on nanoparticle type, and concentrations are shown in equations below. The unit of concentration is weight percent (wt %).

SiO_2

$$Recovery\ (\%) = 46.6 + 133.2\sqrt{Concentration} - 247.2\ Concentration$$ ----- **Eq. 10**

Al_2O_3

$$Recovery(\%) = 45.8 + 120.0\sqrt{Concentration} - \ 247.2\ Concentration$$ ----- **Eq. 11**

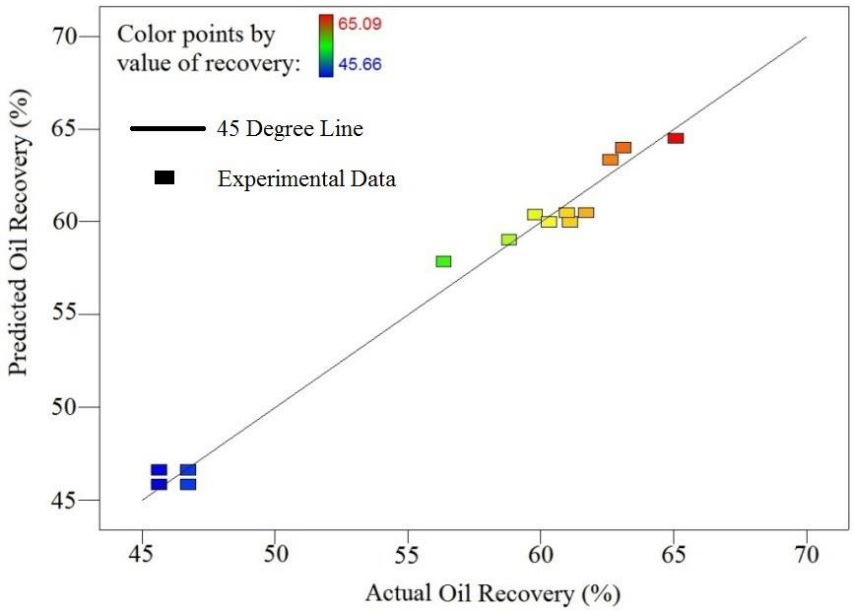

Figure 32: Predicted oil recovery vs. actual experimental data

Figure 32 shows how the oil recovery predicted by the model matches the actual experimental data. As shown in the figure, the data points fall very close to the 45º slope line. The maximum difference between the experimental values and the predicted values

is approximately 1.5%, which is not significant in comparison to the increase in the oil recovery over simple water alternating gas injection.

4.3.1 Effect of Type and Concentration of Nanoparticles

As shown in **Figures 30** and **31**, increasing the concentration is resulted in increasing the oil recovery. The dashed lines indicate the 95% confidence interval bands for the predictive model shown in correlations corresponding to the analysis of variance in **Table 19**, and the points are the experimental results. By investigating **Figure 30**, the change in the oil recovery is not significant after a concentration of approximately 0.04-0.05 wt%. However, the model predicts the maximum recovery at approximately 0.06 and 0.065 g/ml, for alumina and silica nanofluid injection, respectively. The model and experimental data suggest that silica nanofluid is slightly more efficient. The experimental results and predicted model both suggest a non-linear effect of nanoparticle concentration on oil recovery.

Figure 31 shows the effect of nanoparticle concentration on oil recovery for a WAG ratio of 1:2. The model predicts the same behavior as far WAG ratio of 1:1. The maximum oil recovery was obtained at a concentration of approximately 0.06 g/ml (600 ppm) for both silica and alumina nanofluids. Therefore, the results indicate that the effect of WAG ratio on oil recovery is not significant in this particular set of experiments.

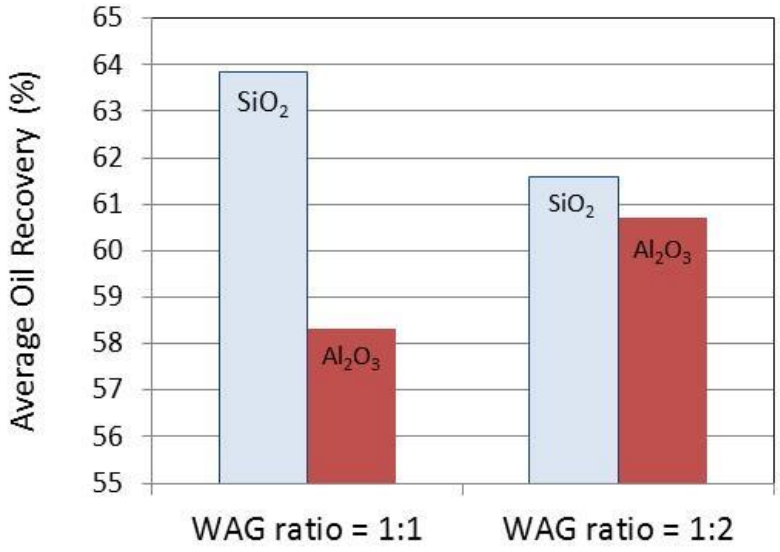

Figure 33: Interaction between nanoparticle type and WAG ratio (experimental results)

A statistically significant difference in recovery between alumina and silica nanofluids was observed during flooding. SiO_2 nanofluid injection was shown to be more efficient in terms of oil recovery. **Figure 33** shows the effect of the type of nanoparticles on average oil recovery that was obtained from the experiments. The silica nanofluid injection case resulted in higher oil recovery. The model predicts approximately 5% more recovery using silica nanofluid, which is in a good agreement with the experimental results.

Figure 34 shows an example of the emulsion generated during SiO_2 nanofluid injection. As shown in **Figure 35**, such a phenomenon was not observed during Al_2O_3 nanofluid injection. This phenomenon might be a possible explanation for the higher recovery using the WAG ratio of 1:2 (SiO_2). Sharma et al. (2014) also reported stabilized emulsion

generation using silica nanoparticles. Silica nanoparticles were observed to generate stable oil in water emulsion. In order to recover these emulsions, they need to be carried in the water phase to the outlet.

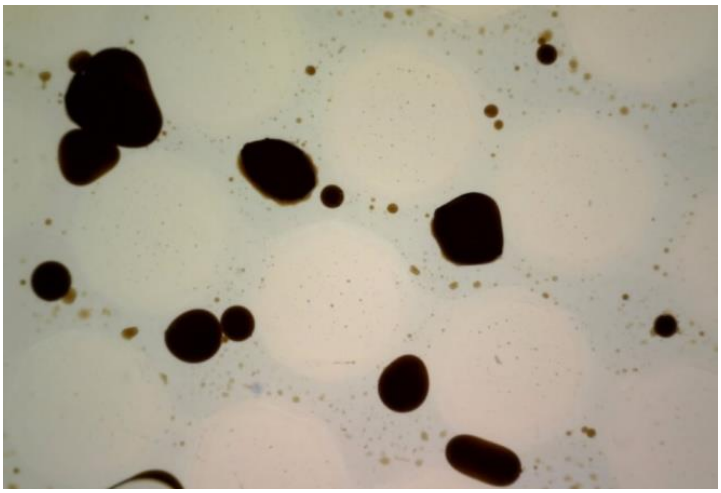

Figure 34: Oil in water emulsion observed during waterflooding with brine enriched with 0.08 g/ml SiO_2 nanoparticles [run #12]

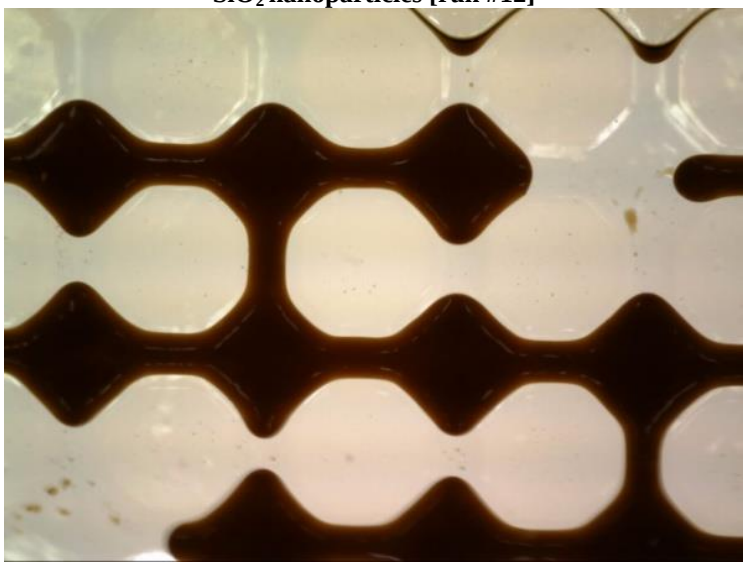

Figure 35: No emulsion was observed during waterflooding with brine enriched with 0.08 g/ml Al_2O_3 nanoparticles [run #2]

The model predicts that the interaction between nanoparticle type and the concentration plays an important role in the regression model. However, WAG ratio was shown to be insignificant in the model. **Figure 33** illustrates that for silica nanofluid injection; more oil was recovered in WAG ratio of 1:1. On the other hand, for alumina nanofluid injection, higher recovery was obtained at WAG ratio of 1:2. Experimental data show that the variations in oil recovery by changing the WAG ratio are approximately 2 - 3% (**Figure 33**), which is not significant. Therefore, both the model and the experimental data show that the effect of WAG ratio on the oil recovery is not significant for this particular set of experiments. However, it should be noted that in general WAG ratio is considered as one of the most important factors in WAG processes.

Figure 36 shows a photo captured during water alternating gas injection in which the distribution of oil, brine with nanoparticles, and gas in the pore system of strongly water-wet glass micro-model can be seen. The wetting brine phase is shown saturating a film along the entire micromodel glass solid, along the pore and pore throat walls. Oil is shown spreading over the brine phase in the presence of the air that is being injected.

Figure 37 shows how the residual oil was distributed during waterflooding. As shown in the photo, residual oil tends to be trapped in the pore bodies due to the wettability state of the glass micromodel which is strongly water-wet, whereby water injection is an imbibition process.

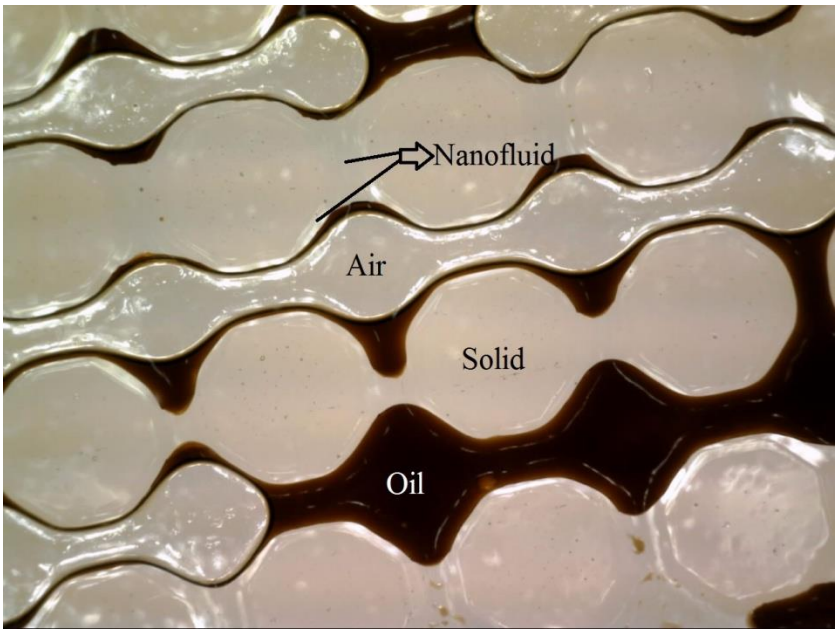

Figure 36: Distribution of oil, brine with 0.08 g/ml Al_2O_3 nanoparticles, and air in the micromodel [run #2]

Figure 37: Distribution of oil and brine during waterflooding [run #7]

4.4 Modeling (IFT Experiments)

The experimental results (**Table 20**) show that by increasing the concentration of nanoparticle in the brine, IFT will drop dramatically. Increasing the temperature has also caused IFT to be reduced significantly. Interfacial tension is not very sensitive to pressure. However, pressure is a very important factor due to its interaction with other variables. **Figure 38** shows the overall behavior of IFT with respect to concentration in different states of pressure and temperature. It should be mentioned that this figure depicts the results of the model predicted by ANOVA. As shown in the figure, concentration of nanoparticles has a significant impact on interfacial tension. However, IFT did not change significantly for concentrations more than 600 ppm. The results of the model shown in **Figure 38** indicate that at higher temperature IFT is more sensitive to changes in pressure, which highlights the effect of interaction between pressure and temperature on IFT. Overall, by increasing the temperature, the effect of pressure on IFT becomes more significant. The dashed lines indicate the 95% confidence interval bands for the predictive model corresponding to the analysis of variance in **Table 21**. The results of our experiments perfectly match with the results found in literature. For example, Roustaei et al. (2012) reported IFT reduction (oil and water) to approximately 2 (mN/m).

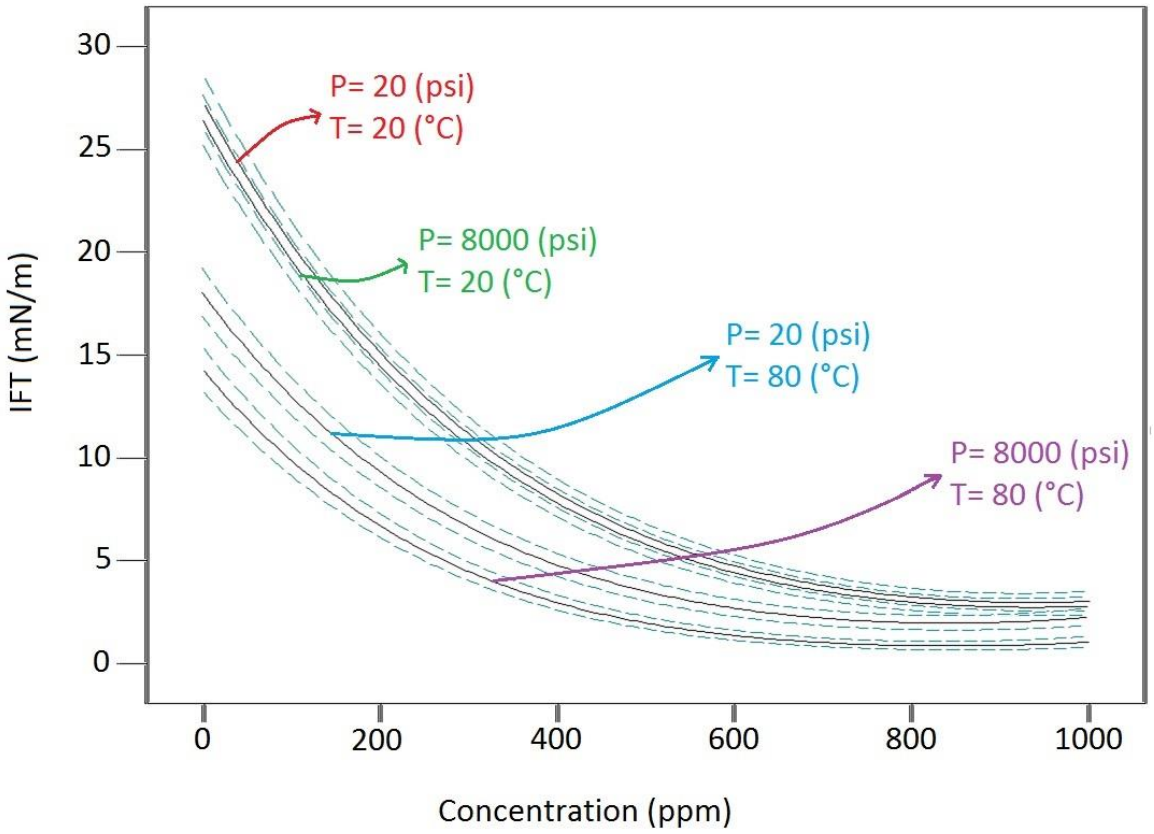

Figure 38: IFT vs. concentration in different states of pressure and temperature

The ANOVA table (**Table 21**) demonstrates that the model is significant, and the lack of fit is not significant. After trying several models with the interaction and higher terms included and excluded, the predicted model with the best fit was found to include the concentration (C), pressure (P), temperature (T), nanoparticle type (N), interaction between concentration and temperature (CT), interaction between pressure and temperature (PT), interaction between pressure and nanoparticle type (PN), and

concentration to the power of two (C^2). The results of the analysis of variance indicate that concentration is the most important factor, and has the largest impact on IFT.

SiO_2

$$\sqrt{IFT} = 5.52 - (7.69 \times 10^{-3} \times C) - (4.23 \times 10^{-6} \times P) - (0.02 \times T) + (1.20 \times 10^{-5} \times C \times T) - (8.50 \times 10^{-7} \times P \times T) + (3.98 \times 10^{-6} \times C^2)$$ ----- **Eq. 12**

Al_2O_3

$$\sqrt{IFT} = 5.52 - (7.69 \times 10^{-3} \times C) - (2.07 \times 10^{-5} \times P) - (0.02 \times T) + (1.20 \times 10^{-5} \times C \times T) - (8.50 \times 10^{-7} \times P \times T) + (3.98 \times 10^{-6} \times C^2)$$ ----- **Eq. 13**

Table 22: Variables and their corresponding units

Variable	Unit
Interfacial tension (IFT)	mN/m
Pressure (P)	psia
Temperature (T)	°C
Concentration (C)	ppm

Interfacial tension was correlated based on the variables in the experiment. The predicted model, based on ANOVA, suggests the following equations for IFT. The predicted models for IFT based on nanoparticle type are shown in equations below. **Table 22** shows the variables in the following equations and their corresponding units.

Figure 39 indicates how the IFT predicted by the model matches the actual experimental IFT. The figure demonstrates that data points fall very close to the 45° slope line. The maximum difference between the experimental values and the predicted values is approximately 5%, which is not considered significant.

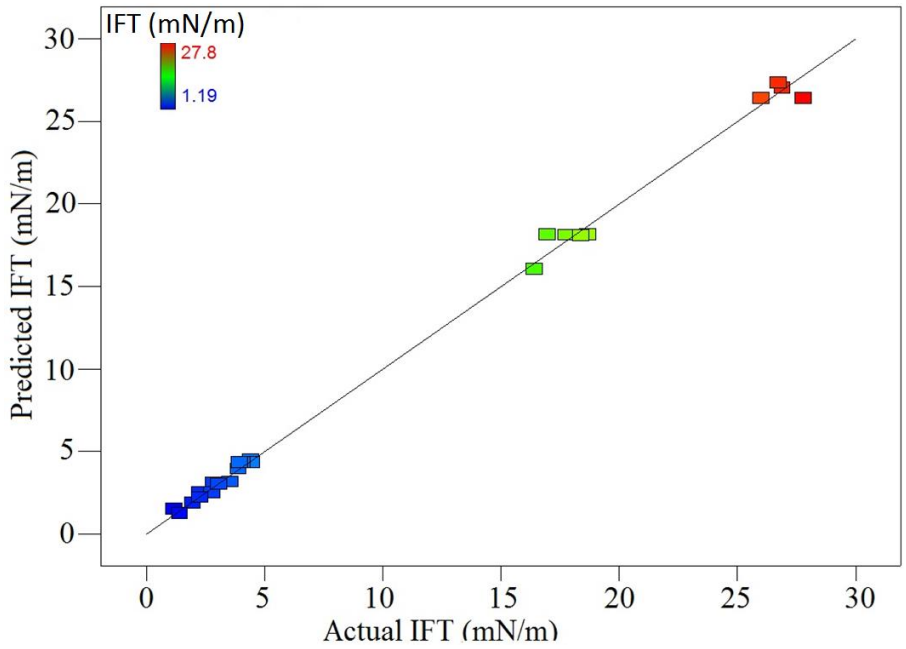

Figure 39: Predicted IFT vs. actual experimental data

4.4.1 Silica Nanoparticles (SiO_2) – Low Pressure (20 psia)

Figure 40 shows the effect of silica nanoparticle concentration on the interfacial tension between oil and the nanofluid for a low pressure system in different temperatures. As shown in the figure, by increasing the concentration, IFT decreases significantly up to the concentration of approximately 500 ppm. The figure suggests that interfacial tension is independent of temperature at a high concentration of silica nanoparticles in the nanofluid. However, the effect of temperature on IFT became significant at low concentration of silica nanoparticles. It should be mentioned that this figure is only for low pressure of 20 psia. The points in the figure below demonstrate the experimental data points.

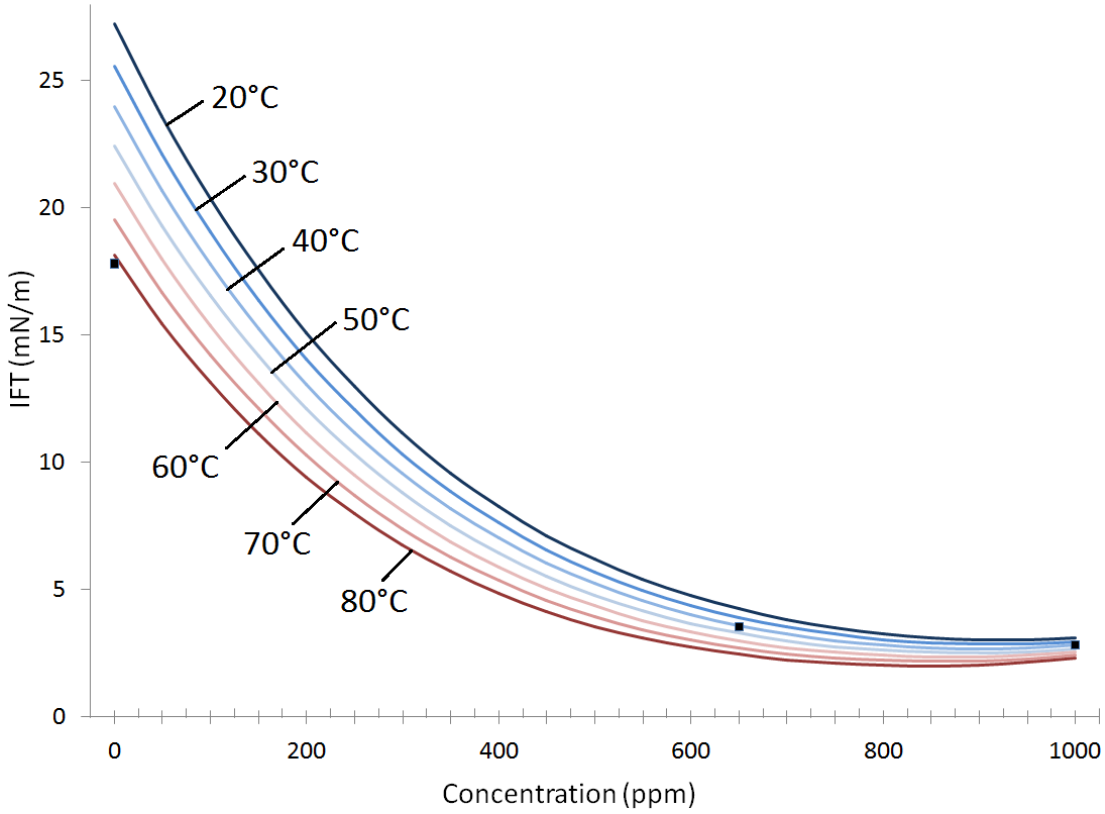

Figure 40: IFT vs. SiO_2 concentration for low pressure system (20 psia)

4.4.2 Silica Nanoparticles (SiO_2) – High Pressure (8000 psia)

Figure 41 shows the effect of silica nanoparticle concentration on the interfacial tension between oil and the nanofluid for a high pressure system at different temperatures. As was observed in the low pressure system, by increasing the concentration, IFT decreases significantly up to the concentration of approximately 500 ppm. However, as shown in the figure, IFT is temperature dependent even at high concentrations of silica nanoparticles. Comparing the **Figure 40** and **41**, we can say that for a low pressure

system, IFT is less dependent of temperature at high concentration of silica nanoparticles. However, **Figure 41** demonstrates temperature dependency of IFT for all concentrations, which shows the interaction effects between pressure, temperature, and concentration. Also, the interfacial tension values are smaller for the high pressure system in comparison to the low pressure system. Overall, by increasing temperature, concentration, and pressure, IFT decreases. The points in the figure below demonstrate the experimental data points. Overall, IFT is more dependent on temperature and concentration than pressure.

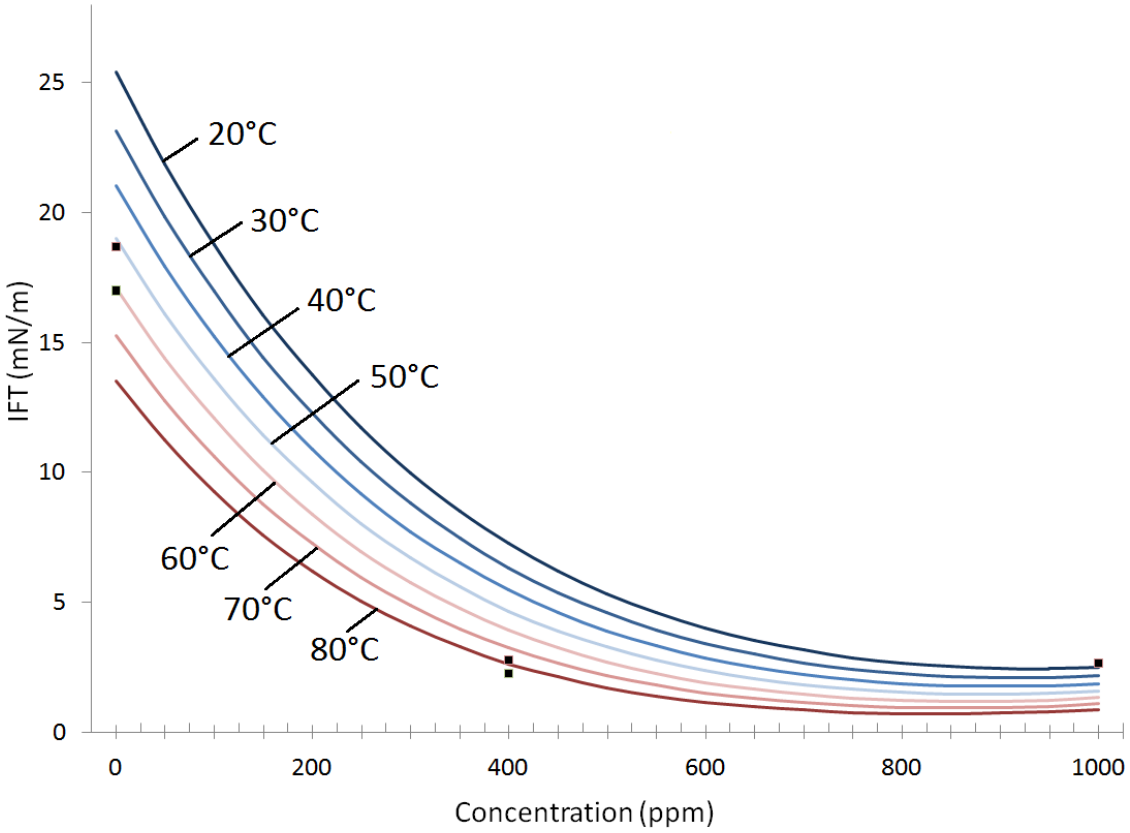

Figure 41: IFT vs. SiO_2 concentration for high pressure system (8000 psia)

4.4.3 Alumina Nanoparticles (Al_2O_3) – Low Pressure (20 psia)

For alumina nanofluid, the interfacial tension behavior was observed to be the same as the silica nanofluid case. **Figure 42** shows that IFT is decreasing by increasing the alumina nanoparticle concentration. Also, IFT is decreasing with decreasing with increasing temperature at low concentrations, and is independent of temperature at high concentration of alumina nanoparticles.

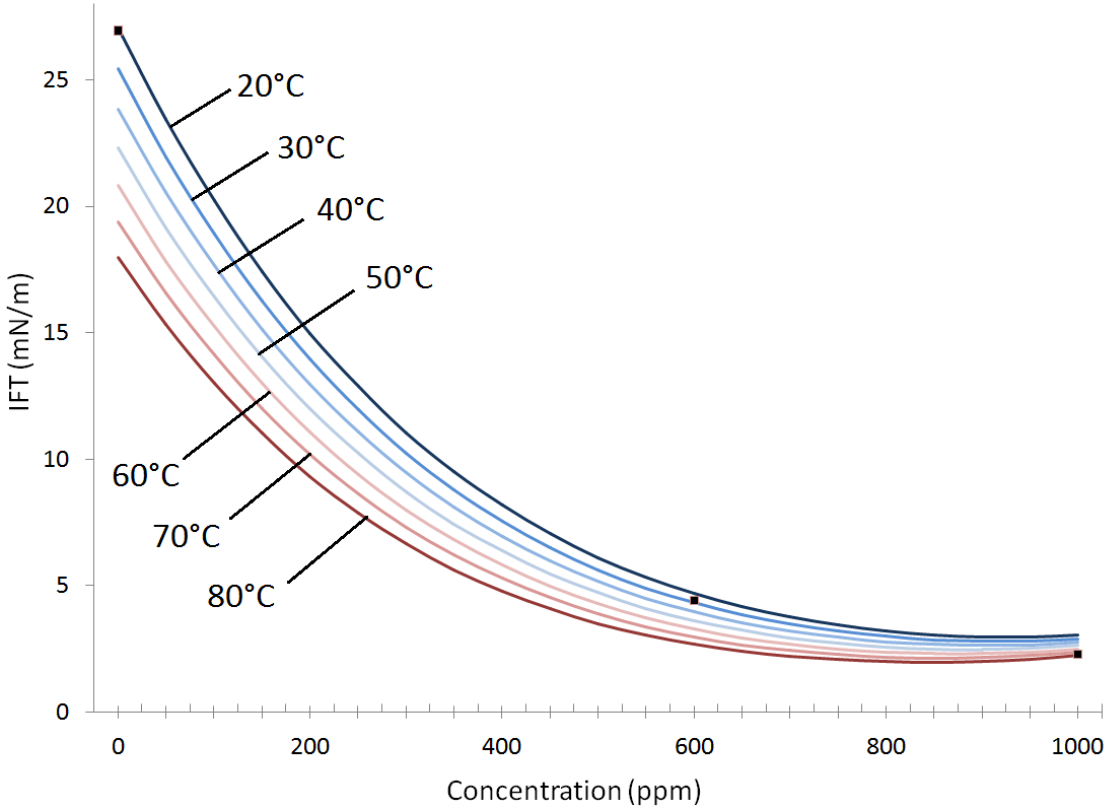

Figure 42: IFT vs. Al_2O_3 concentration for low pressure system (20 psia)

4.4.4 Alumina Nanoparticles (Al_2O_3) – High Pressure (8000 psia)

Figure 43 shows the behavior of IFT with respect to concentration of alumina nanoparticles for a high pressure system at different temperatures. As shown in the figure, IFT is decreasing with increasing concentration and temperature. The important difference between the high and low pressure systems (**Figure 42** and **43**) is that interfacial tension is independent of temperature for the low pressure system at high concentration of alumina nanoparticles, but is always temperature dependent for high pressure system. The points in the figure below demonstrate the experimental data points.

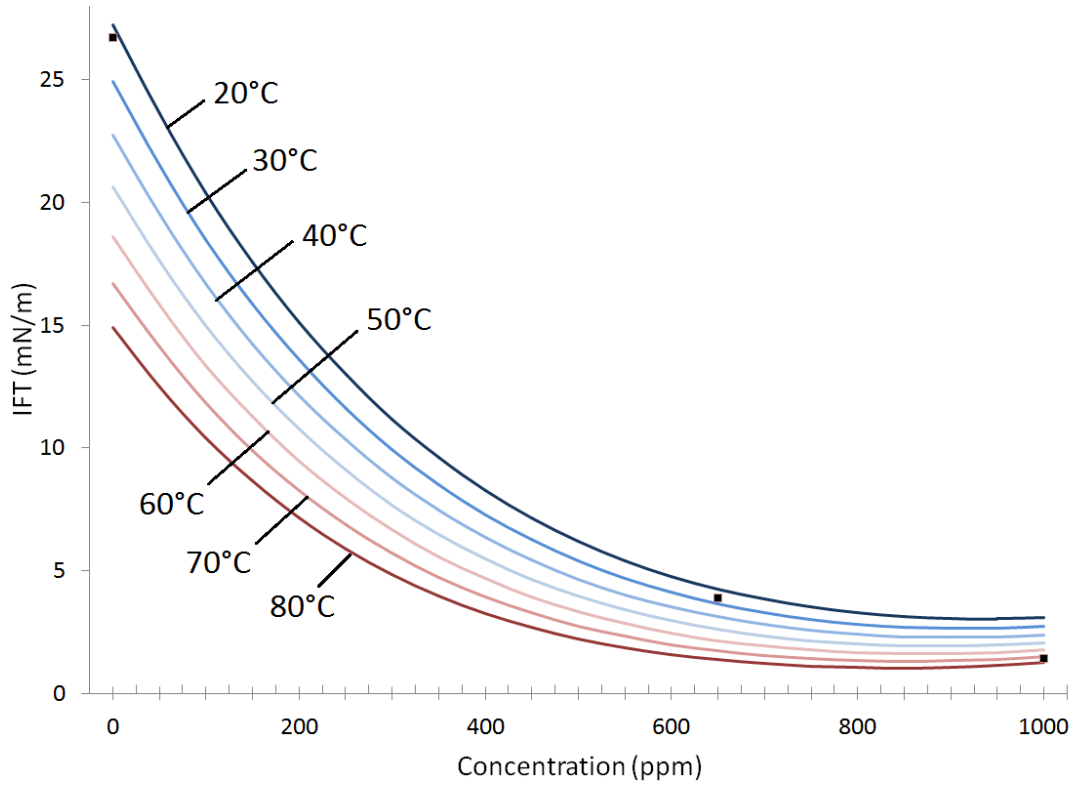

Figure 43: IFT vs. Al_2O_3 concentration for high pressure system (8000 psia)

4.4.5 Interaction Effect

The significant interaction effects on IFT are:

- Interaction between concentration and temperature (CT)
- Interaction between pressure and temperature (PT)
- Interaction between pressure and nanoparticle type (PN)

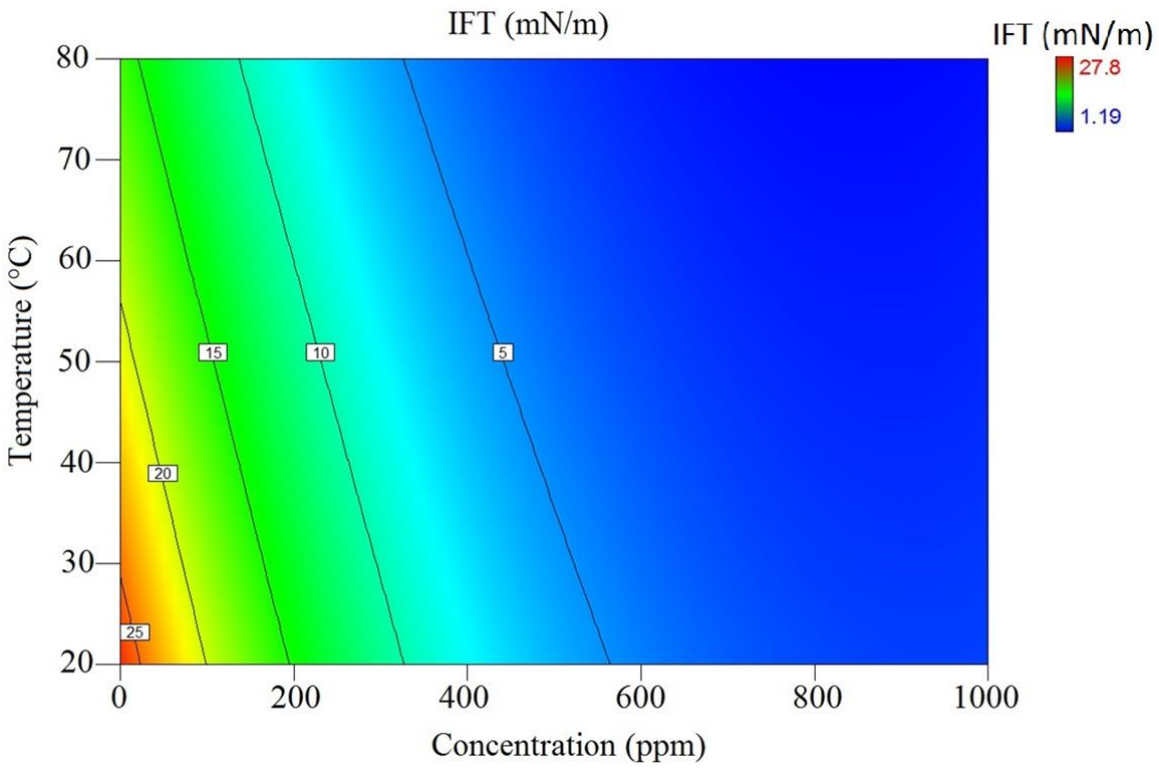

Figure 44: Interaction between concentration and temperature (4010 psia)

Figure 44 shows the contour plot for the effect of concentration×temperature (CT) interaction on interfacial tension. As shown in the figure below, a maximum IFT is obtained at the lowest temperature and concentration. It should be mentioned that to

draw this plot, the average value of IFT for silica and alumina nanoparticle cases was used. Also, the pressure is 4010 psia for this plot.

Figure 45 shows the PT (pressure and temperature) interaction effect on IFT for zero concentration (brine and oil) case. As shown in the figure, IFT decreases with increasing temperature and pressure. Therefore, it can be concluded that IFT is strongly temperature and pressure dependent at low concentrations of nanoparticles in the nanofluid. The highest IFT was obtained at low pressure, low temperature, and zero concentration of nanoparticles. By increasing the temperature (to 80°C) and the pressure (to 8000 psi) IFT reduced to approximately 16 (mN/m) in an approximately 36000 ppm brine without any nanoparticles. **Figure 46** shows the PT interaction effect on IFT for high concentration of nanoparticles (1000 ppm) in the nanofluid. **Figure 46** indicates that IFT has a very weak temperature and pressure dependency at high concentration of nanoparticles. The interfacial tension difference between high pressure-high temperature and low pressure-low temperature cases is approximately 2 (mN/m), which is considered to be insignificant. Therefore, the effect of concentration on IFT is the most important effect. In both **Figures 45** and **46**, the average value of IFT for alumina and silica nanofluid cases was used.

Since nanoparticle type is a qualitative factor, we are not able to plot the contour map for PN (pressure and nanoparticle type). However, the ANOVA table (**Table 21**) shows that

the p-value for PN interaction is 0.0627, which indicates that the effect of this interaction can be considered as insignificant. Overall, both the experimental results, and the predicted model show that silica nanoparticles are more effective in reducing IFT.

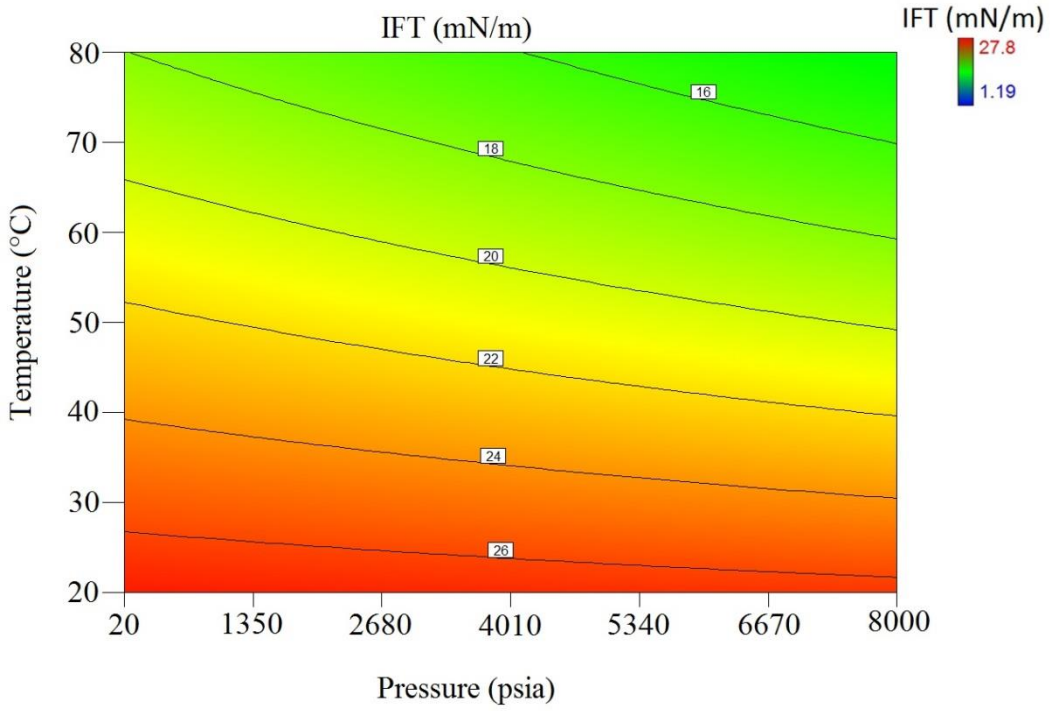

Figure 45: Interaction between pressure and temperature with no nanoparticles

The analysis of variance showed that concentration to the power of two (C^2) is also an important term in the model, which makes the IFT correlation nonlinear. **Figure 47** shows how interfacial tension behaves in a nonlinear fashion with respect to concentration. For example, using brine only (zero concentration of nanoparticles), by changing temperature from 20 to 80 °C IFT will decrease from approximately 26 mN/m to approximately 16 mN/m. However, at 1000 ppm concentration of nanoparticles, by

changing temperature from 20 to 80 °C, IFT remains almost constant (at a very low value due to high concentration of nanoparticles). Nanoparticles are able to reduce IFT between oil and water to a small value 2 mN/m. Our results are consistent with available literature at ambient condition (Roustaei et al. 2012). However, due to limited literature available studying IFT of nanofluid and oil at different pressure and temperature, we are not able compare our results with literature completely. It should be mentioned that the average value of IFT in terms of nanoparticle type was also used for this figure.

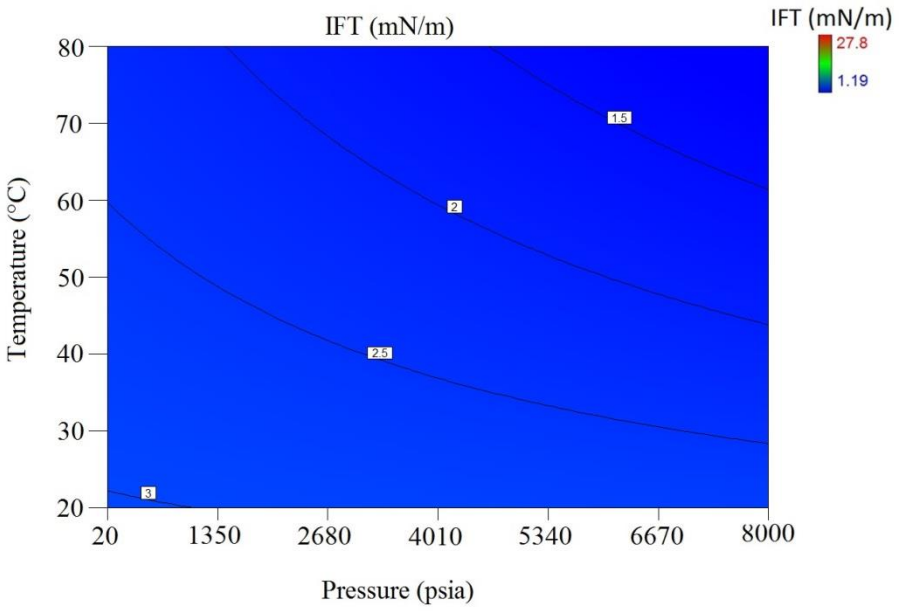

Figure 46: Interaction between pressure and temperature at high concentration of nanoparticles

In order to be able to compare the significance of all the effects in a single equation, we need to use all the factors at a similar scale. For each specific state of a factor, one coded value was assigned. Then, IFT was brought to an equation in terms of coded factors.

Table 23 shows the actual and coded values for the high and low levels of factors. The final correlation in terms of coded factors is shown below. The significant factors from most to least important are:

- Concentration (C)
- Concentration to the power of two (C^2)
- Temperature (T)
- Interaction between concentration and temperature (CT)
- Pressure (P)
- Interaction between pressure and temperature (PT)
- Interaction between pressure and nanoparticle type (PN)
- Nanoparticle type (N)

$$Coded\ value = \frac{actual\ value - mean}{half\ of\ range}$$ ----- **Eq. 14**

Table 23: Actual and coded values of variables

Factor	Actual	Coded
C: Concentration (ppm)	0	-1
	1000	+1
P: Pressure (psia)	20	-1
	8000	+1
T: Temperature (°C)	20	-1
	80	+1
N: Nanoparticle type	SiO_2	-1
	Al_2O_3	+1

$$\sqrt{IFT} = 2.040 - 1.550C - 0.140P - 0.400T + 0.041N + 0.180CT - 0.100PT + 0.050PN + 1.000C^2$$ ----- **Eq. 15**

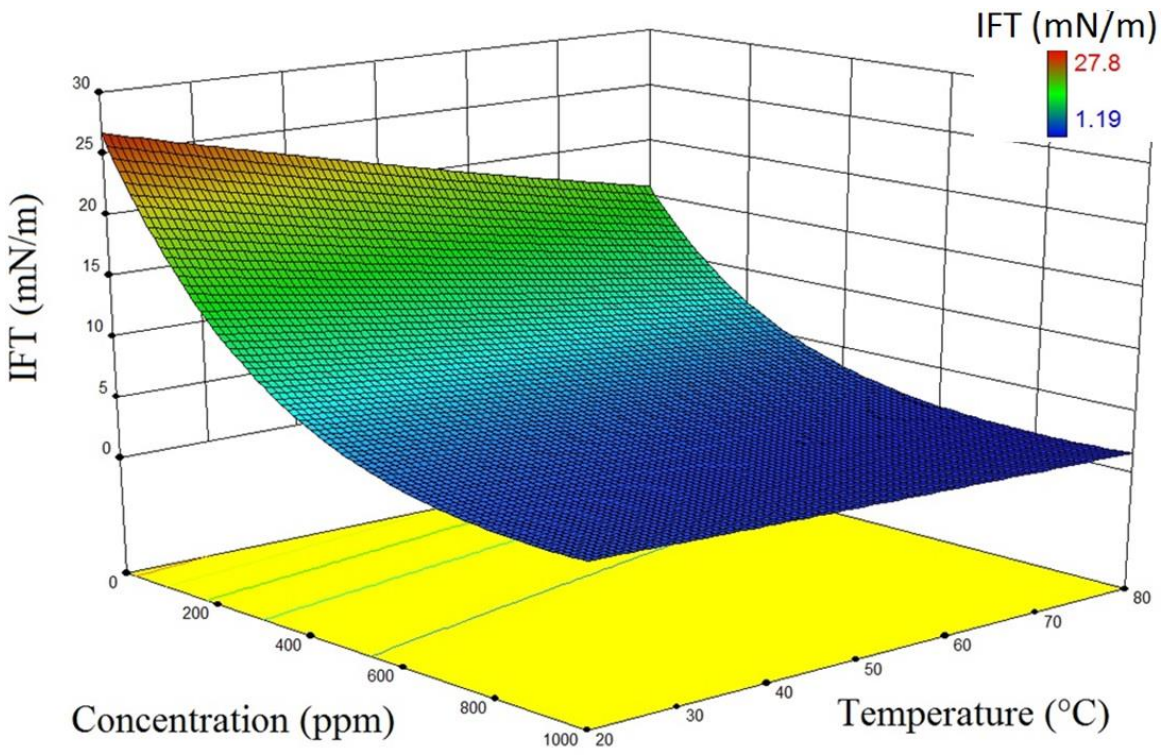

Figure 47: Nonlinear behavior of interfacial tension

4.5 Waterflooding Experiments

Oil saturation in the micromodel experiments can be measured at any time by image analysis. Standard image analysis using MATLAB® software was used to determine the oil recovery, which is discussed in **Appendix A**. The difference between the initial state of the black pixels and the final state was interpreted as oil recovery.

Figure 48 shows the oil recovery at different pore volumes injected. Comparing the recovery of alumina nanofluid and polymer solution (10 ppm) both with μ = 1.75 cP at

experimental conditions, we can see that the oil recovery for the alumina nanofluid is higher. Since the viscosity enhancement was not significant, the recovery improvement is thought to be due to IFT reduction using nanoparticles. Moreover, we can see that silica nanofluid with μ=1.06 cP but the lowest interfacial tension (will be discussed more) has the highest oil recovery. This higher oil recovery might be resulted from improvement of microscopic sweep efficiency. Nanoparticles have the ability to decrease the interfacial tension between oil and water and improving microscopic efficiency, which will be discussed in detail in IFT measurements section later. The recovery values used for the polymer 10 ppm case are the average value of test # 2 and 4. The standard deviation was measured to be 1.89% recovery according to recovery values measured for these two tests. The standard deviation is also shown in **Figures 48**. As shown in the figure, the recovery values for alumina, silica and DI water are outside of this standard deviation giving us confidence in the experimental results. As shown in the figure, the oil production profile for silica nanofluid is different than all other cases. Oil production is hindered before breakthrough in the silica nanofluid case. This might be due to emulsion generation in the form of oil/water. Production of these emulsions after breakthrough causes a big jump in oil recovery (**Figure 34**).

Figure 49 shows the ultimate oil recovery, oil recovery at breakthrough, and breakthrough time for different scenarios of injection. As shown in the figure, oil recoveries obtained for the alumina and silica nanofluids are approximately 8 and 11%

higher than the oil recovery by DI water injection respectively (17 and 23 % increase relative to DI waterflooding), showing a significant improvement of oil recovery. Alumina and silica nanofluids improved the recovery of polymer (10 ppm) injection by approximately 5 and 8% respectively (10 and 16 % increase relative to polymer flooding). The oil recovery of polymer (10 ppm) injection compare to DI water injection is approximately 3 % higher (6% increase relative to DI waterflooding), which is showing the effect of viscosity improvement of the injected fluid. However, it should be mentioned that the effect of IFT reduction is more significant.

As shown in **Figure 49**, injected fluids with the same viscosities have approximately similar breakthrough time. Moreover, breakthrough time was delayed significantly by injecting with half speed. This can be explained by the fact that more stable front movement can be obtained by lowering the injection flow rate. Comparing Tests 1 and 7, we can see that they both have approximately the same recovery at breakthrough. However, ultimate oil recovery is significantly higher for silica nanofluid case. This higher oil production after breakthrough might be due to emulsion generation using silica nanoparticles. A comparison between Tests 2, 4 and 8 shows that the effect of IFT reduction on the ultimate oil recovery is significant.

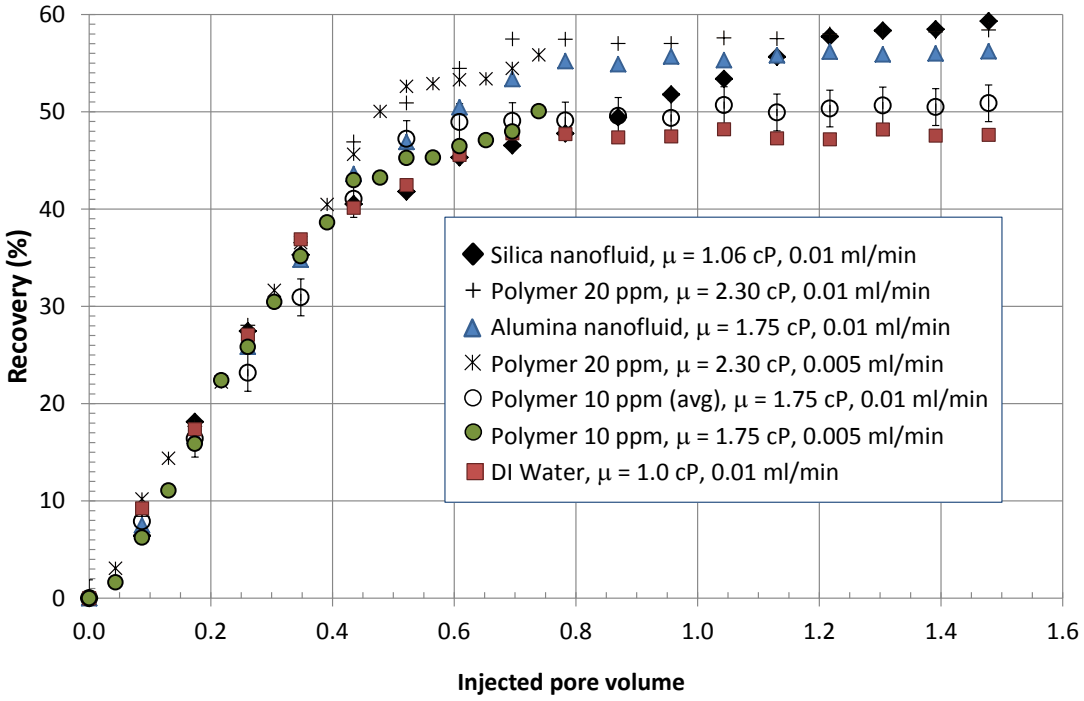

Figure 48: Oil recovery vs. injected pore volume

One replicate test was performed for the polymer (10 ppm) solution to have a better estimate of error in the experiments. The difference in recovery of the polymer (10 ppm) and polymer (10 ppm) replicate was approximately 2%. This difference in recoveries might be due to experimental errors or image analysis errors. An additional experiment at half flow rate was also performed to see the effect of flow rate on breakthrough time and ultimate recovery. Decreasing the injection flow rate causes a more stable front movement, which increases the breakthrough time significantly. However, ultimate recovery did not change by decreasing the flow rate.

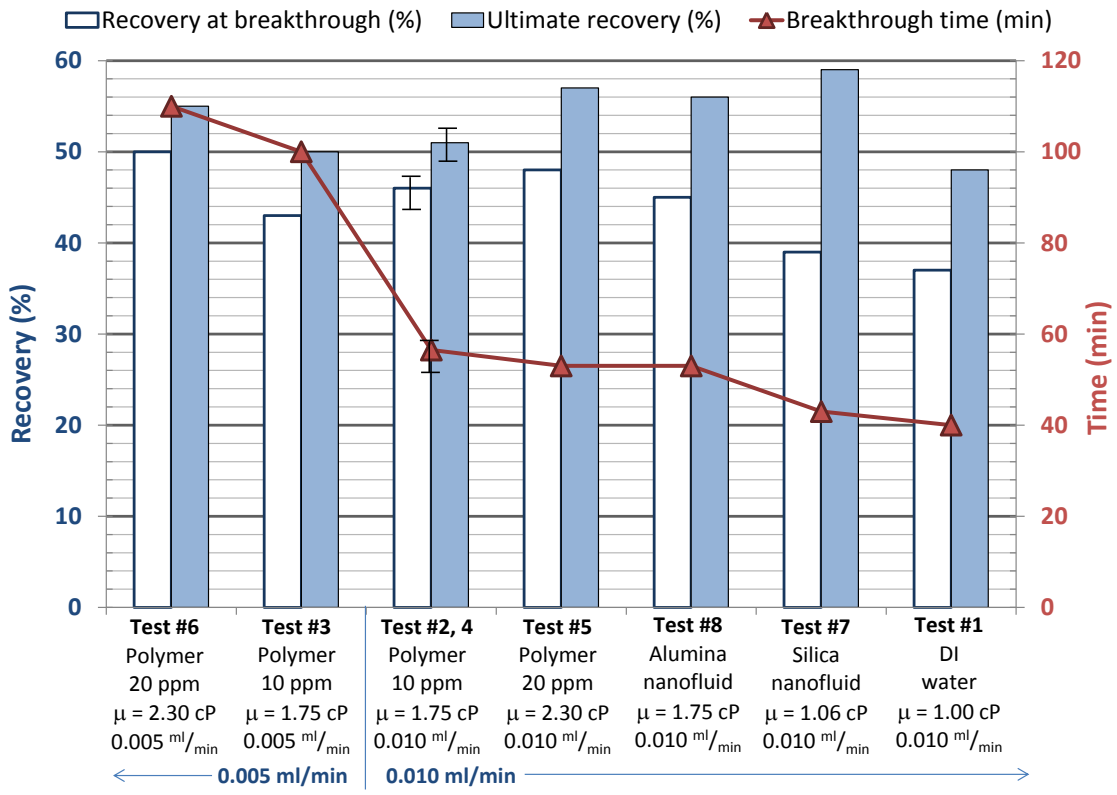

Figure 49: Ultimate recovery, recovery at breakthrough, and breakthrough time for the experiments

Overall, nanofluid injection has higher recovery compared to polymer/DI waterflooding. The fact that nanoparticles are active on the interface of oil and water might be the reason for this improvement. Therefore, we studied the interfacial tension of nanofluid/polymer solution/DI water with oil to better understand the surface activation by nanoparticles, which will be discussed in more detail. Mobility control might be another reason for enhanced oil recovery of nanofluid/ polymer injection over DI waterflood. In the next

section the viscosity measurements for nanofluid, polymer solution and DI water will be discussed more.

In the following sections it will be explained why we get higher oil recovery using nanoparticles (viscosity and IFT measurements).

4.5.1 Viscosity Measurements

As discussed before, nanoparticles are capable of increasing the viscosity of water. However, most of these viscosity measurements were conducted under fixed pressure and temperature. In order to understand the behavior of viscosity with respect to different factors and their interactions, we need to change all the factors at the same time. Response surface methodology (optimal design) was employed to investigate the effect of each factor: concentration of nanoparticles, pressure, temperature, nanoparticle type, and their interaction on the response (viscosity). A calibration experiment was performed using DI water to ensure that the results are accurate. The details of calibration experiment are discussed in **Appendix B**.

In this study, Design Expert Software® was used for the design of experiments. **Table 24** shows the 24 viscosity measurements based on optimal design. Concentration, pressure, and temperature are quantitative factors varying from 0 to 5 wt%, 20 to 8000 psia, and 20 to 80°C respectively.

Table 24: Viscosity measurements

Run	Concentration (wt%)	Pressure (psia)	Temperature (°C)	Nanoparticle type	Viscosity (cP) ± 0.01
*1	5.00	8000	55.4	Al_2O_3	0.78
*2	5.00	8000	55.4	Al_2O_3	0.80
*3	2.50	4010	50.0	SiO_2	0.66
*4	2.50	4010	50.0	SiO_2	0.66
5	0.00	4110	79.8	DI water	0.36
6	5.00	20	80.0	Al_2O_3	0.53
*7	2.50	4010	50.0	SiO_2	0.66
8	5.00	20	20.0	SiO_2	1.06
9	0.00	4848	22.4	DI water	0.86
10	5.00	4010	24.4	Al_2O_3	1.82
11	5.00	5207	79.8	SiO_2	0.40
*12	2.90	8000	80.0	Al_2O_3	0.40
13	1.85	20	33.8	SiO_2	0.81
14	0.00	8000	22.6	DI water	0.84
15	0.00	20	20.0	DI water	1.07
16	3.80	3611	61.6	Al_2O_3	0.74
17	5.00	8000	21.3	SiO_2	0.92
18	1.00	4010	38.0	Al_2O_3	0.75
*19	2.90	8000	80.0	Al_2O_3	0.43
20	1.43	20	61.7	Al_2O_3	0.51
21	0.00	8000	79.5	DI water	0.34
22	0.00	20	80.4	DI water	0.37
23	0.55	7880	42.5	SiO_2	0.57
24	5.00	4010	27.8	Al_2O_3	1.69

The VISCOlab PVT viscometer (manufactured by Cambridge Viscosity) was used for measuring the viscosity. A billet for the range of 0.25 to 5.00 cP was used for the experiments. After loading the pump, the system was set to the desired temperature and pressure. Before measuring any data, the system was bled through the relief valves to rid

the system of any air. Then, viscosity was measured under stable pressure and temperature conditions. After running each test, the system was flushed with an appropriate solvent to clean all the lines and fittings, and then vacuumed. Bias was avoided by performing the experiments in random order. As shown in the table, * indicates replicate runs. A standard deviation of 0.01cP was calculated based on the replicate values. The detail of standard deviation calculation will be discussed in **Appendix B**. The viscometer was calibrated using DI water. As shown in **Table 24**, the viscosity measured for the DI water at ambient condition was 1.07 cP (run #15), which is slightly different than the available data for the DI water viscosity in literature. This discrepancy might be due to experimental errors.

Table 25 shows the analysis of variance (ANOVA) results for the viscosity measurements. The prediction interval provides the upper and lower levels for 95% confidence level. The p-value represents the probability of the occurrence of a given event. When the p-value is less than 0.05 (1-95% confidence) the factor is considered significant. The analysis of variance is model dependent, so it is up to the user to suggest models that describe the data. We systematically tried and compared several different models (linear, quadratic, etc.) with the inclusion and elimination of higher order and interaction terms. The goal was to find the simplest model to best fit the results. The results of the ANOVA table demonstrate that all the individual factors have significant effect on viscosity (p-value < 0.05). Moreover, the interaction between concentration and

nanoparticle type and second order terms of pressure and temperature were shown to be important and should be considered in the model.

Table 25: Analysis of variance for viscosity measurements

Source	Sum of Squares	Mean Square	F Value	p-value
Model	2.320	0.330	359.11	<0.0001
Concentration (C)	0.160	0.160	176.93	<0.0001
Pressure (P)	0.023	0.023	25.09	<0.0001
Temperature (T)	1.840	1.840	1990.49	<0.0001
Nanoparticle type (N)	0.079	0.079	85.15	<0.0001
Concentration x Nanoparticle Type (CN)	0.069	0.069	74.98	<0.0001
Pressure^2 (P^2)	0.011	0.011	12.14	0.0021
Temperature^2 (T^2)	$4.323x10^{-3}$	$4.323x10^{-3}$	4.68	0.0416
Lack of fit	0.019	$1.096x10^{-3}$	3.26	0.0976

Figure 50 shows how the viscosity predicted by the model matches the actual experimental data. In an ideal situation (perfect model) the experimental points should be exactly on the 45° slope line. As shown in the figure, the data points fall very close to the 45° slope line, which confirms that lack of fit is not significant as it was shown in the ANOVA table.

Figure 51 and **52** show the effect of nanoparticles concentration on the viscosity. The black points are indicating the experimental measurements. **Figure 51** demonstrates that by increasing the concentration of alumina (Al_2O_3) nanoparticles in the DI water, the viscosity increases. It should be mentioned that 5 wt% nanoparticles can be considered as very high concentration. However, these high concentrations of nanoparticles were used

to qualitatively study the usage of nanoparticles for mobility control purposes. **Figure 52** shows that adding silica (SiO_2) nanoparticles to DI water does not change the viscosity significantly. Moreover, as shown in the figure, viscosity decreases with increasing temperature. The effect of pressure on the viscosity of nanofluid is slightly more significant at lower temperatures. In fact, the viscosity values at high temperature (80 °C) are similar for different states of pressure, which is showing the insignificance of pressure effect on viscosity at high temperature. Overall, the effect of temperature and concentration was found to be more significant on viscosity than the effect of pressure. The dashed lines indicate the 95% confidence interval bands for the predictive model.

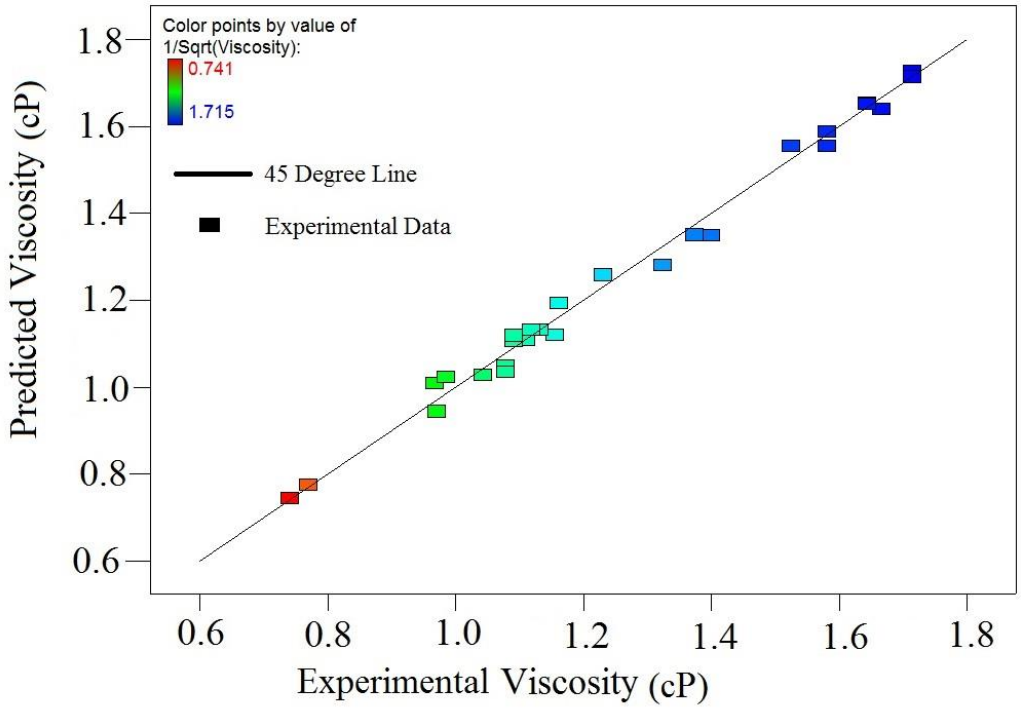

Figure 50: Predicted viscosity vs. experimental viscosity measurements

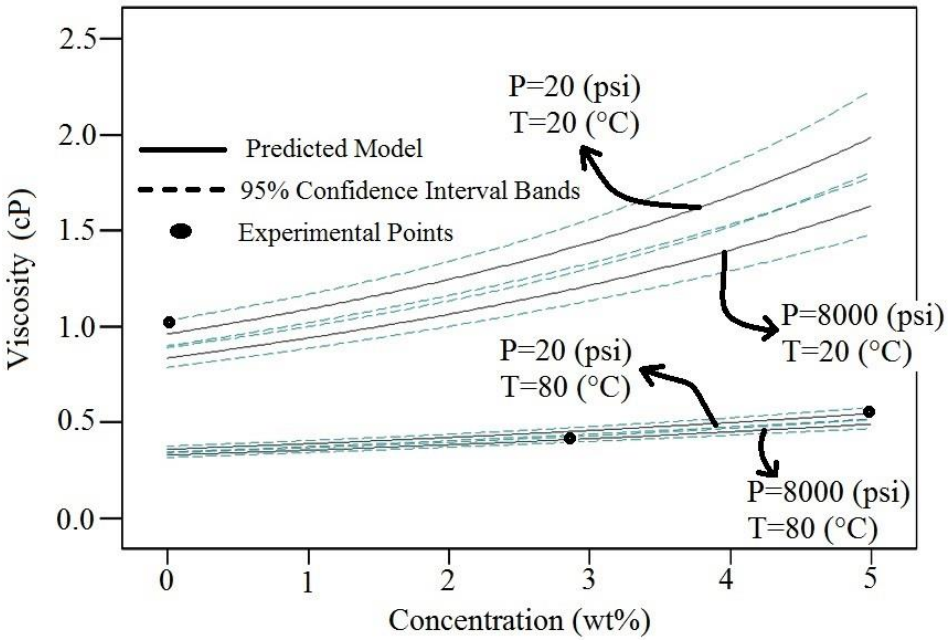

Figure 51: Effect of nanoparticles concentration on alumina (Al_2O_3) nanofluid viscosity

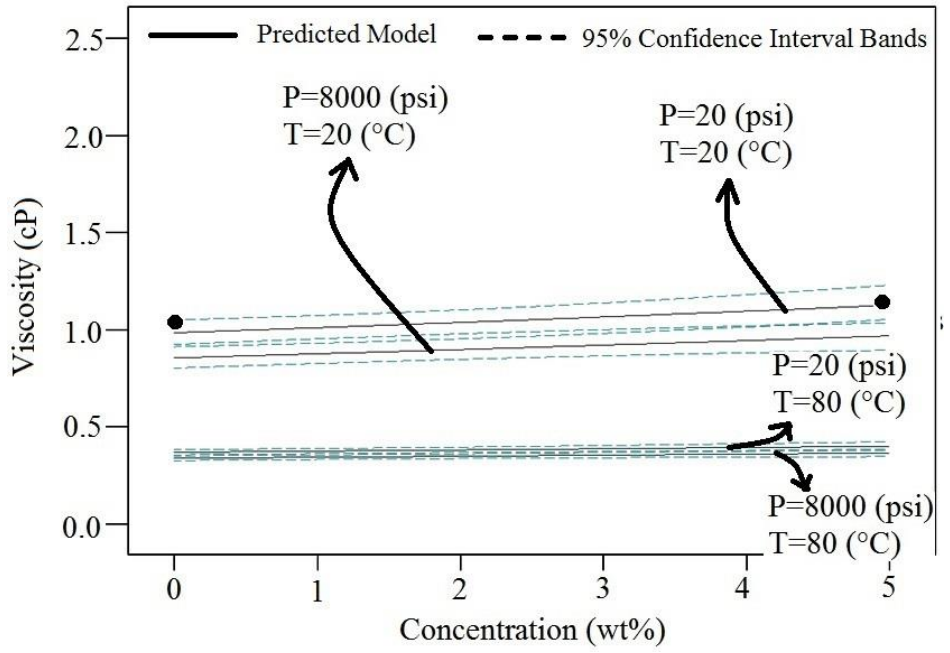

Figure 52: Effect of nanoparticles concentration on silica (SiO_2) nanofluid viscosity

Figure 53, **54**, **55** and **56** show the effect of interaction between pressure and temperature on the measured viscosity of nanofluid. As shown in the ANOVA table, the effect of second order terms of pressure and temperature are significant. We can see this non-linearity effect in the figures. Again, pressure is shown to have little effect. **Figure 54** indicates that viscosity behaves more non-linear while using alumina nanoparticles at higher concentration. Moreover, by looking at **Figure 54**, we can see that the maximum viscosity was obtained while using alumina nanoparticles at medium pressure, low temperature, and high concentration. For silica nanofluid increasing the concentration of nanoparticles in DI water does not affect the viscosity significantly. However, viscosity increases significantly by increasing the concentration of alumina nanoparticles in DI water. Increasing the concentration of alumina nanoparticles increases the effect of non-linearity behavior of viscosity (**Figure 53** and **54**). Overall, the model predicts that the viscosity of DI water can increase to a maximum value of approximately 2 cP using alumina nanoparticle. As shown in **Figure 55** and **56**, the viscosity behaves approximately linear for silica nanofluid. Moreover, by increasing temperature, viscosity decreases significantly. These Figures confirm that the effect of temperature and concentration on viscosity is significantly more than the effect of pressure.

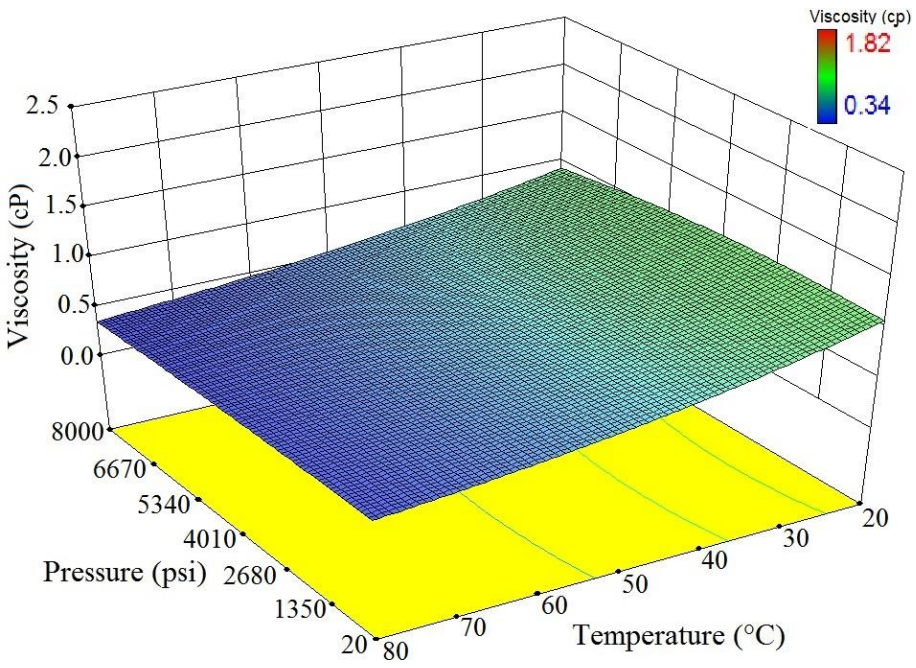

Figure 53: 3D map of viscosity vs. pressure and temperature (Al_2O_3, 1 wt%)

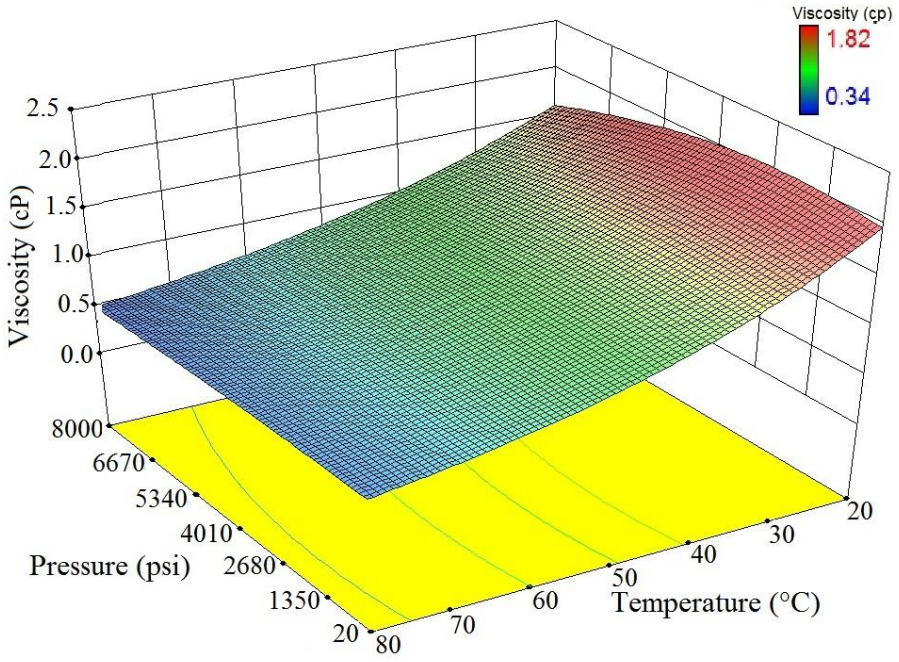

Figure 54: 3D map of viscosity vs. pressure and temperature (Al_2O_3, 5 wt%)

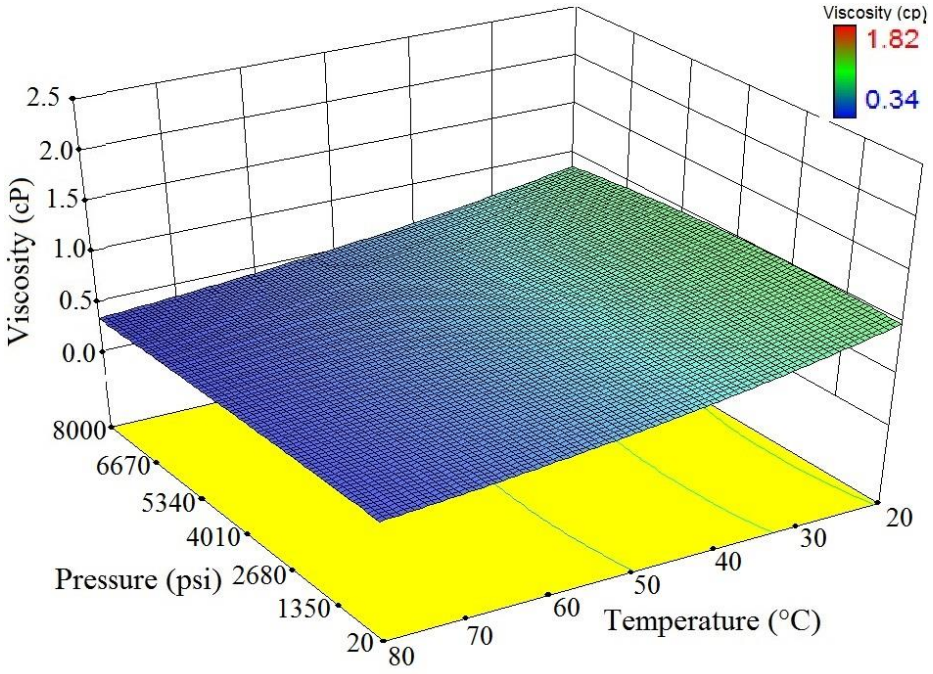

Figure 55: 3D map of viscosity vs. pressure and temperature (SiO_2, 1 wt%)

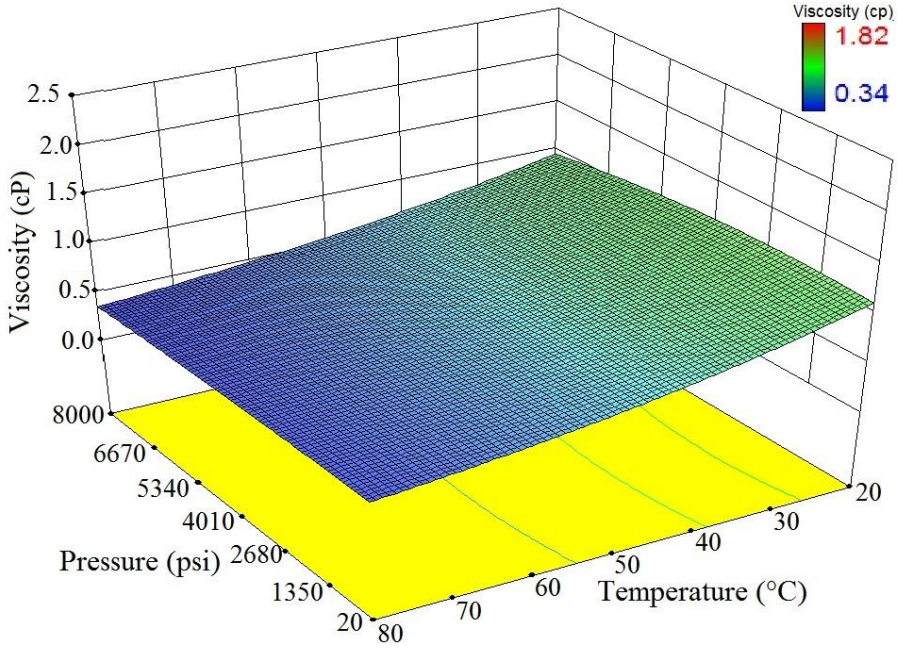

Figure 56: 3D map of viscosity vs. pressure and temperature (SiO_2, 5 wt%)

4.5.2 Interfacial Tension Measurements

As it was discussed, the results of waterflooding experiments indicated that oil recovery of nanofluid injection is higher than DI water/polymer injection. This higher oil recovery might be due to viscosity enhancement (as shown in section 4.5.1) or interfacial tension reduction. To this end, numbers of interfacial tension measurements were performed to show the ability of these specific nanoparticles in reducing the IFT between DI water and oil.

An Interfacial Tension Meter (IFT 700, manufactured by Vinci Technologies) was used to determine interfacial tension between the oil and DI water, polymer solution, and the nanofluid (liquid-liquid interface) at ambient (experimental) conditions. The pendant drop method was used for IFT measurements. An oil drop was created and put in contact with the nanofluid in a cell. A camera connected to a computer records the shape of the oil droplet to derive the interfacial tension. The results of IFT measurements are tabulated in **Table 26** where the value reported is the average value for approximately 70 runs. A calibration experiment was performed using air/DI water/toluene to ensure that the results are accurate. The details of calibration experiment are discussed in **Appendix B**. The standard deviation was calculated for each test separately. The procedure of measuring standard deviation is discussed in **Appendix B**. As shown in the table, interfacial tension decreases significantly by adding nanoparticles to DI water. Moreover, the minimum IFT was obtained while using silica nanoparticles (6.56 mN/m). The results indicate that

nanoparticles are active at the interface of oil and water, which help to improve the microscopic sweep efficiency of waterflooding.

Table 26: Interfacial measurements

Fluid	IFT (mN/m)
DI Water and Oil	29.00
Silica nanofluid (5 wt%) and Oil	6.56 ± 1.06
Alumina nanofluid (5 wt%) and Oil	12.71 ± 0.35
Polymer Solution (10 ppm) and Oil	21.47 ± 1.30

4.5.3 Capillary Number Analysis

As it was mentioned before in **Eq. 7**, capillary number (dimensionless) is the ratio of viscous forces over interfacial tension.

$$N_C = \frac{Viscous\ forces}{Capillary\ forces} = \frac{v\mu}{\gamma}, \text{ ----- Eq. 7}$$

The results of capillary number calculation are tabulated in **Table 27**. As shown in the table, the most significant improvement was observed in silica nanofluid injection ($7.01*10^{-9}$). The velocity was simply calculated dividing the flow rate over the average cross sectional area of the micromodel. The average depth of 160 µm was calculated (based on areal porosity and pore volume). Injecting polymer (10 ppm) with the flow rate of 0.01 (ml/min) has more favorable capillary number compared to capillary number of polymer injection with half speed (0.005 ml/min). The capillary number of polymer injection can be improved to approximately twice using alumina nanofluid with the same viscosity. This improvement is due to IFT reduction using alumina nanoparticles.

Nanoparticles are shown to be effective in terms of capillary number improvement, since they are able to increase the viscosity and reduce IFT at the same time. It should be noted that the Darcy velocity is used, obtained from the flow rate and the cross sectional area.

Table 27: Capillary number for different scenarios of injection

Injected Fluid	Viscosity (Pa.s)	Flow rate (m^3/s)	Velocity (m/s)	Interfacial tension (N/m)	Capillary number
DI water	0.00100	$1.67*10^{-10}$	$3.78*10^{-7}$	0.02900	$5.61*10^{-9}$
Silica nanofluid	0.00106	$1.67*10^{-10}$	$3.78*10^{-7}$	0.00656	$2.63*10^{-8}$
Alumina nanofluid	0.00175	$1.67*10^{-10}$	$3.78*10^{-7}$	0.01271	$2.24*10^{-8}$
Polymer, 10 ppm	0.00175	$1.67*10^{-10}$	$3.78*10^{-7}$	0.02147	$1.33*10^{-8}$
Polymer, 10 ppm (half speed)	0.00175	$8.33*10^{-11}$	$1.89*10^{-7}$	0.02147	$6.63*10^{-9}$

5. Safety and Environmental Prospects

5.1 Potential Hazards

The micromodel system has the potential to become a pressurized system, and therefore uncontrolled discharges of the fluid could cause serious injury and/or death to personnel in the immediate area. Also, the micromodel and some syringes are constructed of glass, and therefore have the potential to crack and/or splinter and/or eject sharp glass sharps if it is damaged by impact or over pressurization. This could cause serious injury and/or death to personnel in the immediate area. The system cannot be pressurized over 50 psi. The cleaning procedure for the system involves the use of a toluene and acetone solvent. These chemicals can pose health risks and special precautions and handling techniques must be employed when dealing with these solvents. It should be mentioned that nanoparticles may cause health and safety issues due to inhalation. The surfactants, salts, and oils also may cause health and safety issues.

The IFT meter setup has the potential to become a pressurized system, and therefore uncontrolled discharges of the fluid could cause serious injury and/or death to personnel in the immediate area. The cleaning procedure for the system involves the use of a toluene and acetone solvent. These chemicals can pose health risks and special precautions and handling techniques must be employed when dealing with these solvents.

It should be mentioned that nanoparticles may cause health and safety issues due to inhalation. The surfactants, salts, and oils also may cause health and safety issues.

5.2 Precautions

- Ensure the system is assembled as designed in the P&ID. Any alterations may pose additional health and safety risks which are not stated here.
- Ensure that pressure tests, up to 40 psi, are conducted as directed by the Pressure Systems – Hazard's Description and Testing Procedure.
- Ensure that the pressure in the system never exceeds 40 psi.
- Ensure that the toluene, acetone, nanoparticles, surfactants, salts, and oil being used is properly stored in either the fume hood or the ventilated cabinets below the fume hood. Large quantities of oil, toluene, and acetone should be stored in the fire cabinets while not being used.
- Ensure that proper toluene gloves and breathing masks are used whenever toluene is handled.
- Ensure that proper nano rated gloves and breathing masks are used whenever nanoparticles are handled.

All safety precautions mentioned previously for micromodel experiments are applicable for other experiments (viscosity and IFT measurements) as well. Safety goggles, lab coats, safety shoes, nitrile gloves when handling sample, toluene gloves when handling

toluene, and breathing mask when handling toluene, acetone or nanoparticles are required PPE.

5.3 Training

The operation or execution of the procedure requires the user to be trained in, the following:

- Tube Fittings – Assembly Procedure
- Compressed Gas (If dealing with gas phases other than air)
- Solvent Handling

5.4 Personal Protective Equipment

- Safety goggles
- Lab coats
- Safety Shoes
- Nitrile gloves when handling sample
- Toluene gloves when handling toluene
- Breathing mask when handling toluene, acetone or nanoparticles

6. Conclusions and Recommendations

Nanotechnology has found widespread application in a diverse range of industries. Researchers are now investigating whether nanotechnology can be applied to enhance oil recovery (EOR). The goal of enhanced oil recovery (EOR) is to manipulate the fluid-fluid properties and fluid-rock properties between the injected fluid and the residual oil phase to improve recovery efficiency. Water enhanced with nanoparticles (nanofluids) has recently gained research interest for enhanced oil recovery because of the possible physical and chemical properties imparted by the nanoparticles. The application of nanofluids in enhanced oil recovery is strongly dependent on the resulting nanofluid properties.

In this study, nanoparticles were added to the water phase and injected into two dimensional glass (WAG injection) and PMMA (waterflooding) micromodels to study the effect of the nanoparticles qualitatively and quantitatively at low pressures. Silicon oxide (SiO_2) and aluminum oxide (Al_2O_3) nanoparticles, at different concentrations, were dispersed in the brine and injected as the water phase in WAG followed by air as the gas phase. Response Surface Methodology (RSM) was used to investigate the effect of the factors and interactions between the factors on oil recovery. The results from the micromodel studies indicate that adding a small amount of nanoparticles to the water can

enhance residual oil recovery. Fluid characterization experiments were performed to better understand the mechanism of oil recovery using nanoparticles.

Adding nanoparticles to the injected water has been shown to decrease IFT. However, the interfacial tension under different ranges of pressure and temperature had not previously been defined. In this study, silicon oxide (SiO_2) and aluminum oxide (Al_2O_3) nanoparticles, at different concentrations, were dispersed in brine and the IFT between the nanofluid and the oil phases measured. Response Surface Methodology (RSM) was used to investigate the effect of the type and concentration of the nanoparticles, pressure (20 to 8000 psi), and temperature (20 to 80 °C). Further, the effect of interactions between the factors on IFT was also studied. Adding a small amount of nanoparticles to brine can reduce the IFT between brine and oil, thus enhancing oil recovery. Some of the important results of WAG and IFT experiments are listed below:

- The addition of a small amount of nanoparticles to the brine enhanced oil recovery by 15%- 20%. This is potentially due to a reduction in the interfacial tension, which is consistent with previous studies.
- The following factors have a statistically significant effect in the regression model of oil recovery:
    - Concentration of nanoparticles, specifically the square root of the concentration and concentration

- Type of nanoparticles
- Interaction between the concentration and the type of nanoparticles

- Silica nanoparticles are more efficient than alumina nanoparticles in terms of oil recovery. The higher oil recovery during silica nanofluid injection may be due to emulsion generation, which was only observed while using silica nanoparticles.
- The results of interfacial tension measurements indicate that both silica and alumina nanoparticles reduced the IFT of oil-brine system significantly by a factor of 85% and 90% for alumina and silica nanofluid respectively (at a concentration of 500 ppm).
- The model predicts a maximum oil recovery of ~65% while using silica nanoparticles (SiO_2) in brine with a concentration of ~600 - 700 ppm of SiO_2 nanoparticles.
- The following factors have significant effect on IFT:
  - Concentration (C), pressure (P) , temperature (T), and nanoparticle type (N)
  - Interactions: CT, PN, and PT
  - $(Concentration)^2$
- Minimum IFT was obtained at:
  - High concentration of nanoparticles in brine
  - High pressure

    - High temperature
- The effect of WAG ratio on oil recovery showed to be insignificant for these particular set of experiments. It is worth mentioning that only WAG ratios of 1:1 and 1:2 were examined.
- Overall, adding a small amount of nanoparticles to the brine reduced IFT significantly, thus enhancing oil recovery.

Is IFT reduction the only mechanism enhancing oil recovery? The next step toward this experimental work was to perform further experimental work to see if there are other mechanisms enhancing oil recovery. The research question asked is whether oil recovery using nanoparticle enhanced water is due to a more favorable mobility ratio (increased water phase viscosity) or is it due to the effect of the enhanced surface chemistry? We examine the role of increased viscosity of the water phase on oil recovery using nanoparticle enhanced water and polymer enhanced water with similar viscosity (waterflooding) in addition to the WAG experiments. First, the nanoparticle enhanced water is characterized. A statistical design of experiments technique, Response Surface Methodology, is used to investigate the effect of the type of nanoparticles (silicon oxide and aluminum oxide nanoparticles), concentration of the nanoparticles, pressure, and temperature on viscosity. The effect of interactions between the factors on viscosity is also studied. Second, the viscosity measurement results are used to plan micromodel and coreflooding laboratory scale enhanced oil recovery experiments at low pressure and

temperature conditions. The results can be used to help elucidate the role of increasing viscosity versus surface chemistry on oil recovery.

The results of this micromodel waterflooding experiments show that nanoparticle have the ability to increase oil recovery by improving both the microscopic and macroscopic sweep efficiencies. The results of viscosity measurements demonstrated that alumina nanoparticles can increase the viscosity of deionized water. Interfacial tension experiments show how the surface chemistry plays an important role when using nanoparticles as an additive agent to water for EOR purposes. The results of IFT measurements indicate that IFT between oil and DI water can decreases from 29 to 6.56 and 12.71 for silica (5 wt%) and alumina (5 wt%), respectively. The results of micromodel experiments show that this IFT reduction causes higher oil recovery of nanofluid injection in comparison to polymer injection with the same viscosity. Oil recoveries using polymer injection with concentrations of 10 and 20 ppm were 3 and 9% (6 and 19% increase relative to DI waterflooding) higher respectively than oil recovery using DI water injection, which shows the effect of viscosity improvement on accelerating the oil production. The recoveries obtained from silica and alumina nanofluid injection were also higher than the recovery of DI water injection by 11 and 8% respectively (23 and 17 % increase relative to waterflooding). More investigation is required but surface chemistry does seem to play a role in oil recovery using nanofluids. This experimental work shows that nanoparticles are very promising for EOR purposes

due to their specific chemical and physical properties, and the fact they have the ability to improve oil recovery through viscosity improvement and surface chemistry. Overall, the effect of IFT reduction shown to be more significant than viscosity improvement in these specific set of experiments. It should be mentioned that all micromodel experiments were performed at ambient conditions (room temperature and ambient pressure).

6.1 Recommendations for Future Work

The following investigations are suggested to better understand the application of nanotechnology:

- Deeper understanding of how nanoparticles work in EOR (nanotechnology fundamentals).
- Performing economic analysis to capture the feasibility of nano-EOR techniques in field scale.
- As this study was more a qualitative pore scale research, investigation at the core scale, and analytical and numerical modeling of nano-EOR techniques is required to better understand the EOR mechanisms using nanoparticles.
- Conducting the WAG micromodel experiments in high pressure to investigate the effect of miscibility on oil recovery.
- Using different types of gas phase such as propane in the WAG experiments.

- Investigating the effect of pressure, temperature, slug size, pH, salinity, and their interaction with nanoparticle concentration on the efficiency of oil recovery in the WAG micromodel experiments.
- Using different types of micromodels to investigate the effect of factors such as wettability and pore size distribution.
- Investigating other types of nanoparticles.
- Investigating the effect of using nanoparticles on creating stabilized foam.
- Using different types of oil.
- Scaling up the Nano-EOR experimental data to reservoir conditions.
- Comparing the experimental results to simulation results (if any).
- Investigating gas-liquid interfacial tension. For example, measuring IFT between nanofluid and air.
- Introducing other factors such as salinity and pH in the IFT and the viscosity experiments
- Investigating other types of nanoparticles, and their effect on IFT between oil and nanofluid, and viscosity of nanofluid.
- Changing the oil properties such as API gravity, oil composition, and viscosity, to determine their relationship with IFT.

Appendix

A. Image Analysis

A.1 Micromodel Experiments

Oil saturation in the micromodel experiments can be measured at any time by image analysis. Standard image analysis using Matlab software® was used to determine the oil recovery. The difference between the initial state of the black pixels and the final state was interpreted as oil recovery. A number was assigned to each color from 0 (black) to 250 (white). The range between 0 to 150 was considered as oil as per the software recommendations. By summing up the number of pixels between 0 to 150, the oil saturation can be calculated. Oil recovery was defined as:

$$Oil\ recovery\ (\%) = \left[\frac{initial\ oil\ saturation - final\ oil\ saturation}{initial\ oil\ saturation}\right] 100\% \text{ ----- } \mathbf{Eq.\ 9}$$

First, the pictures need to be cropped at the same size. It is very important to use the same cropping path for all pictures. **Figure 57** to **74** shows the cropped pictures of the micromodel experiments from time 0 to 170 with the time interval of 10 minutes. These photos were taken during the waterflooding experiments using silica nanofluid (5 wt%) as the fluid injection. Second, the brightness and contrast of the photos need to be adjusted to the same value. Then, Matlab code will be used to change the photos to black and white. Finally, the number of black pixels will be calculated according to black and white

photos. The number of black pixels for time 0 is the initial oil saturation. **Table 28** shows the procedure of oil recovery measurements.

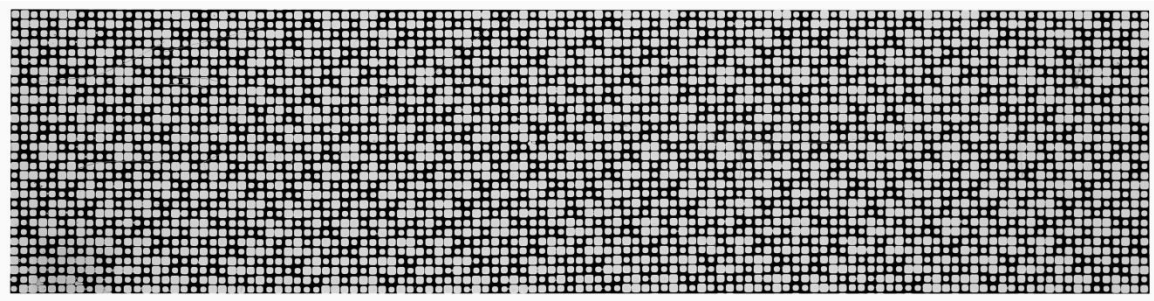

Figure 57: Silica nanofluid micromodel injection at t = 0 (min)

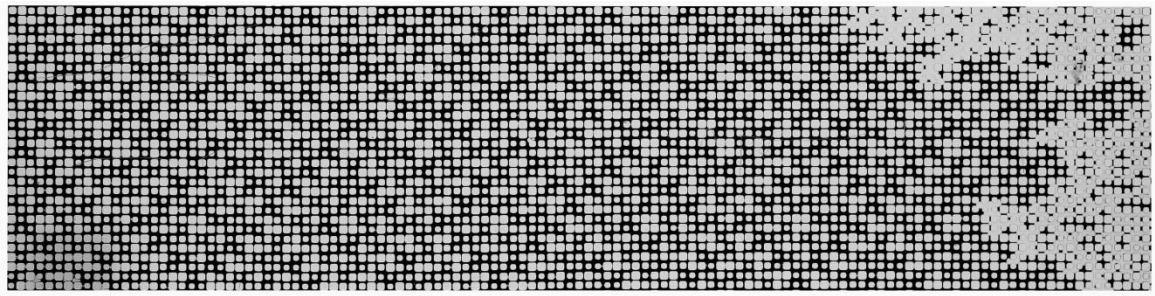

Figure 58: Silica nanofluid micromodel injection at t = 10 (min)

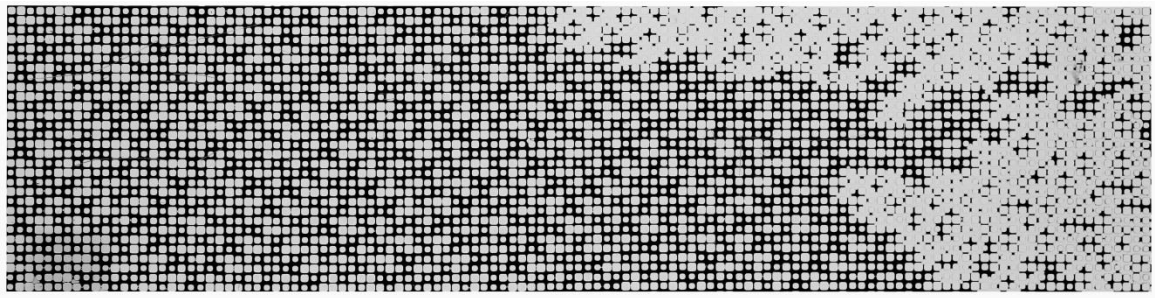

Figure 59: Silica nanofluid micromodel injection at t = 20 (min)

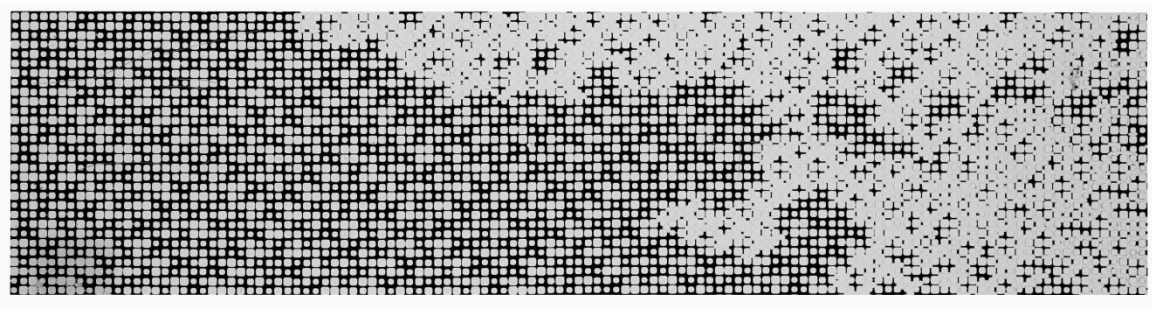

Figure 60: Silica nanofluid micromodel injection at t = 30 (min)

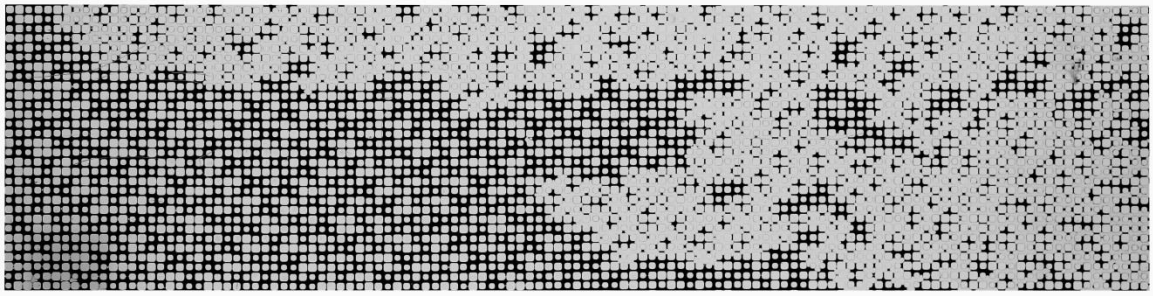

Figure 61: Silica nanofluid micromodel injection at t = 40 (min)

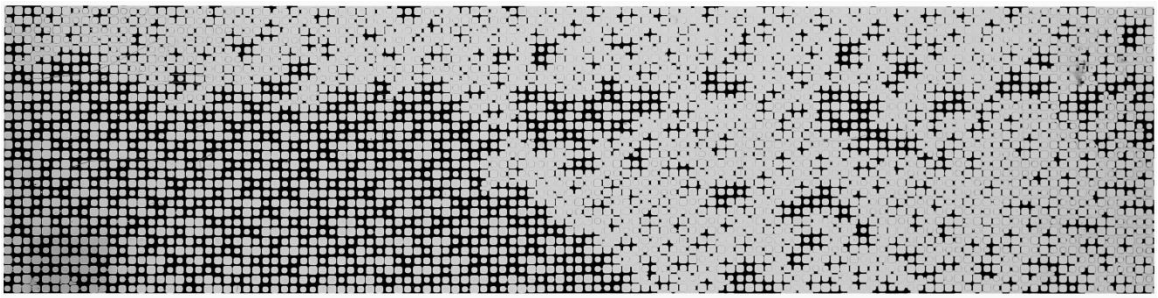

Figure 62: Silica nanofluid micromodel injection at t = 50 (min)

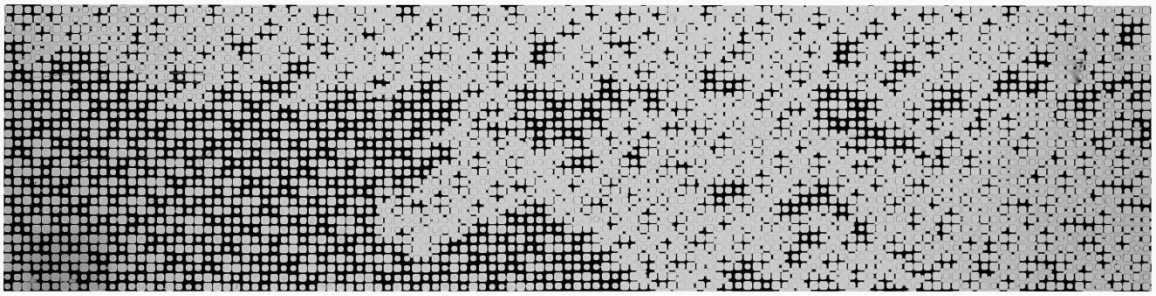

Figure 63: Silica nanofluid micromodel injection at t = 60 (min)

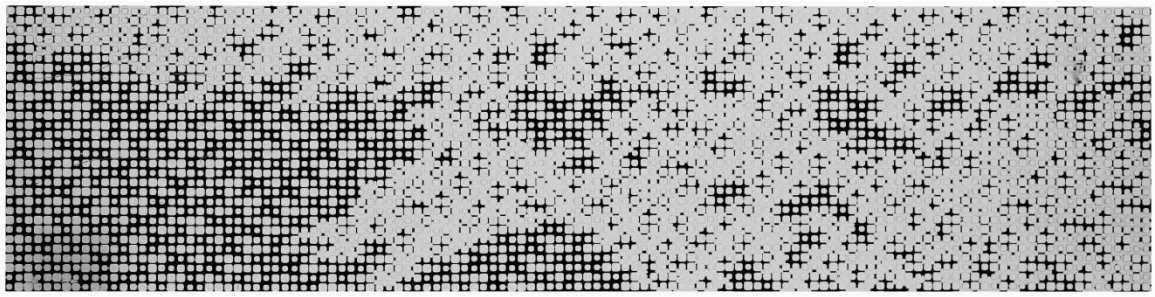

Figure 64: Silica nanofluid micromodel injection at t = 70 (min)

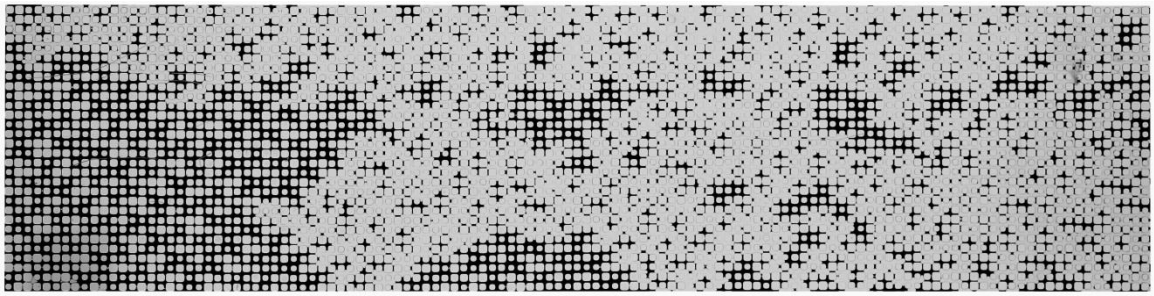

Figure 65: Silica nanofluid micromodel injection at t = 80 (min)

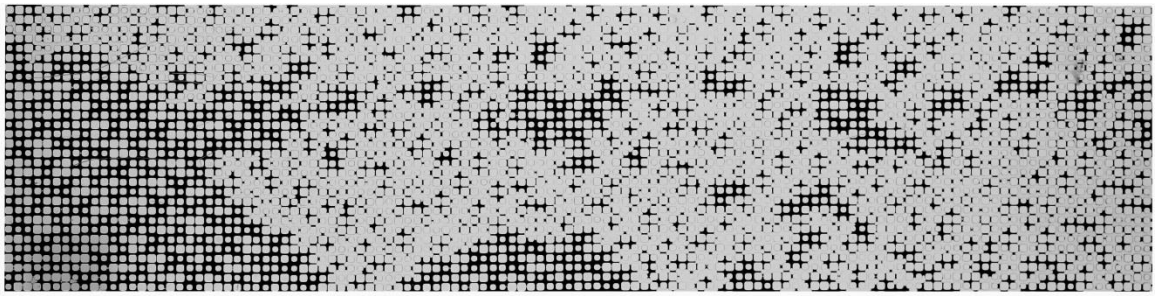

Figure 66: Silica nanofluid micromodel injection at t = 90 (min)

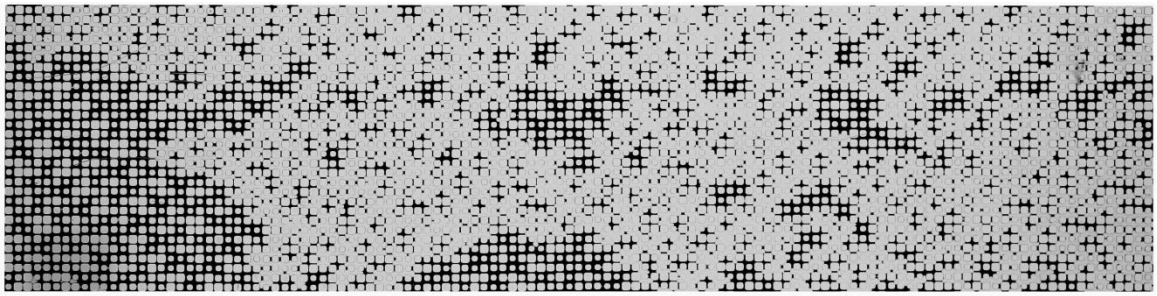

Figure 67: Silica nanofluid micromodel injection at t = 100 (min)

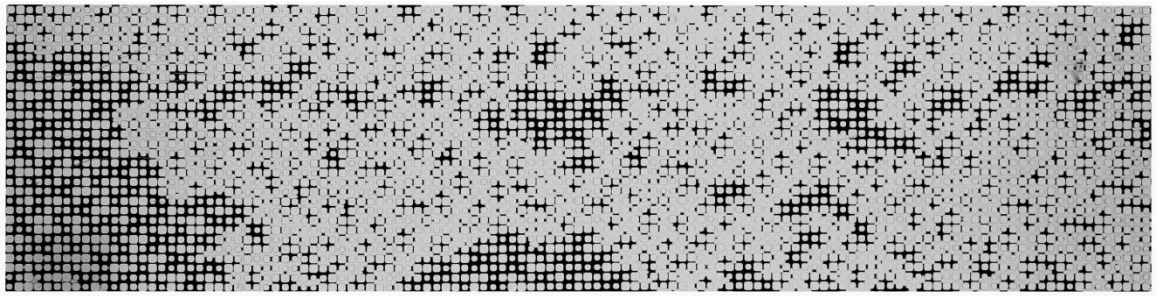

Figure 68: Silica nanofluid micromodel injection at t = 110 (min)

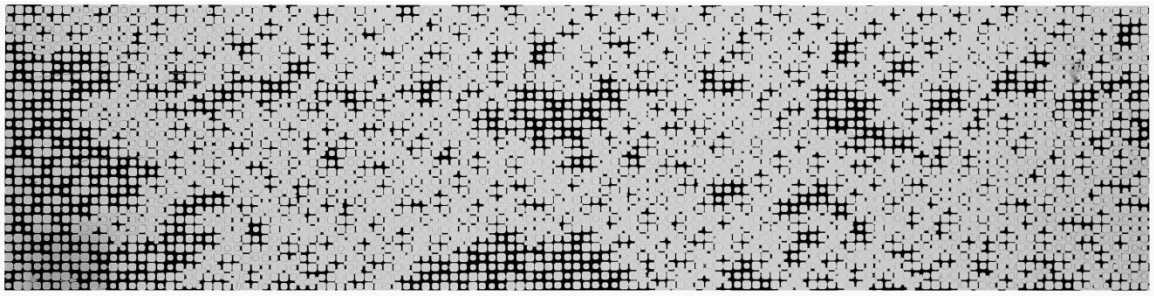

Figure 69: Silica nanofluid micromodel injection at t = 120 (min)

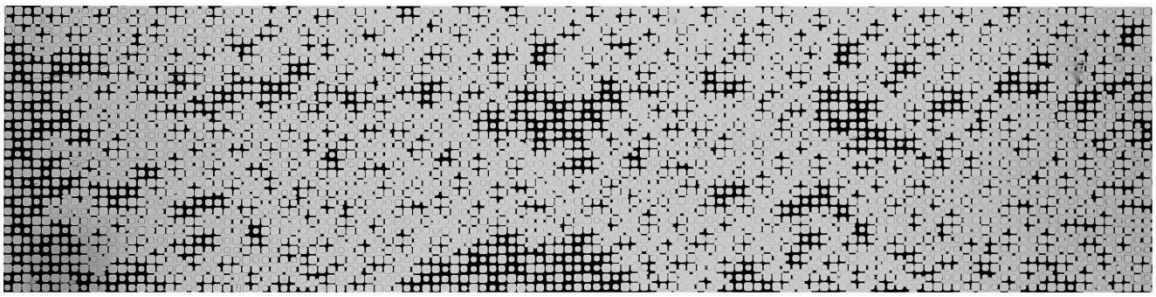

Figure 70: Silica nanofluid micromodel injection at t = 130 (min)

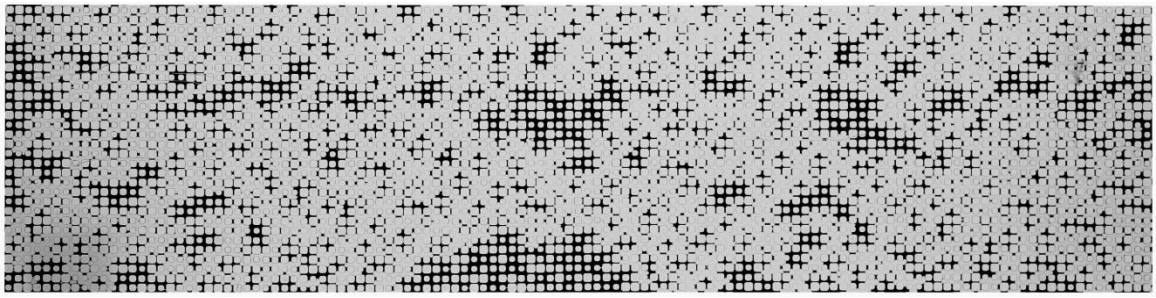

Figure 71: Silica nanofluid micromodel injection at t = 140 (min)

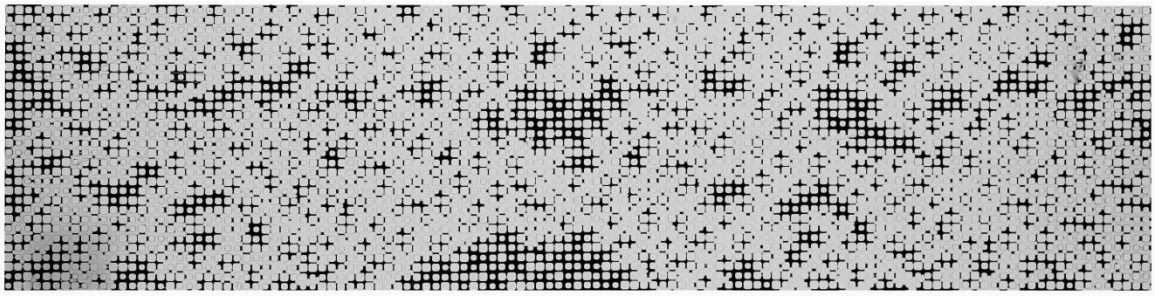

Figure 72: Silica nanofluid micromodel injection at t = 150 (min)

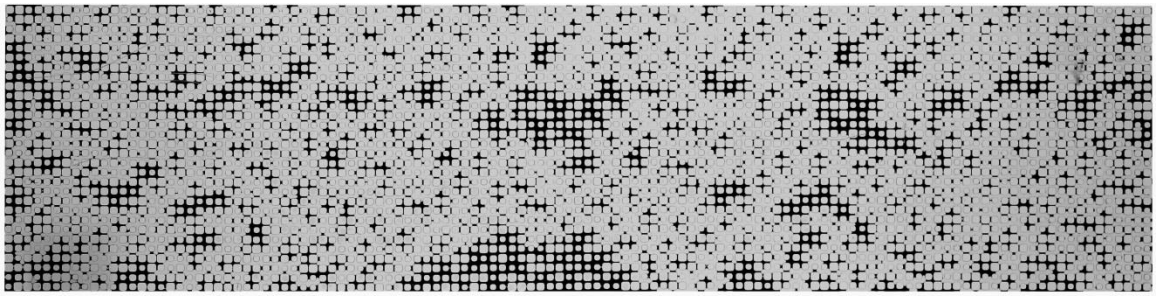

Figure 73: Silica nanofluid micromodel injection at t = 160 (min)

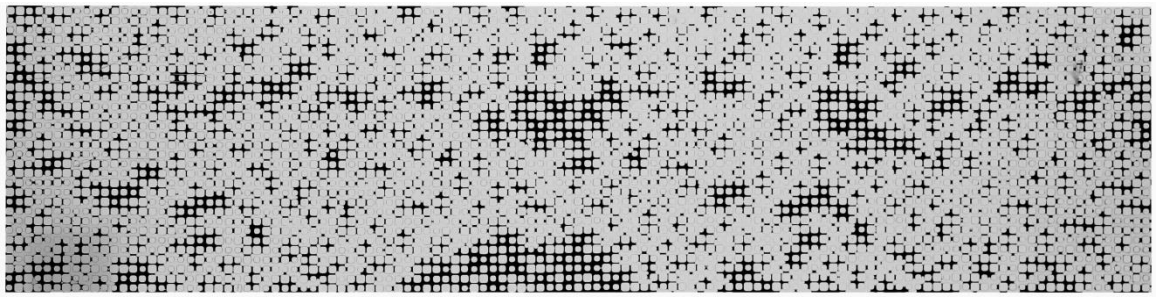

Figure 74: Silica nanofluid micromodel injection at t = 170 (min)

Table 28: Oil recovery measurements by image analysis

Time (min)	# of black pixels	Oil recovery	Oil recovery (%)
0	2437797	0.000000	0.00
10	2281182	0.064244	6.42
20	1996119	0.181179	18.12
30	1768299	0.274632	27.46
40	1577744	0.352799	35.28
50	1450162	0.405134	40.51
60	1419025	0.417907	41.80
70	1333490	0.452994	45.30
80	1303470	0.465308	46.53
90	1273493	0.477605	47.76
100	1233246	0.494115	49.41
110	1175838	0.517664	51.77
120	1136488	0.533805	53.38
130	1080949	0.556588	55.66
140	1030622	0.577232	57.72
150	1015486	0.583441	58.34
160	1012546	0.584647	58.47
170	991806	0.593155	59.32

B. Error Analysis

B.1 Viscosity Measurements

The viscosity measurement device measures the viscosity for a given time interval. The software calculates the standard deviation of measurements for a certain fluid sample. It is recommended to report the viscosity when the standard deviation is smaller than 1 percent. **Figure 75** shows an example output photo of viscosity measurement software. This photo is for viscosity measurements of silica nanofluid (2.5 wt%) at temperature of 50 °C and pressure of 4010 psi. As shown in the figure, the standard deviation (blue

curve) is updating at any time. A significant standard deviation fluctuation can be seen at early time. However, the standard deviation is stabilizing eventually. When 1 percent standard deviation was reached, the viscosity value is recorded.

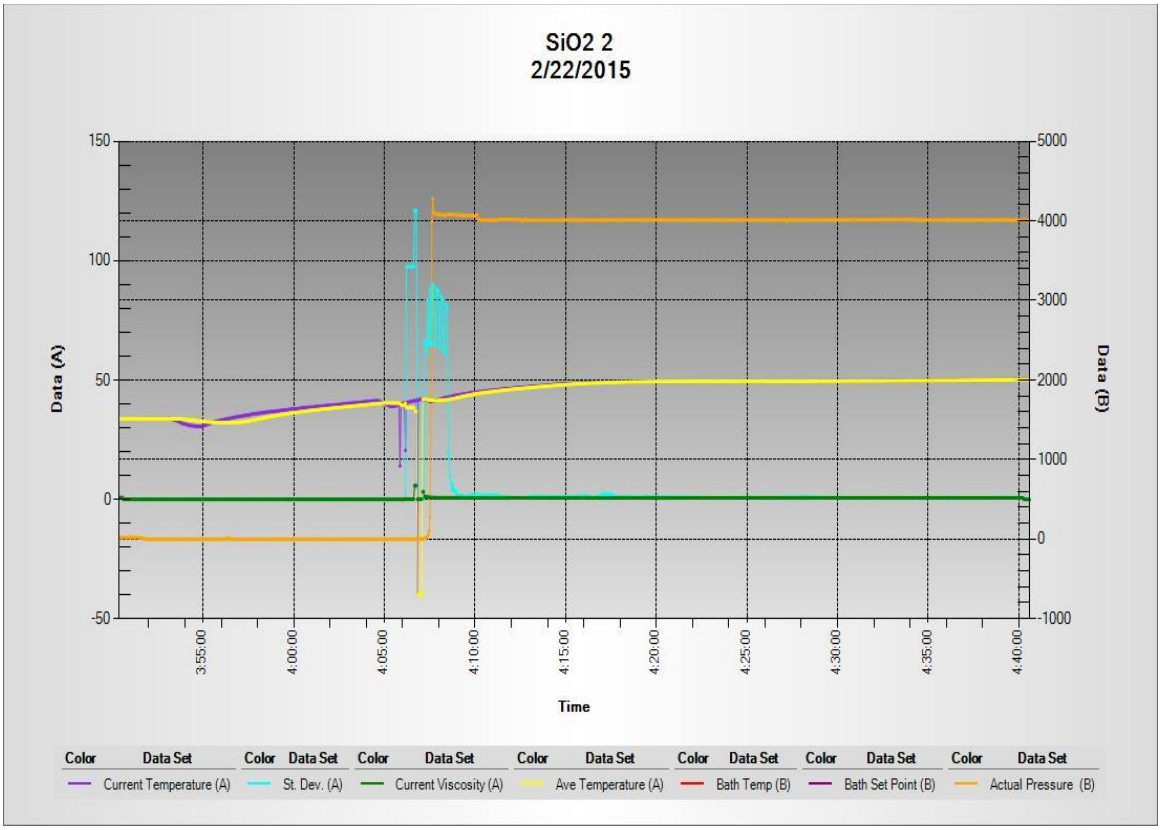

Figure 75: Silica nanofluid viscosity measurements (2.5 wt%, T=50°C, P=4010 psi)

Table 29 shows an example of the viscosity data for silica nanofluid. As shown the standard deviation starts from 121.0328 %, and decreases by time. The viscosity of 0.66119 can be reported as the silica nanofluid viscosity at these certain conditions

(standard deviation = 0.464740 %). It should be noted that the data in the table are the selected data from approximately 600 measurements.

Table 29: Silica nanofluid viscosity measurements (2.5 wt%, T=50°C, P=4010 psi)

Run	Current viscosity (cP)	Average viscosity (cP)	Standard deviation (%)
1	5.72541	2.31060	121.0328
2	0.76900	1.33193	90.12442
3	0.70305	0.94027	79.99218
4	0.69548	0.94064	61.35207
5	0.71005	0.79763	19.55142
6	0.71213	0.77575	17.13622
7	0.71705	0.74538	9.714330
8	0.71686	0.73416	6.960400
9	0.71327	0.72412	3.970840
10	0.71630	0.71313	2.284400
11	0.71176	0.71042	1.807990
12	0.67616	0.67392	1.494910
13	0.67237	0.67258	1.211740
14	0.67370	0.67142	1.063140
15	0.67541	0.67235	0.936940
16	0.66802	0.67271	0.875390
17	0.66764	0.67182	0.546180
18	0.64716	0.65056	0.489000
19	0.65683	0.65779	0.474290
20	0.66119	0.65774	0.464740

To measure the total error of the viscosity experiments 7 replicate runs were performed (**Table 24**). Then, the standard deviation corresponding to these replicate run was calculated. **Table 30** shows the detail of standard deviation calculation for viscosity measurements based on replicate runs. Total standard deviation is calculated from the following equation:

$$Total\ standard\ deviation = \sqrt{\frac{STD1^2 + STD2^2 + STD3^2}{Total\ \#\ of\ runs}}$$

$$= \sqrt{\frac{0.01^2 + 0.00^2 + 0.01^2}{7}} \sim 0.01$$

Table 30: Standard deviation of viscosity measurements based on replicate runs

Run	Viscosity (μ)	Average Viscosity (Aμ)	$(\mu\text{-}A\mu)^2$	Sum $(\mu\text{-}A\mu)^2$	Standard Deviation	Total Standard Deviation
1	0.78	0.790	0.0001	0.0002	STD1=0.01	0.01
2	0.80		0.0001			
3	0.66	0.660	0.0000	0.0000	STD2=0.00	
4	0.66		0.0000			
7	0.66		0.0000			
12	0.40	0.415	0.0002	0.0004	STD3=0.01	
19	0.43		0.0002			

B.1.1 Viscosity Calibration Experiment

Deionized water was used to calibrate the viscosity measurement apparatus. **Table 31** shows the results of viscosity calibration experiment. The results show that the maximum difference observed between the measure viscosity and the actual viscosity (obtained from literature) is 0.02 cP, which can be considered as insignificant. Based on the fluid that we want to measure the viscosity of it, different piston (billet) needs to be used. For example, a piston for the range of 0.25 to 5.00 cP was used in this set of experiments. It is recommended to perform the calibration experiment for the whole range. However, due to limited data available in literature and limited time, only DI water was used in this particular set of experiments.

Table 31: Viscosity calibration results

Temperature °C	Viscosity (Actual) cP	Viscosity (experimental) cP
20	1.00	1.01
24	0.91	0.89
25	0.90	0.88
26	0.88	0.87

B.2 Interfacial Tension Measurements

Two different approaches were followed for measuring the error of IFT experiments. The error corresponding to each run can be measured separately. For each run of IFT measurement, approximately 80 data (average) were taken. **Table 32** shows the standard deviation measured for the interfacial tension between crude oil and alumina nanofluid (5 wt%) at ambient conditions. Total standard deviation was calculated based on following equation:

$$Standard\ Deviation = \sqrt{\frac{Sum((IFT - \overline{IFT})^2)}{Total\ \#\ of\ Runs}} = \sqrt{\frac{10.01826}{83}} = 0.35\ (\frac{mN}{m})$$

Table 32: IFT measurements for crude oil and alumina nanofluid (standard deviation)

Run	IFT (mN/m)	$(\mathbf{IFT} - \overline{\mathbf{IFT}})^2$
1	13.44	0.527991
2	13.28	0.321070
3	13.28	0.321070
4	13.28	0.321070
5	13.28	0.321070
6	13.28	0.321070
7	13.28	0.321070
8	13.11	0.157315
9	13.11	0.157315
10	13.11	0.157315
11	12.76	0.002174
12	13	0.082157
13	12.95	0.055994
14	13.03	0.100255
15	12.66	0.002848
16	12.61	0.010685
17	12.61	0.010685
18	12.84	0.016035
19	12.55	0.026690
20	12.61	0.010685
21	12.61	0.010685
22	12.79	0.005872
23	12.66	0.002848
24	12.53	0.033625
25	12.68	0.001114
26	12.71	0.000000
27	12.63	0.006951
28	12.47	0.059229
29	12.37	0.117903
30	12.3	0.170875
31	12.3	0.170875
32	12.63	0.006951
33	12.63	0.006951

34	12.3	0.170875
35	12.3	0.170875
36	12.3	0.170875
37	12.22	0.243414
38	12.52	0.037392
39	12.3	0.170875
40	12.3	0.170875
41	12.3	0.170875
42	12	0.508897
43	12.45	0.069364
44	12.47	0.059229
45	12.47	0.059229
46	12.22	0.243414
47	12.55	0.026690
48	12.37	0.117903
49	12.3	0.170875
50	12.34	0.139405
51	12.3	0.170875
52	12.25	0.214712
53	12.37	0.117903
54	12.3	0.170875
55	13.28	0.321070
56	13.28	0.321070
57	13.47	0.572489
58	13.28	0.321070
59	13.19	0.227176
60	13.11	0.157315
61	13.11	0.157315
62	13.11	0.157315
63	12.68	0.001114
64	13.03	0.100255
65	12.92	0.042696
66	12.76	0.002174
67	12.68	0.001114
68	12.95	0.055994

69	12.95	0.055994
70	12.89	0.031198
71	12.79	0.005872
72	12.68	0.001114
73	12.71	0.000000
74	12.68	0.001114
75	12.89	0.031198
76	12.68	0.001114
77	12.45	0.069364
78	12.68	0.001114
79	12.53	0.033625
80	12.53	0.033625
81	12.53	0.033625
82	12.53	0.033625
83	12.53	0.033625
	$\overline{\text{IFT}} = 12.71$	$\text{Sum}((\text{IFT} - \overline{\text{IFT}})^2) = 10.01826$
Total Standard Deviation = 0.35 (mN/m)		

The other approach is to replicate an experiment at different times, and measure the standard deviation based on the replicate experiments. As shown in **Table 20**, 7 replicates were conducted for the IFT measurements between oil and nanofluid (nanoparticles dispersed in brine). **Table 33** shows the details of standard deviation measurement based on replicate experiments for IFT between oil and nanofluid. 3 sets of unique experiments were repeated, and the standard deviation related to each one was calculated separately. Then, total standard deviation was calculated from the following equation:

$$Total\ standard\ deviation = \sqrt{\frac{STD1^2 + STD2^2 + STD3^2}{Total\ \#\ of\ runs}} = \sqrt{\frac{0.23^2 + 0.26^2 + 0.86^2}{7}}$$

$$= 0.35\ (\frac{mN}{m})$$

Table 33: Standard deviation of IFT measurements based on replicate runs

Run	IFT (mN/m)	Average IFT (AIFT)	(IFT-AIFT)^2	Sum (IFT-AIFT)^2	Standard Deviation	Total Standard Deviation
4	2.26	2.52	0.0676	0.1352	STD1=0.26	0.35
18	2.78		0.0676			
8	4.48	4.17	0.0961	0.1526	STD2=0.23	
11	3.95		0.0484			
13	4.08		0.0081			
20	16.96	17.82	0.7396	1.4792	STD3=0.86	
24	18.68		0.7396			

B.2.1 IFT Measurements Calibration

For calibrating the IFT measurements apparatus, interfacial tension of DI water/air, and toluene/air system was measured, and compared to the reference value. For each experiment, different number of data was collected, and standard deviation was calculated for each experiment. **Table 34** shows the details of standard deviation calculation (IFT) for air/DI water system. As shown in the table, the interfacial tension measured for air/DI water system at 25 °C was 71.08 ± 1.04 (mN/m). The actual value is 72.00 (mN/m). As shown the measured value and the actual value are within the standard deviation. The standard deviation for IFT of air/toluene system was also measured. The details of this

standard deviation calculation are tabulated in **Table 35**. As shown in the table, the interfacial tension measured for air/toluene system at 25 °C was 27.64 ± 0.32 (mN/m). The actual value is 27.85 (mN/m). As shown in **Table 35**, the measured value and the actual value are within the standard deviation.

Table 34: Standard deviation for IFT of air/DI water system

Run	**IFT (mN/m)**	$(\mathbf{IFT} - \overline{\mathbf{IFT}})^{\mathbf{2}}$
1	71.00	0.006306
2	73.08	4.002353
3	71.67	0.348794
4	72.37	1.665618
5	73.08	4.002353
6	70.34	0.546730
7	71.00	0.006306
8	70.34	0.546730
9	71.67	0.348794
10	71.00	0.006306
11	70.78	0.089647
12	70.34	0.546730
13	70.34	0.546730
14	68.99	4.365642
15	70.34	0.546730
16	70.34	0.546730
17	71.67	0.348794
	$\overline{\text{IFT}}$ =71.08	Sum$((\text{IFT} - \overline{\text{IFT}})^2)$ =18.47129
Total Standard Deviation = 1.04 (mN/m)		

Table 35: Standard deviation for IFT of air/toluene system

Run	IFT (mN/m)	$(\mathbf{IFT} - \overline{\mathbf{IFT}})^2$
1	27.63	0.000137
2	27.54	0.010343
3	27.45	0.036749
4	27.54	0.010343
5	27.76	0.013995
6	27.23	0.169497
7	27.50	0.020079
8	27.54	0.010343
9	27.50	0.020079
10	27.50	0.020079
11	27.50	0.020079
12	27.17	0.222501
13	27.12	0.272171
14	27.12	0.272171
15	27.12	0.272171
16	27.12	0.272171
17	27.36	0.079355
18	27.17	0.222501
19	27.12	0.272171
20	27.12	0.272171
21	28.03	0.150777
22	27.72	0.006131
23	27.76	0.013995
24	27.76	0.013995
25	28.03	0.150777
26	28.26	0.382295
27	28.03	0.150777
28	27.65	6.89E-05
29	27.43	0.044817
30	27.65	6.89E-05
31	27.65	6.89E-05
32	27.70	0.003399
33	27.65	6.89E-05

34	27.70	0.003399
35	27.65	6.89E-05
36	27.65	6.89E-05
37	27.43	0.044817
38	27.10	0.293439
39	27.48	0.026147
40	27.83	0.035457
41	27.97	0.107781
42	28.24	0.357963
43	27.83	0.035457
44	28.20	0.311699
45	27.83	0.035457
46	28.02	0.143111
47	27.83	0.035457
48	27.97	0.107781
49	27.83	0.035457
50	28.20	0.311699
51	27.83	0.035457
52	27.97	0.107781
53	28.02	0.143111
	$\overline{\text{IFT}} = 27.64$	$\text{Sum}((\text{IFT} - \overline{\text{IFT}})^2) = 5.577947$
Total Standard Deviation = 0.32 (mN/m)		

B.3 Waterflooding Micromodel

For waterflooding experiments, 1 replicate run was performed for polymer (10 ppm) flooding with the flow rate of 0.01 ml/min (test #2 and #4 in **Table 6**). We have two values for oil recovery at each time (time interval = 10 minutes). Standard deviation can be calculated for each pair of oil recovery separately. Then, total standard deviation can be calculated as the average of these values. **Table 36** shows the detail of standard deviation calculation for micromodel experiments.

Total standard deviation can be calculated as follow:

$$Total\ Standard\ Deviation = \sqrt{\frac{Sum(STD_i^2)}{Total\ \#\ of\ runs}} = \sqrt{\frac{64.30365}{18}}$$

$$= 1.89\ (\%\ recovery)$$

Table 36: Standard deviation calculation for oil recovery of micromodel flooding

Time (min)	Oil Recovery (Test #2)	Oil Recovery (Test #4)	Average Oil Recovery	Sum of Squares	Standard Deviation	(Standard Deviation)^2
0	0.00	0.00	0.00	0.00000	0.000	0.00000
10	9.70	6.09	7.895	6.51605	1.805	3.25802
20	17.71	15.09	16.400	3.43220	1.310	1.71610
30	25.72	20.61	23.165	13.05605	2.555	6.52802
40	34.65	27.20	30.925	27.75125	3.725	13.87563
50	46.21	35.86	41.035	53.56125	5.175	26.78063
60	47.92	46.48	47.200	1.03680	0.720	0.51840
70	50.05	47.81	48.930	2.50880	1.120	1.25440
80	50.40	47.69	49.045	3.67205	1.355	1.83602
90	49.95	48.25	49.100	1.44500	0.850	0.72250
100	50.73	48.41	49.570	2.69120	1.160	1.34560
110	49.60	49.12	49.360	0.11520	0.240	0.05760
120	51.52	49.84	50.680	1.41120	0.840	0.70560
130	50.76	49.10	49.930	1.37780	0.830	0.68890
140	51.60	49.06	50.330	3.22580	1.270	1.61290
150	51.69	49.60	50.645	2.18405	1.045	1.09202
160	51.56	49.40	50.480	2.33280	1.080	1.16640
170	51.94	49.80	50.8700	2.28980	1.070	1.14490
						Sum=64.30365

C. Raw Data

It should be mentioned that all raw data is kept/backed up on Hibernia EOR Lab Server.

C.1 Micromodel Experiments

Figure 76 to **93** show the raw pictures taken during waterflooding micromodel experiments using silica nanofluid (5 wt%) with the injection flow rate of 0.01 ml/min. The pictures were taken every 30 seconds. Following photos show the micromodel injection for every 10 minutes starting from t = 0 (min) to t = 170 (min).

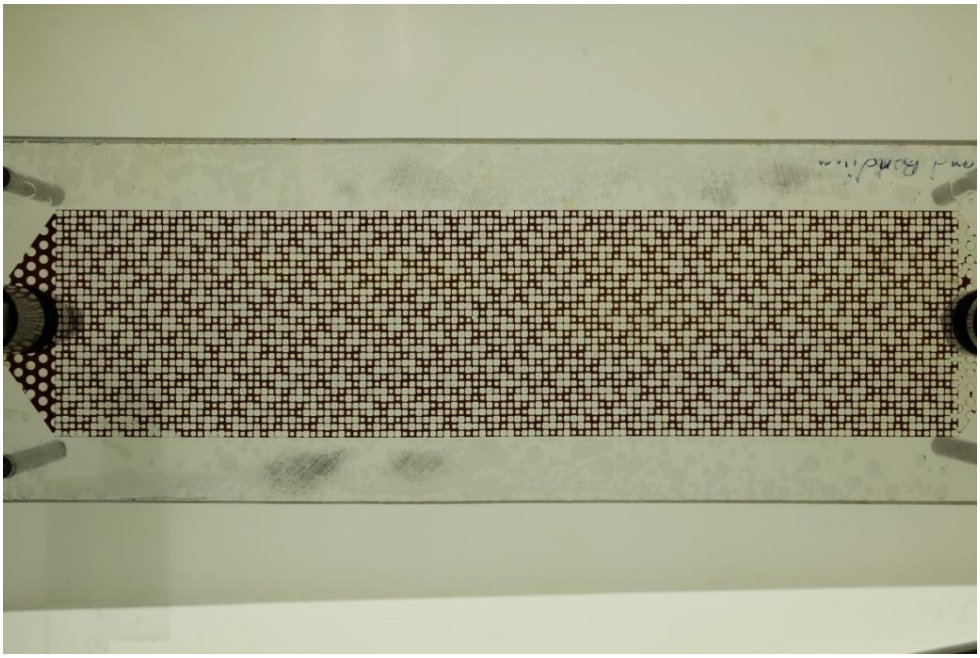

Figure 76: Silica nanofluid micromodel injection, t=0 min

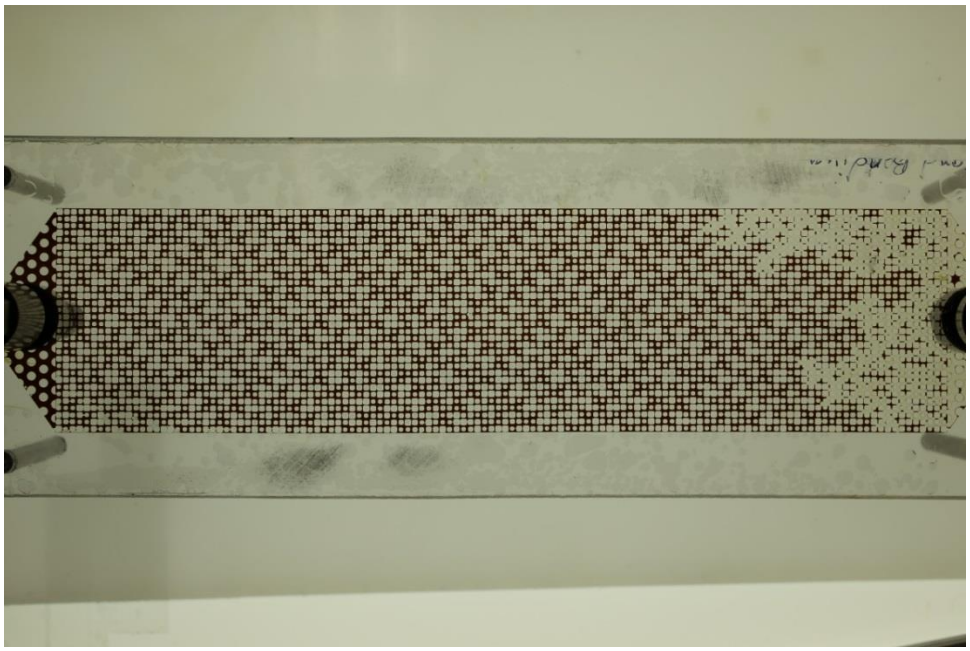

Figure 77: Silica nanofluid micromodel injection, t=10 min

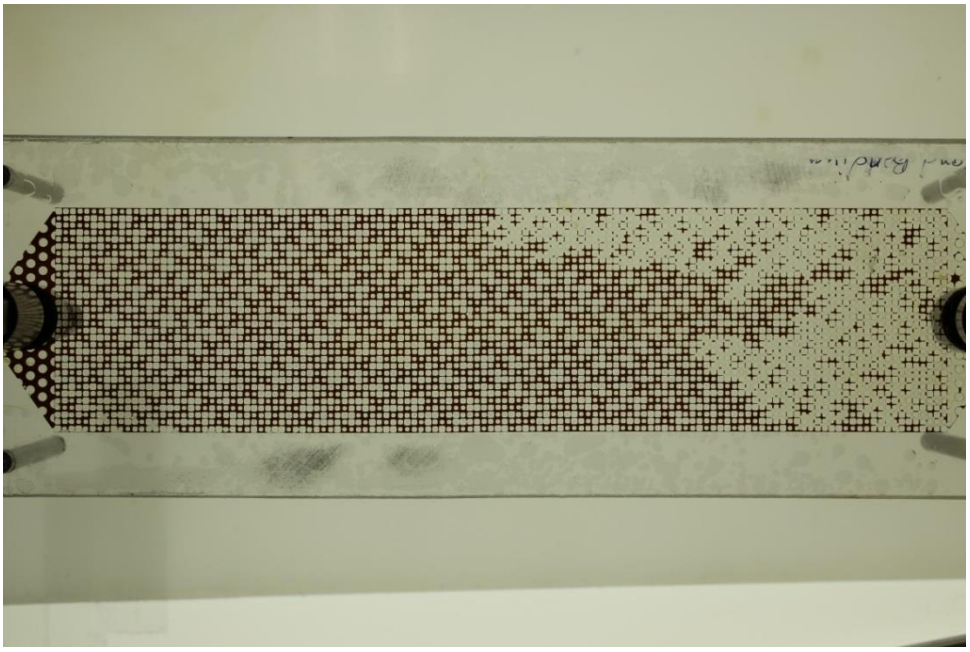

Figure 78: Silica nanofluid micromodel injection, t=20 min

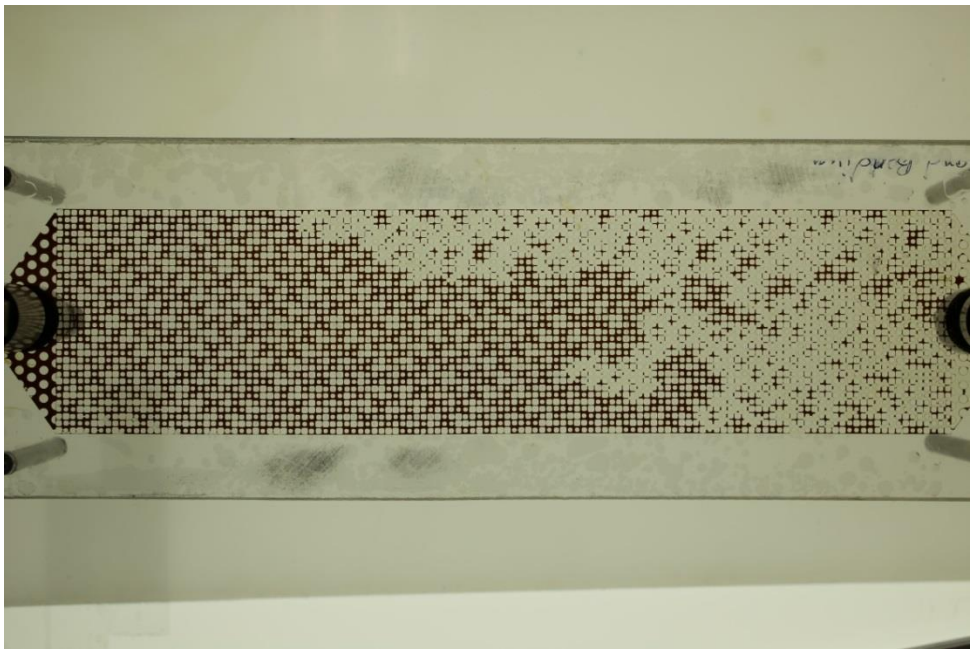

Figure 79: Silica nanofluid micromodel injection, t=30 min

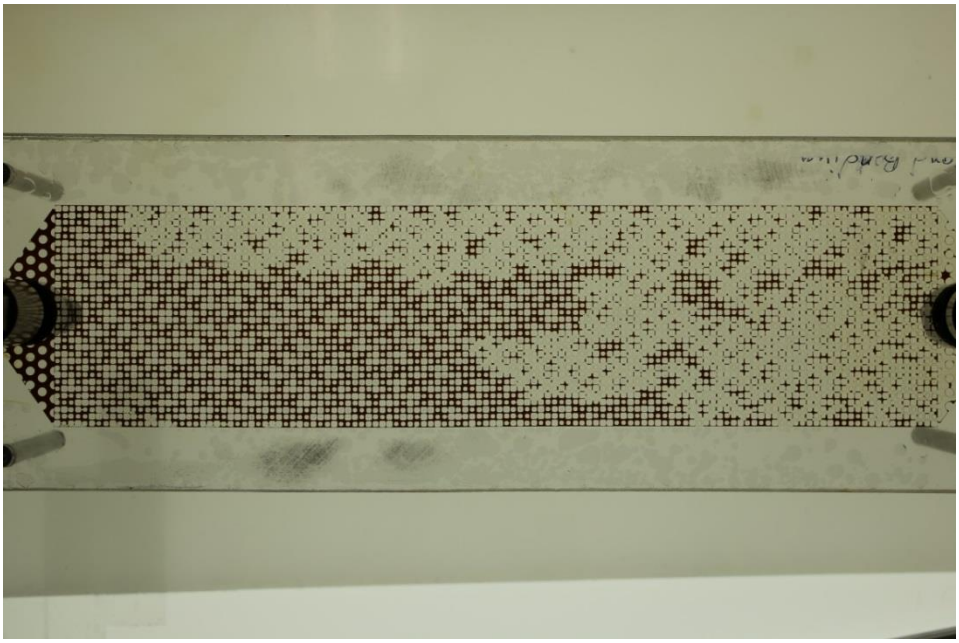

Figure 80: Silica nanofluid micromodel injection, t=40 min

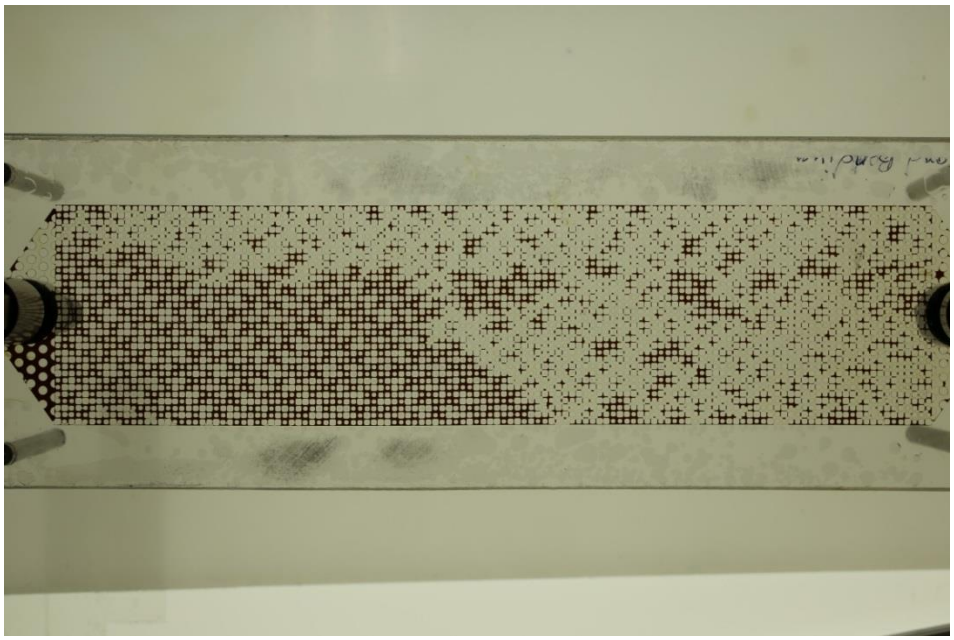

Figure 81: Silica nanofluid micromodel injection, t=50 min

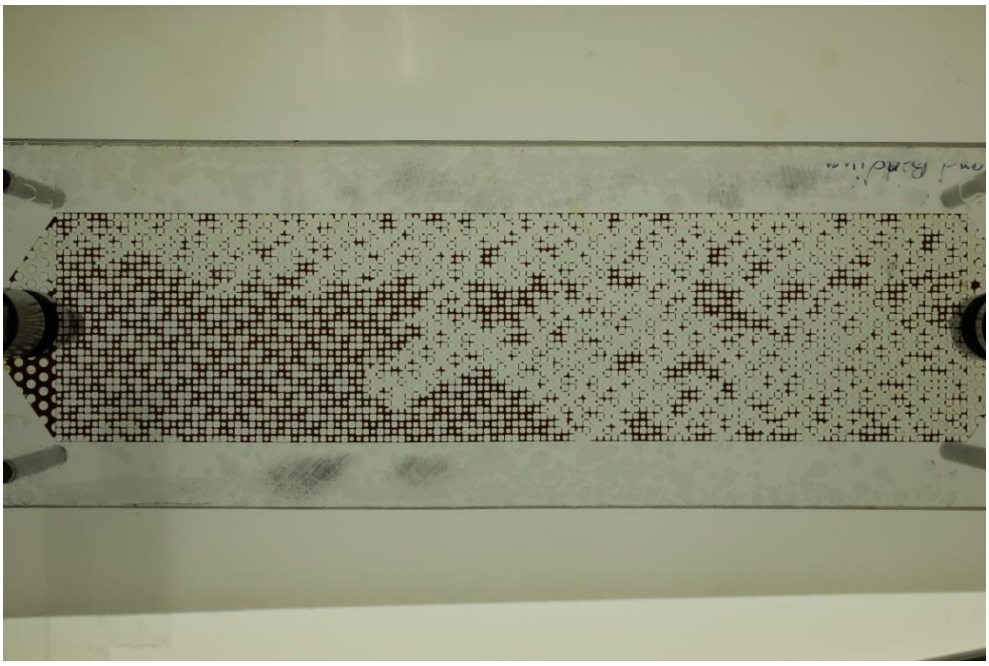

Figure 82: Silica nanofluid micromodel injection, t=60 min

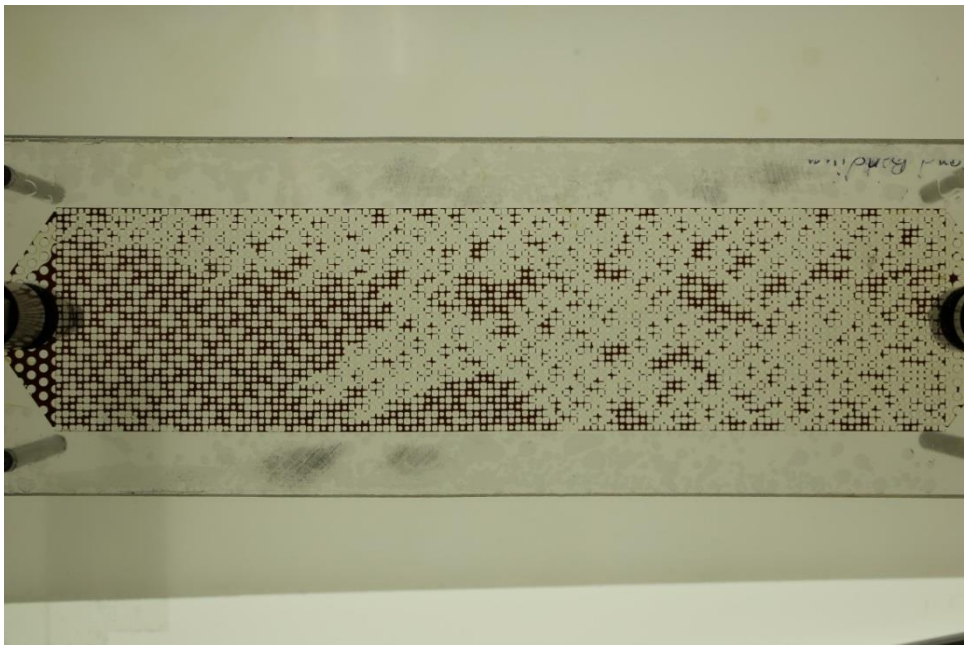

Figure 83: Silica nanofluid micromodel injection, t=70 min

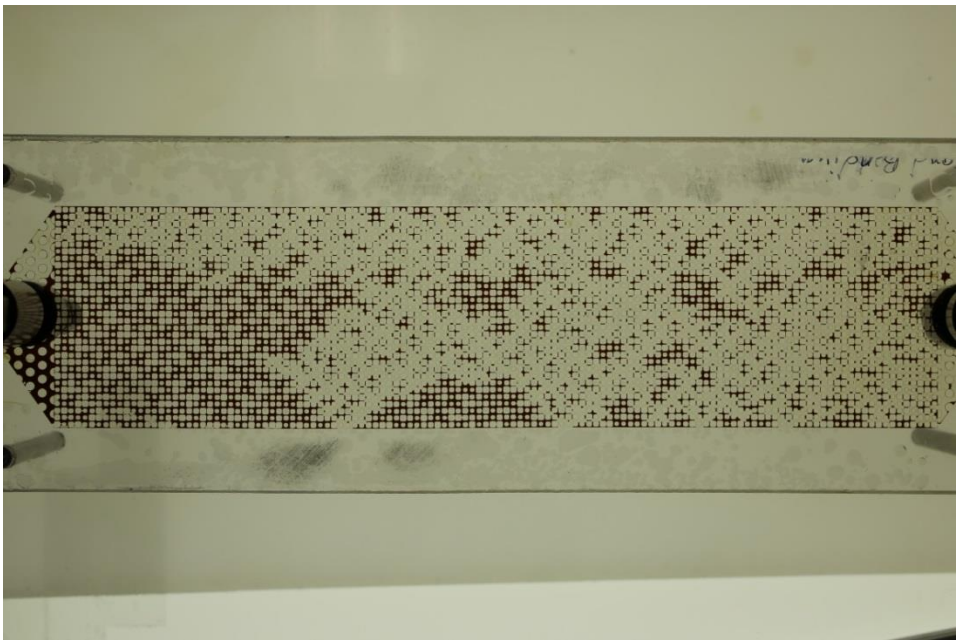

Figure 84: Silica nanofluid micromodel injection, t=80 min

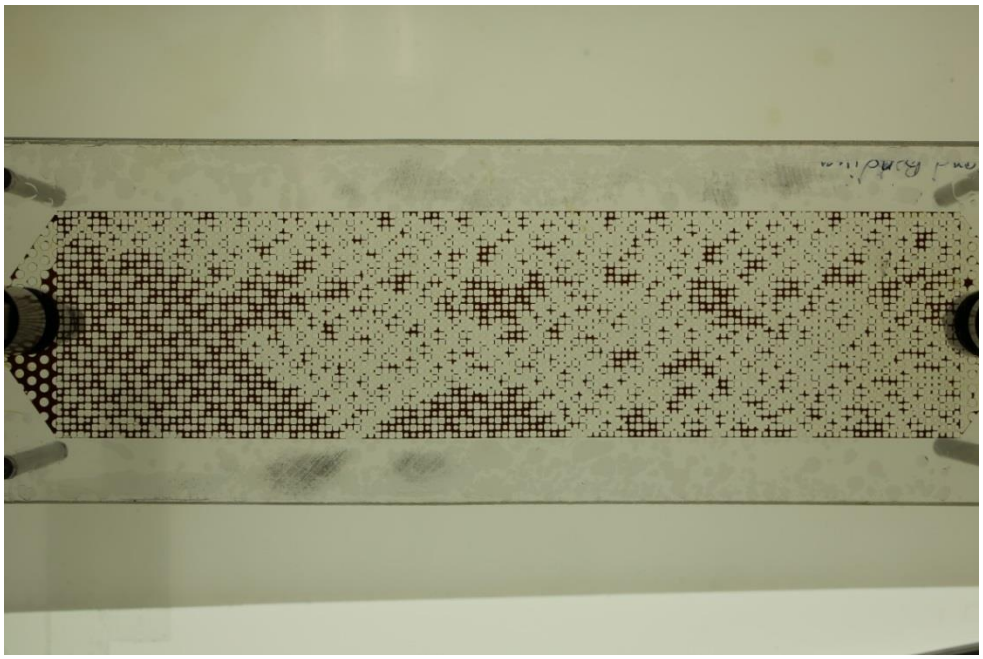

Figure 85: Silica nanofluid micromodel injection, t=90 min

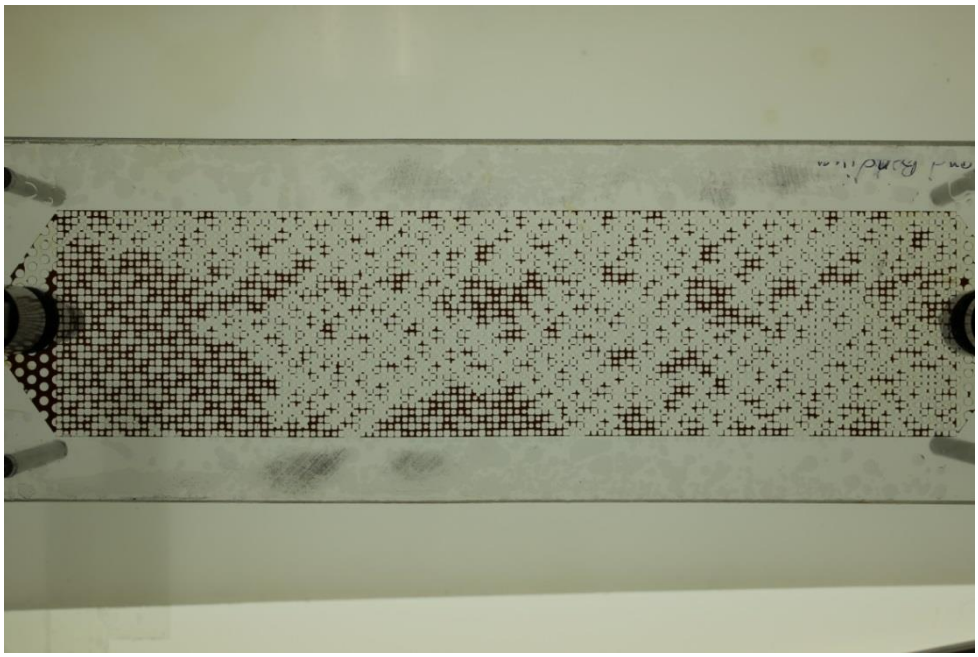

Figure 86: Silica nanofluid micromodel injection, t=100 min

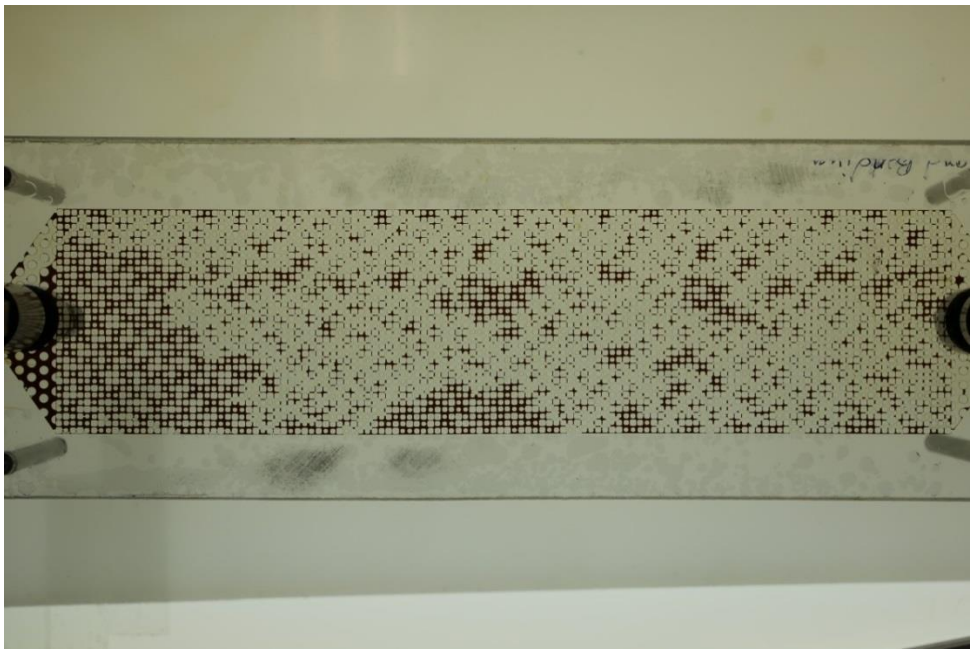

Figure 87: Silica nanofluid micromodel injection, t=110 min

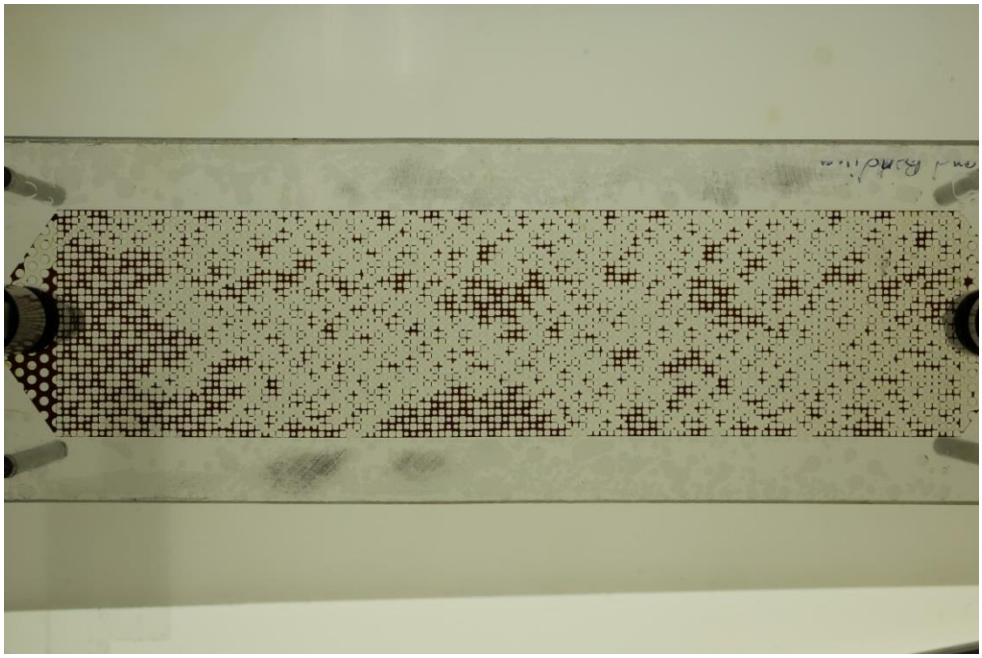

Figure 88: Silica nanofluid micromodel injection, t=120 min

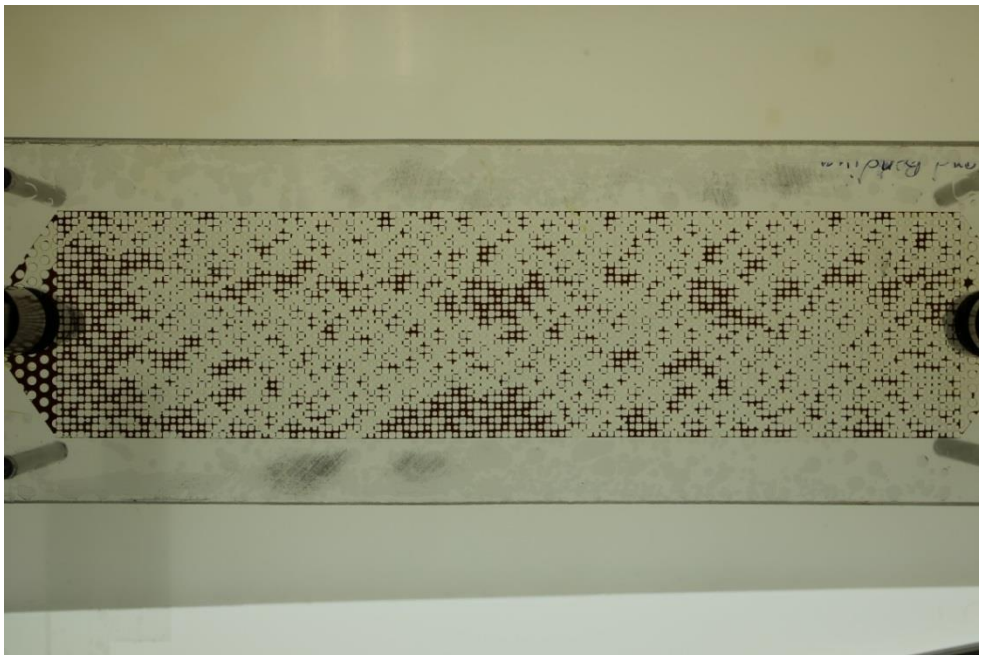

Figure 89: Silica nanofluid micromodel injection, t=130 min

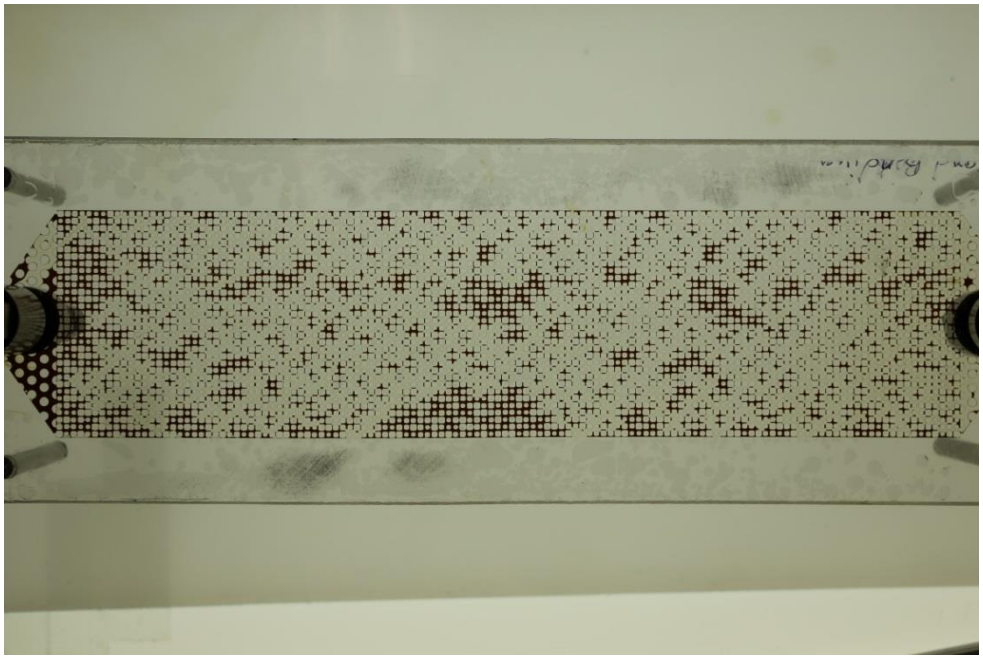

Figure 90: Silica nanofluid micromodel injection, t=140 min

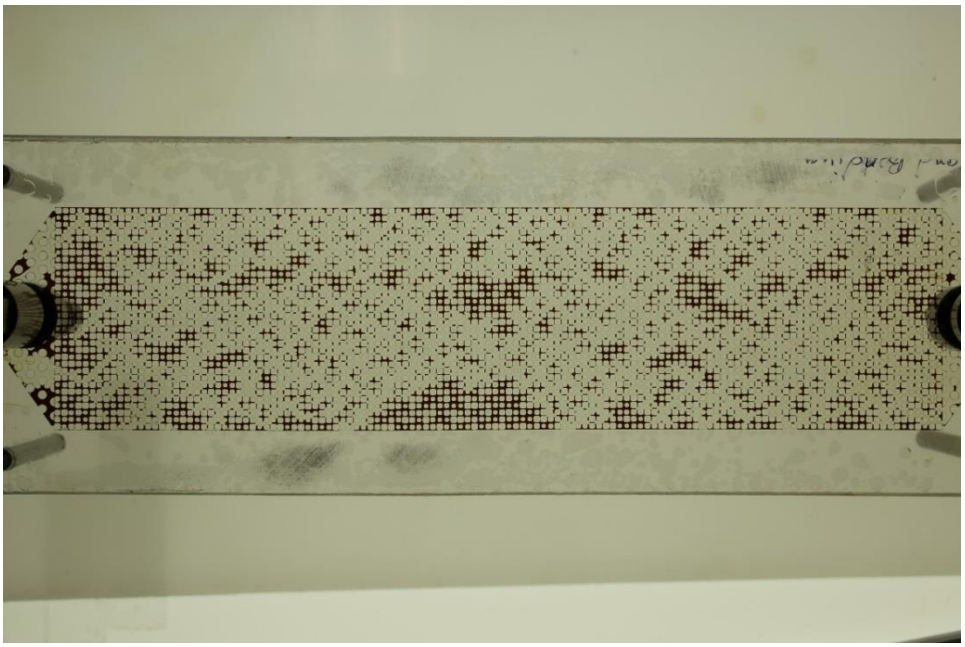

Figure 91: Silica nanofluid micromodel injection, t=150 min

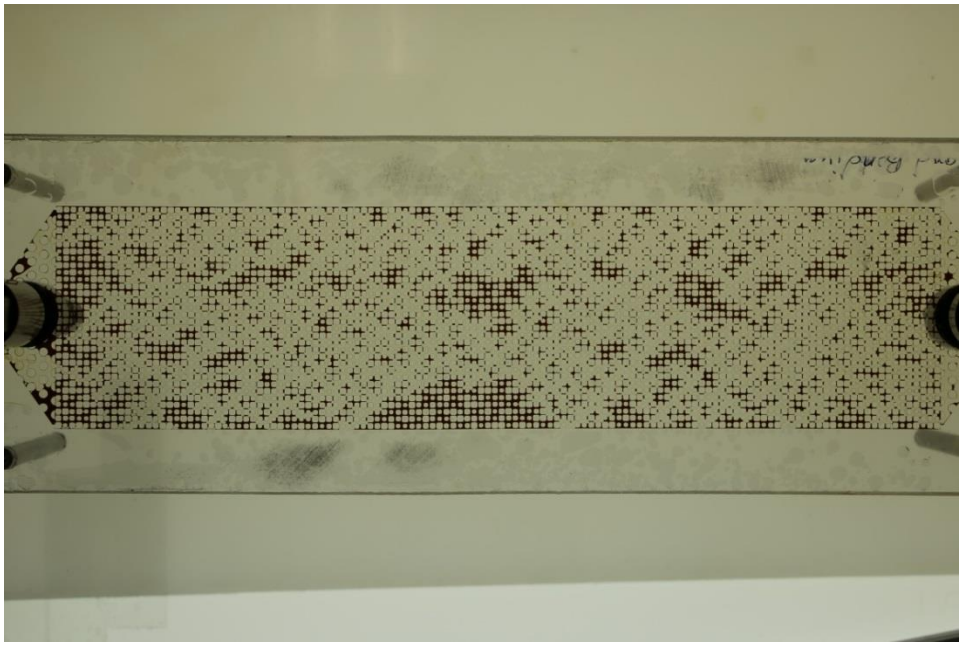

Figure 92: Silica nanofluid micromodel injection, t=160 min

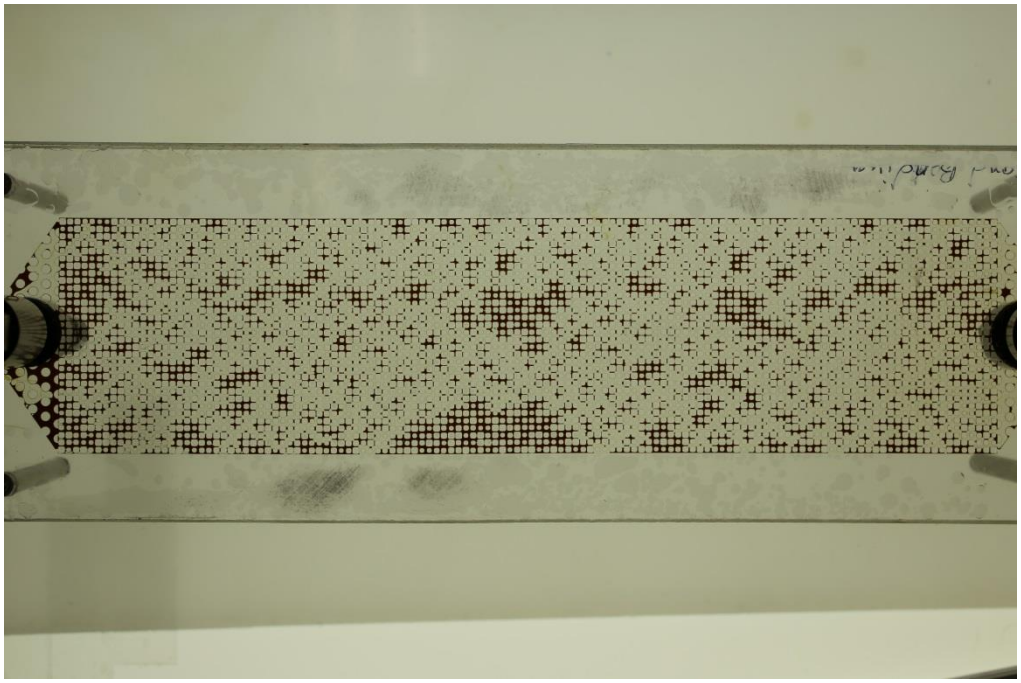

Figure 93: Silica nanofluid micromodel injection, t=170 min

C.2 Interfacial Tension Measurements

Figure 94 to **103** shows examples of interfacial tension measured between crude oil and alumina nanoparticles dispersed in DI water (5 wt%). These photos are taken straight from the software of IFT meter setup.

Figure 94: Interfacial tension between oil and alumina nanofluid (example #1)

Figure 95: Interfacial tension between oil and alumina nanofluid (example #2)

Figure 96: Interfacial tension between oil and alumina nanofluid (example #3)

Figure 97: Interfacial tension between oil and alumina nanofluid (example #4)

Figure 98: Interfacial tension between oil and alumina nanofluid (example #5)

Figure 99: Interfacial tension between oil and alumina nanofluid (example #6)

Figure 100: Interfacial tension between oil and alumina nanofluid (example #7)

Figure 101: Interfacial tension between oil and alumina nanofluid (example #8)

Figure 102: Interfacial tension between oil and alumina nanofluid (example #9)

Figure 103: Interfacial tension between oil and alumina nanofluid (example #10)

C. 3 Viscosity Measurements

Figure 104, **105**, **106** and **107** show some examples for the viscosity measurements data for DI water, alumina nanofluid, silica nanofluid, and polymer solution respectively.

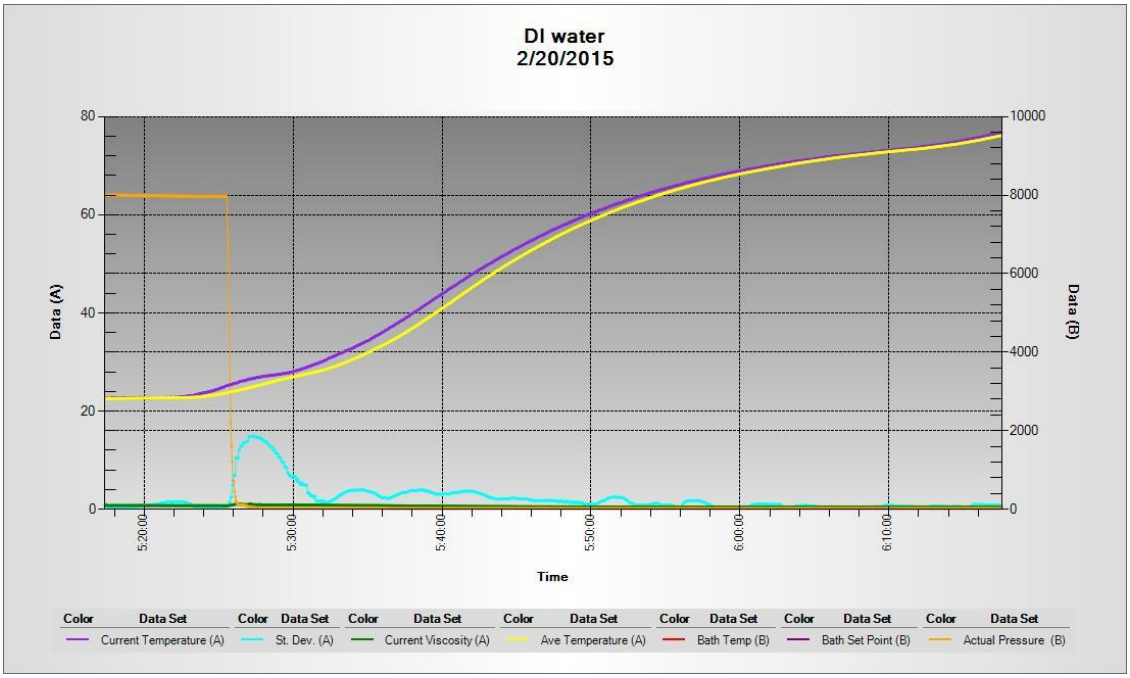

Figure 104: Viscosity measurements for DI water

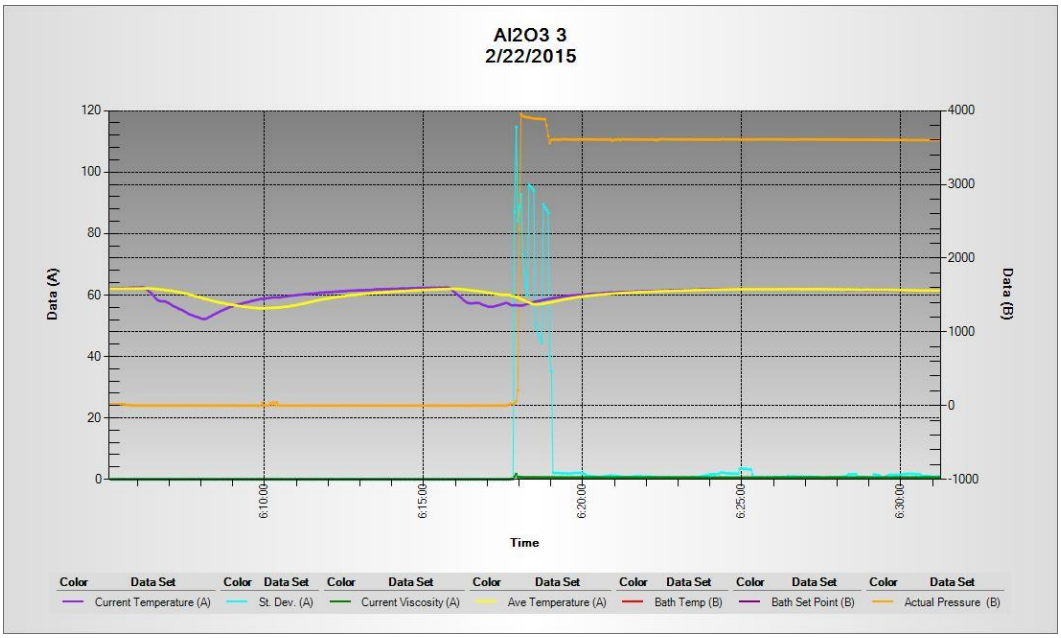

Figure 105: Viscosity measurements for alumina nanofluid

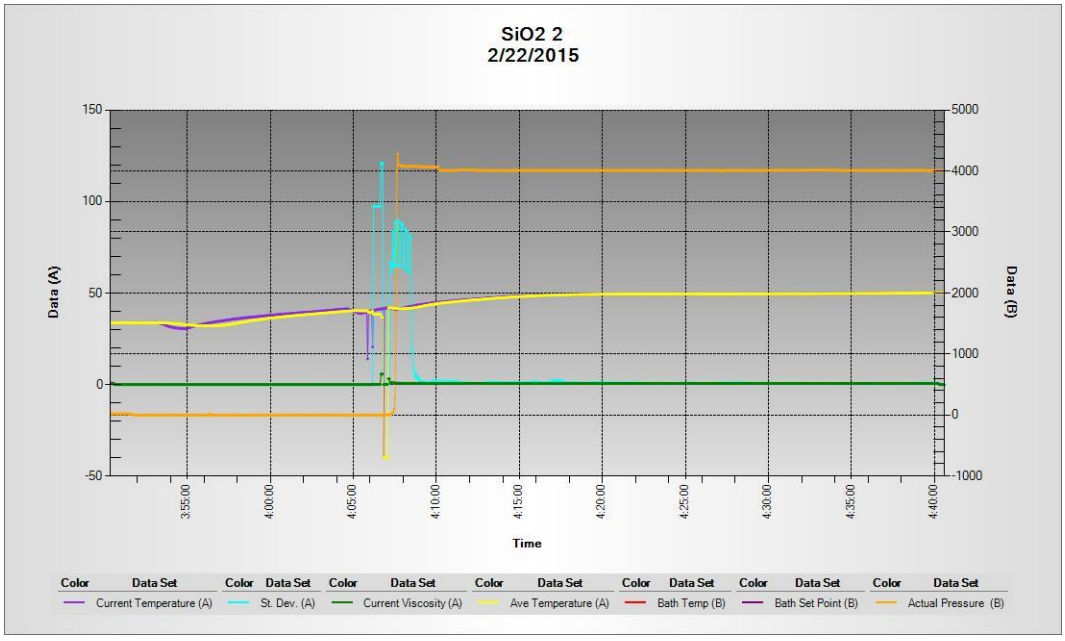

Figure 106: Viscosity measurements for silica nanofluid

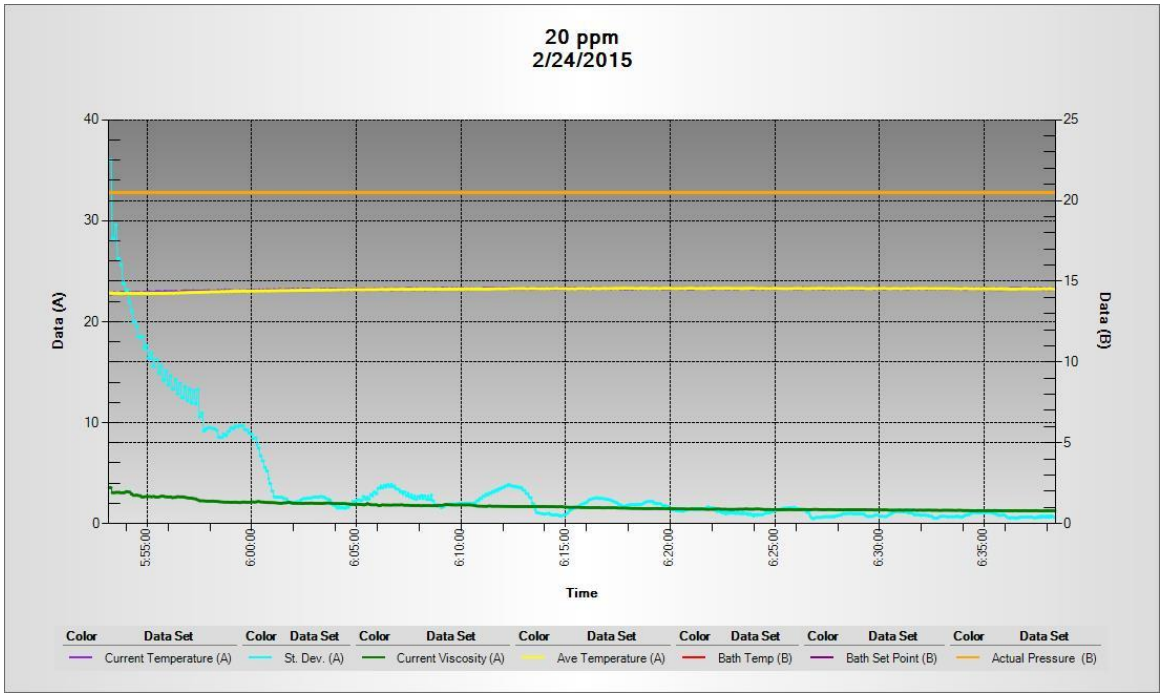

Figure 107: Viscosity measurements for polymer solution

Bibliography

Agbalaka, C.C., Dandekar, A.Y., Patil, S.L., Khataniar, S., and Hemsath, J. 2008. The effect of wettability on oil recovery: a review. Paper SPE 114496 presented at SPE Asia Pacific Oil and Gas Conference and Exhibition, Perth, Australia, 20-22 October.

Agenet, N., Perriat, P., Brichart, T., Crowther, N., Martini, M., and Tillement, O. 2012. Fluorescent Nanobeads: a First Step Toward Intelligent Water Tracers. Paper SPE 157019 presented at the SPE International Oilfield Nanotechnology Conference and Exhibition, Noordwijk, 12-14 June.

Aminzadeh, B., DiCarlo, D.A., Chung, D.H., Kianinejad, A., Bryant, S.L., and Huh, C. 2012. Effect of Nanoparticles on Flow Alteration during CO_2 Injection. Paper SPE 160052 presented at the SPE Annual Technical Conference and Exhibition. Antonio, USA, 8 – 10 October.

Anderson, M.J., and Whitcomb, P.J. 2005. RSM simplified: optimizing processes using response surface methods for design of experiments. Productivity Press, New York.

Ayatollahi, S., and Zerafat, M.M. 2012. Nanotechnology-assisted EOR techniques: New solutions to old challenges. Paper SPE 157094 presented at the SPE International Oilfield Nanotechnology Conference and Exhibition, Noordwijk, 12-14 June.

Bagrezaie, M.A., and Pourafshary, P. 2014. Screening Different Water Alternating Carbon Dioxide Injection Scenarios to Achieve to the Highest Macroscopic Sweep Efficiency in a Non Fractured Carbonate Reservoir. Paper SPE-172267-MS presented at the SPE Annual Caspian Technical Conference and Exhibition. Astana, Kazakhstan, 12-14 November.

Bahralolom, I.M., and Orr Jr, F.M. 1988. Solubility and extraction in multiple-contact miscible displacements: comparison of N2 and CO2 flow visualization experiments. *SPE Reservoir Engineering* **3**(1): 213-219.

Bawa, R., Bawa, S.R., Maebius, S.B., Flynn,T., and Wei, C. 2005. Protecting new ideas and inventions in nanomedicine with patents. *Nanomedicine: Nanotechnology, Biology and Medicine* **1**(2): 150-158.

Bensaba, F. 2013. *Nanoparticles Technologies.* Academic Press, Ottawa, Ontario, Canada.

Borel, J.P. 1981. Thermodynamical size effect and the structure of metallic clusters. *Surface Science*, **106**(1-3): 1-9

Brown, H.W. 1951. Capillary Pressure Investigations. *Journal of Petroleum Technology,* **3**(03).

Burnett, D.B., and Dann, M.W. 1981. Screening Tests For Enhanced Oil Recovery Projects. Paper SPE-9710-MS presented at the Permian Basin Oil and Gas Recovery Conference, Midland, Texas, 12-13 March.

Buzea, C., Blandino, I.I.P., and Robbie, K. 2007. Nanomaterials and nanoparticles: Source and toxicity. *Biointerphases* **2**(4): MR17-MR172.

Chakraborty, S., Agrawal, G., DiGiovanni, A., and Scott, D.E. 2012. The Trick Is The Surface-Functionalized Nanodiamond PDC Technology. Paper SPE 157039 presented at the SPE International Oilfield Nanotechnology Conference and Exhibition, Noordwijk, 12-14 June.

Chatzis, I., and Morrow, N. R. 1981. Measurement and conditions for entrapment and mobilization of residual: US Department of Energy Final Report. DOE/BETC/3251-12.

Chatzis, I., and Morrow, N.R. 1984. Correlation of Capillary Number Relationships for Sandstone. *SPE Journal*, **24**(05).

Cheek, R.E., Menzie, D.E. 1955. Fluid Mapper Model Studies of Mobility Ratio. Paper SPE-432-G.

Chen, M., Chuang, Y., and Tseng, F. 2008.Self-masked high aspect-ratio polymer nanopillars. *Nanotechnology* **19**(50): 505301.

Chol, S.U.S. 1995. Enhancing thermal conductivity of fluids with nanoparticles. *ASME-Publications-Fed* **231**: 99-106.

Choudhary, M.A., Wani, M.R., Al-Mahmeed, A., and Al-Rashidi, H. 2012. Challenges and Risk Management Strategy for Enhanced Oil Recovery Projects in Carbonate Reservoirs of a Giant Field in Middle East. Paper SPE 154631 presented at the SPE EOR Conference at Oil and Gas West Asia, Muscat, 16-18 April.

Dehghan, A.A., Farzaneh, S.A., Kharrat, R., Ghazanfari, M.H., and Rashtchian, D. 2010. Pore-Level Investigation of Heavy Oil Recovery During Water Alternating Solvent Injection Process. *Transport in Porous Media* **83**(3): 653-666.

Dixit, A.B., Buckley, J.S., McDougall, S.R., and Sorbie, K.S. 2000. Empirical Measures of Wettability in Porous Media and the Relationship between Them Derived From Pore-Scale Modelling. *Transport in Porous Media* **40**(1): 27-54.

Dong, M., Dullien, F.A.L., and Chatzis, I. 1995. Imbibition of Oil in Film over Water in Edges of Capillaries with an Angular Cross Section. *Journal of Colloid Interface Science* **172**(1): 21-36.

Ehtesabi, H., Ahadian, M.M., and Taghikhani, V. 2014. Enhanced Heavy Oil Recovery Using TiO_2 Nanoparticles: Investigation of Deposition during Transport in Core Plug. *Energy and Fuels*, **29**(1): 1 – 8.

El-Amin, M.F., Sun, S., and Salama, A. 2013. Enhanced Oil Recovery by Nanoparticles Injection: Modeling and Simulation. Paper SPE 164333 presented at the SPE Middle East Oil and Gas Show and Conference, Manama, Bahrain, 10-13 March

Einstein, A. 1905. On the motion – required by the molecular kinetic theory of heat – of small particles suspended in a stationary liquid. *Annalen der Physik* **17**(4): 549-560.

Emami Meybodi, H., Kharrat, R., and NasehiAraghi, M. 2011. Experimental studying of pore morphology and wettability effects on microscopic and macroscopic displacement efficiency of polymer flooding. *Journal of Petroleum Science and Engineering* **78(**2): 347-363.

Esfandyari Bayat, A., Junin, R., Samsuri, A., Piroozian, A., and Hokmabadi, M. 2014. Impact of metal oxide nanoparticles on enhanced oil recovery from limestone media at several temperatures. *Energy and Fuels,* **28**(10): 6255 – 6266.

Espinosa, D., Caldelas, F., Johnston, K., Bryant, S.L., and Huh, C. 2010. Nanoparticle-Stabilized Supercritical CO_2 Foams for Potential Mobility Control Applications. Paper SPE 129925 presented at the 2010 SPE Improved Oil Recovery Symposium. Tulsa, USA, 24 – 28 April.

Fei, D., Dingtain, K., Alexandru, C. 2011. Viscosity affected by nanoparticles aggregation in Al_2O_3-water nanofluids. *Nanoscale Research Letters,* **6**(1): X1 – 5.

Fletcher, A. J. P., Weston, S., Haynes, A. K., and Clough, M. D. 2013. The Successful Implementation of a Novel Polymer EOR Pilot in the Low Permeability Windalia Field. Paper SPE-165253-MS presented at the SPE Enhanced Oil Recovery Confernece, Kuala Lumpur, Malaysia, 2 – 4 July.

Friedheim, J., Young, S., De Stefano, G., Lee, J., and Guo, Q. 2012. Nanotechnology for Oilfield Applications – Hype or Reality?. Paper SPE 157032 presented at the SPE International Oilfield Nanotechnology Conference and Exhibition, Noordwijk, 12-14 June.

Gharibshahi, R., Jafari, A., Haghtalab, A., and Karambeigi, M. S. 2015. Application of CFD to evaluate the pore morphology effect on nanofluid flooding for enhanced oil recovery. *RSC Advances*, **5**(37): 28938-28949.

Greff, J., and Babadagli, T. 2011. Use of Nano-Metal Particles as Catalyst under Electromagnetic Heating for Viscosity Reduction of Heavy Oil. Paper IPTC 14720 Presented at the International Petroleum Technology Conference. Bangkok, Thailand, 7-9 February.

Hamedi-Shokrlu, Y., and Babadagli, T. 2014. Stabilization of nanometal catalysts and their interaction with oleic phase in porous media during enhanced oil recovery. *Industrial & Engineering Chemistry Research*, **53**(20): 8464-8475.

Hendraningrat, L. and Shidong, L. 2012. A glass micromodel experimental study of hydrophilic nanoparticles retention for EOR project. Paper SPE 159161 presented at the SPE Russian Oil and Gas Exploration and Production Technical Conference and Exhibition, Moscow, 16-18 October.

Hendraningrat, L., Li, S., and Torster, O. 2013. Effect of some parameters influencing enhanced oil recovery process using Silica Nanoparticles: An experimental investigation. Paper SPE-165955 presented at the SPE Reservoir Characterization and Simulation Conference and Exhibition. Abu Dhabi, UAE, 16 – 18 September.

Hendraningrat, L., and Torsæter, O. 2014. Experimental Investigation of Wettability Alteration Due to Various Nanoparticles: An EOR Implication with Nanofluids. Paper SCA2014-082 presented at the International Symposium of the Society of Core Analysts, Avignon, 8-11 September.

Hook, J. R. 2003. An introduction to porosity. *Petrophysics,* **44**(03).

Hunter, T.N., Pugh, R.J., Franks, G.V., and Jameson, G.J. 2008. The role of particles in stabilizing foams and emulsions. *Advances in Colloid and Interface Science* **137**(2): 57-81.

Jafari, S., Khezrnejad, A., Shahrokhi, O., Ghazanfari, M.H., and Vossoughi, M. 2015. Experimental Investigation of Heavy Oil Recovery by Continuous/WAG Injection of

CO2 Saturated with Silica Nanoparticles. *International Journal of Oil, Gas and Coal Technology* **9**(2).

James, L. A., Rezaei, N., and Chatzis, I. 2008. VAPEX, warm VAPEX and hybrid VAPEX: the state of enhanced oil recovery for in situ heavy oils in Canada. *Journal of Canadian Petroleum Technology* **47** (4): 12-18.

James, L.A. 2009. Mass transfer mechanisms during the solvent recovery of heavy oil. PhD dissertation, Waterloo U., Waterloo, Ontario.

Joonaki, E., and Ghanaatian, S. 2014. The Application of Nanofluids for Enhanced Oil Recovery: Effect on Interfacial Tension and Coreflooding Process. *Petroleum Science and Technology*, **32**(21): 2599 – 2607.

Ju, B., Fan, T., and Ma, M. 2006. Enhanced oil recovery by flooding with hydrophilic nanoparticles. *China Particuology* **192**(2009): 195-202.

Ju, B., and Fan, T. 2009. Experimental study and mathematical model of nanoparticle transport in porous media. *Powder Technology* **192**(2): 195-202.

Kapusta, S., Balzano, L., and Riele, P.T. 2011. Nanotechnology Applications in Oil and Gas Exploration and Production. Paper IPTC 15152 Presented at the International Petroleum Technology Conference held in Bangkok, Thailand, 7-9 February

Khezrnejad, A., James, L.A., Johansen, T.E. 2014. Water Enhancement Using Nanoparticles in Water Alternating Gas (WAG) Micromodel Experiments. Paper SPE-173484-STU presented at the SPE Annual Technical Conference and Exhibition, Amsterdam, The Netherlands, 27-29 October.

Kong, X., and Ohadi, M.M. 2010. Applications of Micro and Nano Technologies in the Oil and Gas Industry - Overview of the Recent Progress. Paper SPE 138241 presented at the Abu Dhabi International Petroleum Exhibition & Conference, Abu Dhabi, UAE, 1-4 November.

Krishnamoorti, R. 2006. Extracting the benefits of nanotechnology for the oil industry. *Journal of Petroleum Technology* **58**: 24-26.

Kumar, S., Yen, T.F., Chilingarian, G.V., and Donaldson, E.C. 1989. Chapter 9 Alkaline Flooding. *Development in Petroleum Science* **17-Part B**: 219-254.

Kurenkov, V. F., Hartan, H. G., and Lobanov, F. I. 2002. Degradation of Polyacrylamide and its Derivation in Aqueous Solutions. *Russian Journal of Applied Chemistry,* **75**(07): 1039 – 1050.

Lake, L. W. 1989. Enhanced Oil Recovery. *Prentice Hall,* New Jersey.

Laroche, C., Vizika, O., and Kalaydjian, F. 1999. Network modeling to predict the effect of wettability heterogeneities on multiphase flow. Paper SPE 56674 presented at the SPE Annual Technical Conference and Exhibition, Houston, 3-6 October

Li, S., Hendraningrat, L., and Torsater, O. 2013. Improved Oil Recovery by Hydrophilic Silica Nanoparticles Suspension: 2-Phase Flow Experimental Studies. Paper IPTC 16707 presented at the International Petroleum Technology Conference. Beijing, China, 26 – 28 March.

Li, S., and Torsæter, O. 2014. An Experimental Investigation of EOR Mechanisms for Nanoparticles Fluid in Glass Micromodel. Presented at the International Symposium of the Society of Core Analysts held in Avignon, France, 8-11 September

Li, W., Zhu, J., Qi, J. 2007. Application of nano-nickel catalyst in the viscosity reduction of Liaohe extra-heavy oil by aqua-thermolysis. *Journal of Fuel Chemistry and Technology* **35**(2): 176-180.

Liu, X., and Civan, F. 1993. Characterization and Prediction of Formation Damage in Two-Phase Flow Systems. Paper SPE 25429 Presented at the Production Operations Symposium held in Oklahoma City, 21-23 March

Maghzi, A., Mohebbi, A., Kharrat, R., and Ghazanfari, M. H. 2011. Pore-scale monitoring of wettability alteration by silica nanoparticles during polymer flooding to heavy oil in a five-spot glass micromodel. *Transport in Porous Media* **87**(3): 653-664.

Maghzi, A., Mohammadi, S., Ghazanfari, M. H., Kharrat, R., and Masihi, M. 2012. Monitoring wettability alteration by silica nanoparticles during water flooding to heavy oils in five-spot systems: A pore-level investigation. *Experimental Thermal and Fluid Science* **40**: 168-176.

Maghzi, A., Mohebbi, A., Kharrat, R., and Ghazanfari, M. H. 2013. An Experimental Investigation of Silica Nanoparticles Effect on the Rheological Behavior of Polyacrylamide Solution to Enhance Heavy Oil Recovery. *Petroleum Science and Technology*, **31**(5): 500-508.

Maghzi, A., Kharrat, R., Mohebbi, A., and Ghazanfari, M. H. 2014. The impact of silica nanoparticles on the performance of polymer solution in presence of salts in polymer flooding for heavy oil recovery. *Fuel*, **123**: 123-132.

Matteo, C., Candido, P., Vera, R., and Francesca, V. 2012. Current and Future Nanotech Applications in the Oil Industry. *American Journal of Applied Sciences* **9**(6): 784-793.

Metin, C.O., Bonnecaze, R.T., and Nguyen, Q.P. 2012. The Viscosity of Silica Nanoparticle Dispersions in Permeable Media. Paper SPE 157056 presented at the SPE

International Oilfield Nanotechnology Conference. Noordwijk, The Netherlands. 12 – 14 June.

Mo, D., Jia, B., Yu, J., Liu, N., and Lee, R. 2014. Study Nanoparticle-Stabilized CO_2 Foam for Oil Recovery at Different Pressure, Temperature, and Rock Samples. Paper SPE-169110-MS presented at the SPE Improved Oil Recovery Symposium. Tulsa, USA, 12 – 16 April.

Mohajeri, M., Hemmati, M., Shekarabi, A.S. 2015. An experimental study on using a nanosurfactant in an EOR process of heavy oil in a fractured micromodel. *Journal of Petroleum Science and Engineering,* **126**: 162-173.

Mohanty, K.K. 2006. Dilute surfactant methods for carbonate formations. Final report. University of Houston and US Department of Energy. Report # DE-FC26-02NT15322, February.

Mohebbifar, M., Ghazanfari, M. H., and Vossoughi, M. 2015. Experimental Investigation of Nano-Biomaterial Applications for Heavy Oil Recovery in Shaly Porous Models: A Pore-Level Study. *Journal of Energy Resources Technology*, **137**(1).

Morelato, P., Rodrigues, L., and Romero, O. L. 2011. Effect of Polymer Injection on the Mobility Ratio and Oil Recovery. Paper SPE-148875-MS presented at the SPE Heavy Oil Conference and Exhibition, Kuwait City, Kuwait, 12 – 14 December.

Morrow, N.R., Lim, H.T., and Ward, J.S. 1986. Effect of crude-oil-induced wettability changes on oil recovery. *SPE Formation Evaluation* **1**(01): 89-103.

Nazari Moghadam, R., Bahramian, A., Fakhroueian, Z., Karimi, A., and Arya, S. 2015. Comparative Study of Using Nanoparticles for Enhanced Oil Recovery: Wettability Alteration of Carbonate Rocks. *Energy and Fuels*, **29**: 2111 – 2119.

Netto, A. S. T. 1993. Pore-Size Distribution in Sandstones: GEOLOGIC NOTE. *Aapg Bulletin*, **77**(6): 1101 – 1104.

Nguyen, P.T., Do, B.P.H., Pham, D.K., Nguyen, Q.T., Dao, D.Q.P., and Nguyen, H.-A. 2012. Evaluation on the EOR Potential Capacity of the Synthesized Composite Silica-Core/ Polymer-Shell Nanoparticles Blended with Surfactant Systems for the HPHT Offshore Reservoir Conditions. Paper presented at the SPE International Oilfield Nanotechnology Conference and Exhibition, 12-14 June, Noordwijk, The Netherlands. doi:10.2118/157127-MS

Nguyen, P., Fadaei, H., and Sinton, D. 2014. Pore-Scale Assessment of Nanoparticle-Stabilized CO2 Foam for Enhanced Oil Recovery. *Energy and Fuels*, **28**(10): 6221 – 6227.

Novy, F., and Sloat, B. 1975. Flood Returns 20 plus % on Investment. *Oil and Gas Journal*, **73**(41): 95 – 98.

Ogolo, N.A., Olafuyi, O.A., and Onyekonwu, M.O. 2012. Enhanced Oil Recovery Using Nanoparticles. Paper SPE 160847 presented at the SPE Saudi Arabia Section Technical Symposium and Exhibition, Al-Khobar, Saudi Arabia, 8-11 April

Onyekonwu, M.O., and Ogolo, N.A. 2010. Investigating the Use of Nanoparticles in Enhancing Oil Recovery. Paper SPE 140744 presented at the 34th Annual SPE International Conference and Exhibition. Calabar, Nigeria, 31 July – 7 August.

Øren, P.E., and Pinczewski, W.V. 1995. Fluid distribution and pore-scale displacement mechanisms in drainage dominated three-phase flow. *Transport in Porous Media* **20**(1-2): 105-13

Owens, F.J., and Poole Jr, C.P. 2008. *The physics and chemistry of nanosolids.* John Wily and Sons.

Pal, S.L., Jana, U., Manna, P.K., Manavalan, R. 2011. Nanoparticle: An overview of preparation and characterization. *Journal of Applied Pharmaceutical Science* **01**(06): 228-234.

Panneerselvam, S., and Choi, S. 2014. Nanoinformatics: Emerging Databases and Available Tools. *International Journal of Molecular Science* **15**(5): 7158-7182.

Qiu, F. 2010.The Potential Application in Heavy Oil EOR with the Nanoparticle and Surfactant Stabilized Solvent-Based Emulsion. CSUG/SPE 134613 Paper Presented at the

Canadian Unconventional Resources & International Petroleum Conference held in Calgary, Canada, 19-21 October

Rodriguez, E., Roberts, M.R., Yu, H., Huh, C., Bryant, S.L. 2009. Enhanced Migration of Surface-Treated Nanoparticles in Sedimentary Rocks. Paper SPE 124418 presented at the SPE Annual Technical Conference and Exhibition. New Orleans, USA, 4 – 7 October.

Roustaei, A., Moghadasi, J., Bagherzadeh, H., and Shahrabadi, A. 2012.An Experimental Investigation of Polysilicon Nanoparticles' Recovery Efficiencies through Changes in Interfacial Tension and Wettability Alteration. Paper SPE 156976 presented at the SPE International Oilfield Nanotechnology Conference and Exhibition, Noordwijk, 12-14 June

Roustaei, A., and Bagherzadeh, H. 2015. Experimental investigation of SiO_2 nanoparticles on enhanced oil recovery of carbonate reservoirs. *Journal of Petroleum Exploration and Production Technology*, **5**: 27 – 33.

Sayegh, S., and Fisher, D. 2008. Enhanced Oil Recovery by CO_2 Flooding in Homogeneous and Heterogeneous 2D Micromodels. *Journal of Canadian Petroleum Technology* **48** (08): 30-36.

Shah, R.D. 2009. Application of Nanoparticle Saturated Injectant Gases for EOR of Heavy Oils. Paper SPE-129539-STU Presented at the SPE Annual Technical Conference and Exhibition, Orleans, Louisiana, 4-7 October

Sharma, M.M., Yen, T.F., Chilingarian, G.V., and Donaldson, E.C. 1985. Chapter 7 Some Chemical and Physical Problems in Enhanced Oil Recovery Operations. *Developments in Petroleum Science* **17**-**Part A**: 223-249.

Sharma, T., Kumar, S.G., and Sangwai, J.S. 2014. Enhanced oil recovery using oil-in-water (o/w) emulsion stabilized by nanoparticles, surfactant and polymer in the presence of NaCl. *Geosystem Engineering*, **17**(3): 195-205.

Shokrlu, Y. H., and Babadagli, T. 2010. Effects of Nano Sized Metals on Viscosity Reduction of Heavy Oil/Bitumen during Thermal Applications. Paper CSUG/SPE 137540 Presented at the Canadian Unconventional Resources and International Petroleum Conference, Calgary, Alberta, 19-21 October

Singh, R., and Mohanty, K.K. 2014. Foams Stabilized by In-Situ Surface Activated Nanoparticles in Bulk and Porous Media. Paper SPE-170942-MS presented at the SPE Annual Technical Conference and Exhibition. Amsterdam, The Netherlands, 27 – 29 October.

Sohrabi, M., Henderson, G.D., Tehrani, D.H., and Danesh, A. 2000. Visualization of oil recovery by water alternating gas (WAG) injection using high pressure micromodels-water-wet system. Paper SPE 63000 presented at the SPE Annual Technical Conference and Exhibition, Dallas, 1-4 October

Sohrabi, M., Tehrani, D.H., Danesh, A., and Henderson, G.D. 2004. Visualization of oil recovery by water-alternating-gas injection using high-pressure micromodels. *SPE Journal* **9**(03): 290-301.

Sun, Q., Li, Z., Li, S., Jiang, L., Wang, J., and Wang, P. 2014. Utilization of Surfactant-Stabilized Foam for Enhanced Oil Recovery by Adding Nanoparticles. *Energy and Fuels,* **28**(4): 2384 – 2394.

Taber, J.J., Martin, F.D., and Seright, R.S. 1997. EOR Screening Criteria Revisited—Part 2: Applications and Impact of Oil Prices. *Society of Petroleum Engineers* **12**(03).

Van Dijke, M. I. J., and Sorbie, K.S. 2003. Pore-scale modelling of three-phase flow in mixed-wet porous media: multiple displacement chains. *Journal of Petroleum Science and Engineering* **39**(3-4): 201-216.

Wang, J., Wang, D., Sui, X., and Bai, W. 2006. Combining Small Well Spacing With Polymer Flooding To Improve Oil Recovery of Marginal Reservoirs. Paper SPE-96946-MS presented at the SPE/DOE Symposium on Improved Oil Recovery. Tulsa, USA, 22 – 26 April.

Wang, Y., Zhao, F., and Bai, B. 2010. Optimized Surfactant IFT and Polymer Viscosity for Surfactant-Polymer Flooding in Heterogeneous Formations. Paper SPE-127391-MS presented at the SPE Improved Oil Recovery Symposium. Tulsa, USA, 24 – 28 April.

Xia, Y., Yang, P., Sun, Y., Wu, Y., Mayers, B., Gates, B., Yin, Y., Kim, F., and Yan, H. 2003.One-Dimensional Nanostructures: Synthesis, Characterization, and Applications. *Advanced materials* **15**(5): 353-389.

Yadali Jamaloei, B., and Kharrat, R. 2010. Analysis of Microscopic Displacement Mechanisms of Dilute Surfactant Flooding in Oil-wet and Water-wet Porous Media. *Transport in Porous Media* **81**(1): 1-19.

Yu, J., Wang, S., Liu, N., and Lee, R. 2014. Study of Particle Structure and Hydrophobicity Effects on the Flow Behavior of Nanoparticle-Stabilized CO_2 Foam in Porous Media. Paper SPE-169047-MS presented at the SPE Improved Oil Recovery Symposium, Tulsa, USA, 12 – 16 April.

Zaid, H.M., Latiff, A., Rasyada, N., and Yahya, N. 2014. The Effect of Zinc Oxide and Aluminum Oxide Nanoparticles on Interfacial Tension and Viscosity of Nanofluids for Enhanced Oil Recovery. *Advanced Material Research,* **1024**: 56-59.

Zhang, X., Gu, H., and Fujii, M. 2007. Pore-scale modeling: Effective thermal conductivity and thermal diffusivity of nanofluids containing spherical and cylindrical nanoparticles. *Experimental Thermal and Fluid Science* **31**(6): 593-599.

Zhao, X., Blunt, M.J., and Yao, J. 2010. Pore-scale modeling: Effects of wettability on waterflood oil recovery. *Journal of Petroleum Science and Engineering* **71**(3-4): 169-178.